Volume 46 | Number 14 | 21 July 2017 | Pages 4113–4376

Chem Soc Rev

Chemical Society Reviews

rsc.li/chem-soc-rev

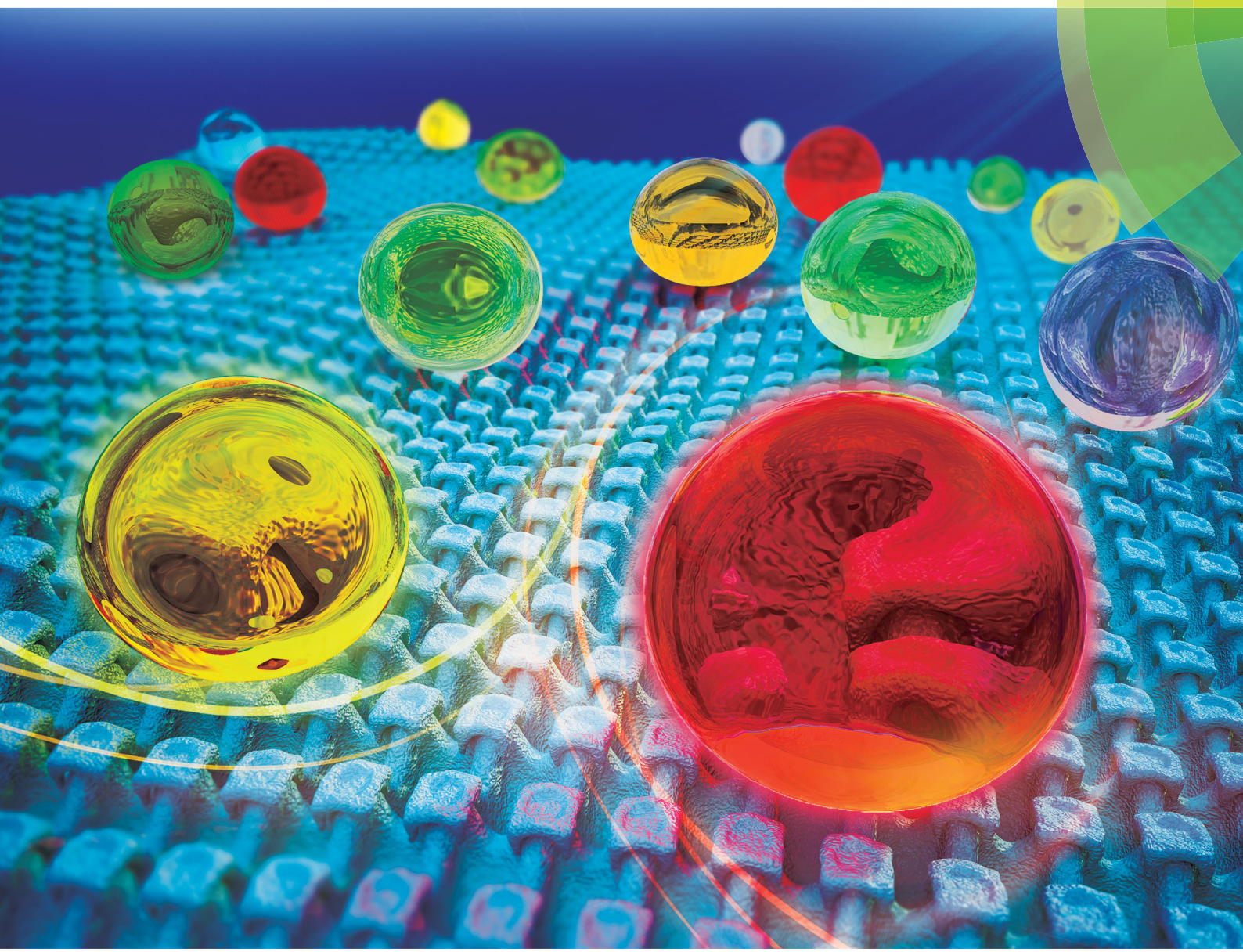

ISSN 0306-0012

ROYAL SOCIETY OF CHEMISTRY

REVIEW ARTICLE

Feng Chen, Qing Yang *et al.*

Superoleophobic surfaces

Chem Soc Rev

REVIEW ARTICLE

View Article Online
View Journal | View Issue

Cite this: Chem. Soc. Rev., 2017, 46, 4168

Superoleophobic surfaces

Jiale Yong,[a] Feng Chen,*[a] Qing Yang,*[b] Jinglan Huo[a] and Xun Hou[a]

Received 19th October 2016

DOI: 10.1039/c6cs00751a

rsc.li/chem-soc-rev

Superoleophobicity is a phenomenon where the contact angles of various oil droplets with low surface tension on a solid surface are larger than 150°. In the past few years, there has been much growing interest in the design and application of superoleophobic surfaces. Such surfaces have great significance for both fundamental research and a variety of practical applications, including oil-repellent coatings, self-cleaning, oil/water separation, oil droplet manipulation, chemical shielding, anti-blocking, designing liquid microlens, oil capture, bioadhesion, guiding oil movement and floating on oil. Herein, we systematically summarize the recent developments of superoleophobic surfaces. This review focuses on the design, fabrication, characteristics, functions, and important applications of various superoleophobic surfaces. Although many significant advances have been achieved, superoleophobic surfaces are still in their "toddler stage" of development. The current challenges and future prospects of this fast-growing field of superoleophobicity are discussed.

1. Introduction

Solid, liquid and gas are the three basic states of matter. The wettability of solid surfaces, which depends on the interfacial interaction of the solid/liquid/gas phase has great significance for the survival of animals/plants and for our daily life, and the materials showing special extreme wettability are particularly captivating.[1–9] Superhydrophobic surfaces and superoleophobic surfaces on which the water droplets and oil droplets present contact angles (CAs) above 150°, are the most widely studied interfaces in wettability, due to their excellent water- or oil-repellent ability.[10–15] Inspired by the natural fascinating features of super-wetting surfaces, people have attempted to change the wettability of various materials either by creating a hierarchical rough microstructure, or by modifying the substrate with a layer of chemical coating for the reason that the wettability of the material surfaces is mainly governed by both the surface

[a] State Key Laboratory for Manufacturing System Engineering and Shaanxi Key Laboratory of Photonics Technology for Information, School of Electronics & Information Engineering, Xi'an Jiaotong University, Xi'an, 710049, P. R. China. E-mail: chenfeng@mail.xjtu.edu.cn

[b] School of Mechanical Engineering, Xi'an Jiaotong University, Xi'an, 710049, P. R. China. E-mail: yangqing@mail.xjtu.edu.cn

Jiale Yong

Dr Jiale Yong is currently a lecturer of Electronic Science and Technology at Xi'an Jiaotong University. He received his BS degree from Xi'an Jiaotong University in 2011. After that, he joined Prof. Chen's research group and received a PhD in Electronic Science and Technology from Xi'an Jiaotong University in 2016. His research interests include femtosecond laser microfabrication, controlling the wettability of solid surfaces, and the bio-inspired design of superhydrophobic and superoleophobic interfaces.

Feng Chen

Prof. Feng Chen is a full professor of the School of Electronics and Information Engineering at Xi'an Jiaotong University, where he directs the Femtosecond Laser Laboratory. He received a BS degree in physics from Sichuan University, China, in 1991, and then began to work for the Chinese Academy of Science (1991 to 2002), where he was promoted to a full professor in 1999. He received a PhD in Optics from the Chinese Academy of Science in 1997. In 2002, he joined Xi'an Jiaotong University, where he became a group leader. His current research interests are femtosecond laser microfabrication and bionic microfabrication.

geometrical microstructure and the surface chemical composition.[16–21] To date, a very large number of superhydrophobic surfaces have been developed, and such artificial materials have a wide variety of practical applications in self-cleaning coatings,[20,22–25] antifouling,[15] anti-fogging/icing/corrosion,[26–29] drag reduction,[30–35] microfluidics,[36–41] lab-on-a-chip,[42–45] cell engineering,[24,46–50] micro-droplet manipulation,[51–55] oil/water separation,[56–60] guiding liquid sliding,[61–64] water collection,[65–67] surface-enhanced Raman scattering (SERS)[68–70] and super-buoyant micro-boats.[71] However, superoleophobic surfaces that will not be wet by organic liquids are difficult to achieve, due to the fact that surface tensions of organic liquids are commonly very low, as shown in Table 1.[72–74] Similar to superhydrophobic surfaces, superoleophobic surfaces have gained more and more attention recently because of their remarkable potential applications, including anti-oil coatings,[75–78] self-cleaning,[22,79,80] oil/water separation,[56,81–88] oil droplet manipulation,[78,80,89–93] chemical shielding,[75] anti-blocking,[79,94] designing liquid microlens,[95] oil capture,[96] bioadhesion,[97] guiding oil movement,[92,98] and floating on oil.[99,100]

There have been three breakthroughs that have made important contributions to the development of superoleophobicity. In 1997, Tsujii *et al.* first reported a superoleophobic surface, which was obtained by modifying an anodized rough aluminum plate with fluorinated monoalkylphosphate.[101] The CA value of a rapeseed oil droplet on this surface was 150°; however, the surface tension of the rapeseed oil is not low (~55 mN m^{-1}). Subsequently, the research on superoleophobicity still developed very slowly, until in 2007, Tuteja *et al.* proposed and demonstrated the importance of re-entrant surface curvature to achieving superoleophobicity, except for ultralow surface free energy and rough microstructures.[72] The surfaces with re-entrant textures generally have overhang, inverted trapezoid, mushroom-like microstructures, and so on.[3,12,72,73,102–108] They further proposed two design parameters for forming stable superoleophobic surfaces.[73,108–120] The concept of re-entrant texture has greatly accelerated the development of this field.[3,12,109,110] In 2009, Jiang *et al.* revealed the internal mechanism of the anti-oil-pollution ability of fish skin in water.[76] The ability stems from the unique underwater superoleophobicity of fish scales. Water can wet the fish skin and be trapped in the rough microstructures of the fish scale surface. The trapped water cushion repels oil and endows the fish scales with superoleophobicity in a water

Table 1 Surface tension of various liquids (at 20 °C from ref. 74)

Liquid	Surface tension (mN m^{-1})	Density (g cm^{-3})
Water	72.8	1.0
Glycerol	64.0	1.26
1,2-Dichloroethane	33.3	1.26
Liquid paraffin	33.1	0.83–0.86
Toluene	28.4	0.87
Chloroform	27.5	1.50
n-Hexadecane	27.5	0.77
n-Tetradecane	26.6	0.76
Dichloromethane	26.5	1.33
Cyclohexane	25.9	0.78
n-Dodecane	25.4	0.75
Cyclohexane	25.0	0.78
n-Decane	23.8	0.73
Gasoline	≈22.0	0.70–0.78
n-Octane	21.6	0.70
n-Heptane	20.1	0.68
n-Hexane	18.4	0.66
n-Pentane	18.3	0.63

Qing Yang

Prof. Qing Yang received her BS degree in Photoelectron Science and Technology in 1992 from Sichuan University. In 2009, she received her PhD from Xi'an Institute of Optics and Fine Mechanics, Chinese Academy of Science. She is currently an associate professor at Xi'an Jiaotong University. Her current research interests are femtosecond laser fine process, microfluidic biochips, and micro-photonics.

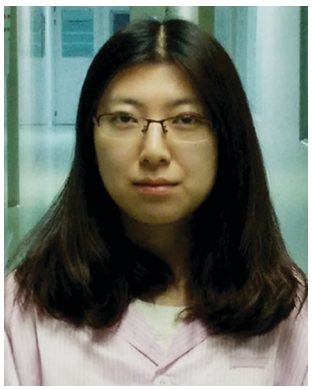

Jinglan Huo

Dr Jinglan Huo is currently a PhD candidate in Prof. Feng Chen's research group at Xi'an Jiaotong University. She received her BS degree in Electronic and Information Engineering from Xidian University in 2015. Her research interests include femtosecond laser microfabrication, superwettability, and cell engineering on superhydrophobic patterned microstructures.

Xun Hou

Prof. Xun Hou received his BS degree in Physics from Northwest University, China, in 1959. From Oct. 1979 to Nov. 1981, he worked at Imperial College in England as a visiting scholar. He was elected as an academician of the Chinese Academy of Sciences in 1991. He is currently a professor at Xi'an Jiaotong University, and he is also the director of the Shaanxi Key Laboratory of Photonics Technology for Information. His research interests mainly focus on photoelectronic materials and devices.

environment. This finding has opened up an important new way for achieving superoleophobicity underwater.[76,79,111–116] By the combination of suitable surface roughness, ultralow or ultrahigh (in underwater case) surface-energy materials and even re-entrant surface texture, various superoleophobic surfaces are continuously being engineered either in air or in water.[3,12–14,76,79,96,108–123] However, superoleophobicity by itself does not fully satisfy the needs of practical application. Endowing superoleophobic surfaces with multiple functions (*e.g.*, controllable oil-adhesion,[78,80,89,91,112,124] anisotropic oil-wettability,[125–127] transparency,[117,120,128,129] durability and self-healing)[121,130–135] and smart properties (respond to external stimulus, *e.g.*, light,[136–138] pH,[139–141] temperature,[142,143] electrical potential,[144,145] magnetic field,[146] density of surroundings[90]) has become the main trend of this research field. The design and realization of more complicated and subtle superoleophobic surfaces have remained as immense challenges.

This review will systematically summarize the recent important developments of superoleophobic surfaces. First, creatures in nature with special superoleophobicity, and classical wetting models are introduced as the background (Section 2). Then, the constructing principle and various properties of superoleophobic surfaces both in air (Section 3) and underwater (Section 4) are reviewed. The next part (Section 5) focuses on the smart superoleophobic surfaces that can response to external stimulation to reversibly switch their static or dynamic wettability. After that, we present a variety of practically functional applications (Section 6). Finally, the challenges and prospects of superoleophobic surfaces are briefly discussed (Section 7).

2. Biological and theoretical backgrounds

2.1 Creatures in nature with special wettability

To survive and adapt to the harsh environment, natural species have evolved all sorts of perfect multifunctional surfaces after millions of years of evolution and natural selection, exhibiting the unification and coordination of structure and performance.[147–150] Therefore, there are many animals and plants having surfaces with diversified wettabilities, such as the self-cleaning property of the lotus leaf (Fig. 1a),[151,152] the high adhesive force of rose petals (Fig. 1b),[153] the anisotropic wettability of the rice leaf (Fig. 1c),[154,155] the directional adhesion of a butterfly wing (Fig. 1d),[156] the anti-fogging ability of a mosquito eye (Fig. 1e),[26] water-collection of a desert beetle (Fig. 1f),[65] underwater long-term air retention of *Salvinia* plants (Fig. 1g),[157] the ability of a water strider to walk and jump on the surface of water (Fig. 1h).[158,159] It is found that both hierarchical microstructures and the chemical composition atop them lead to the specialities of the above creatures, which inspire humans to design and prepare bionic surfaces with special wettability.[63,76,152,160–162] In recent years, many creatures were also found to show superoleophobicity and anti-oil properties.

2.1.1 Springtail skin. Many plant and animal surfaces exhibit extreme water-repellency.[147,148] A trapped air layer usually

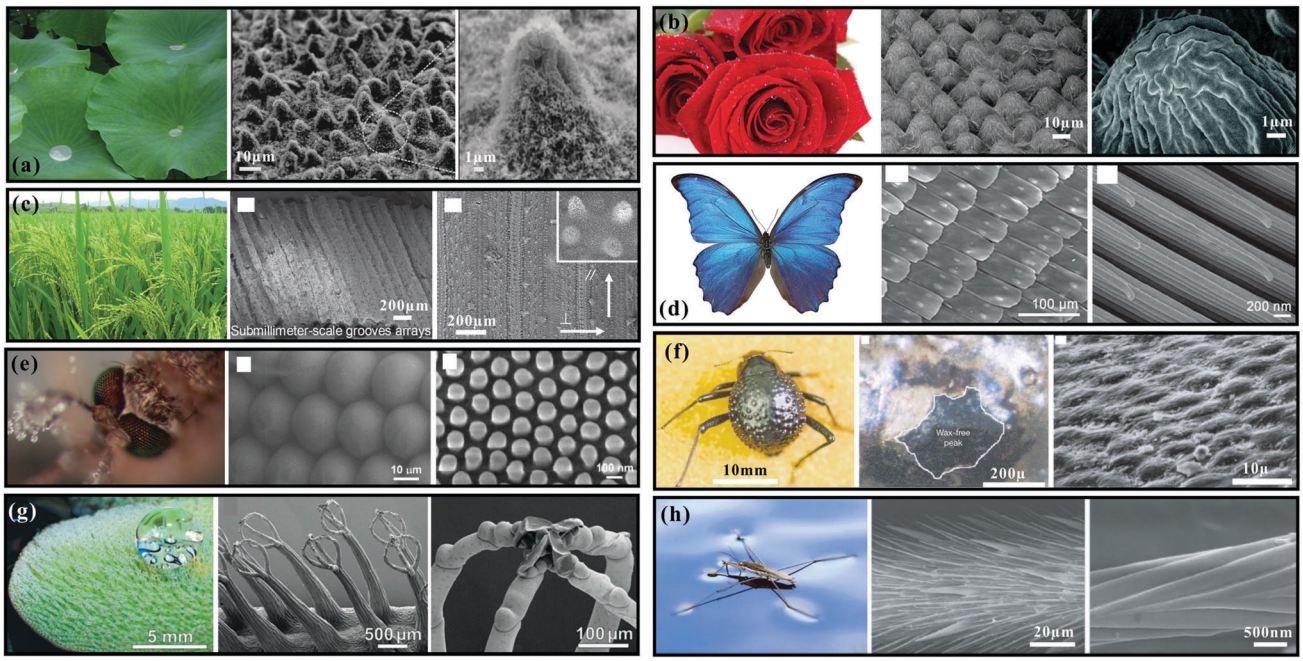

Fig. 1 Photographs and surface microstructures (SEM images) of various natural animals and plants showing special wettability: (a) lotus leaf, (b) red rose petal, (c) rice leaf, (d) a butterfly wing, (e) mosquito eye, (f) back of a desert beetle, (g) *Salvinia* plant, and (h) leg of a water strider. (a) Reproduced from ref. 152 with permission from Wiley, copyright 2008. (b) Reproduced from ref. 153 with permission from ACS, copyright 2008. (c) Reproduced from ref. 155 with permission from Wiley, copyright 2011. (d) Reproduced from ref. 156 with permission from RSC, copyright 2007. (e) Reproduced from ref. 26 with permission from Wiley, copyright 2007. (f) Reproduced from ref. 65 with permission from NPG, copyright 2001. (g) Reproduced from ref. 157 with permission from Wiley, copyright 2010. (h) Reproduced from ref. 158 with permission from NPG, copyright 2004.

forms between surface microstructures and surrounding water after immersing such surfaces in water.[48,136,163,164] The air layer is called the physical gill or plastron, which makes locusts and water spiders able to breathe even in water.[165,166] However, these surfaces are easily wetted by low-surface-tension organic liquids. As a special example, *Springtails* (Fig. 2a) often live in habitats where water is severely polluted by surface-active ingredients forming from decaying organic matter, along with highly damaging/hazardous microorganisms.[167] The springtails' skin not only shows superhydrophobicity, but also similar superoleophobic features, which can stop a variety of organic liquids from wetting the skin. The remarkable water and oil repellency result in a stable plastron when the springtails are immersed in water and even in many organic liquids such as oils or ethanol. To avoid the danger of suffocation in liquid, the springtails can breathe air directly from the plastron in their often rain-flooded habitat. The scanning electron microscope (SEM) image reveals that there are many bristles and rhombic meshes of interconnected nano-granules covering on the skin of springtails (Fig. 2a). Moreover, the profiles of the ridges and granules are negatively overhang, which is the typical re-entrant shape.[3,167,168] The re-entrant microstructures prove to be the forming basis for the anti-oil ability of the springtail skin.

2.1.2 Fish scales. Fish are able to swim freely in oil-contaminated water without their skin being stained. Jiang *et al.* found that the excellent anti-oil capability of fish skin is derived from the superoleophobicity of the scales in water medium, as shown in Fig. 2b and c.[76] Fish scales are mainly formed by a hydrophilic calcium phosphate skeleton and protein, coated with a relatively thin mucus layer. The fan-shaped scales are imbricated on the fish skin. Many oriented micropapillae with length of 100–300 μm and width of 30–40 μm are distributed on the surface of the scales (Fig. 2d). Furthermore, the surfaces of the micropapillae are also not smooth, but have fine-scale roughness (Fig. 2e). Fish scales are superhydrophilic and superoleophilic in air. Water droplets and oil droplets can spread out quickly on the surface of fish scales. Both oil CA (OCA) and water CA (WCA) are close to zero. However, the scales become superoleophobic once immersed in water, where fish generally live, with OCA of 156.4° to an underwater 1,2-dichloroethane droplet (inset of Fig. 2c). The surrounding water medium leads to the wettability transition of fish scales from superhydrophilicity and superoleophilicity (in air) to superoleophobicity (in water). Water can wet and be trapped in the rough microstructures of fish scales, generating an oil-repellent water cushion. When an underwater oil droplet

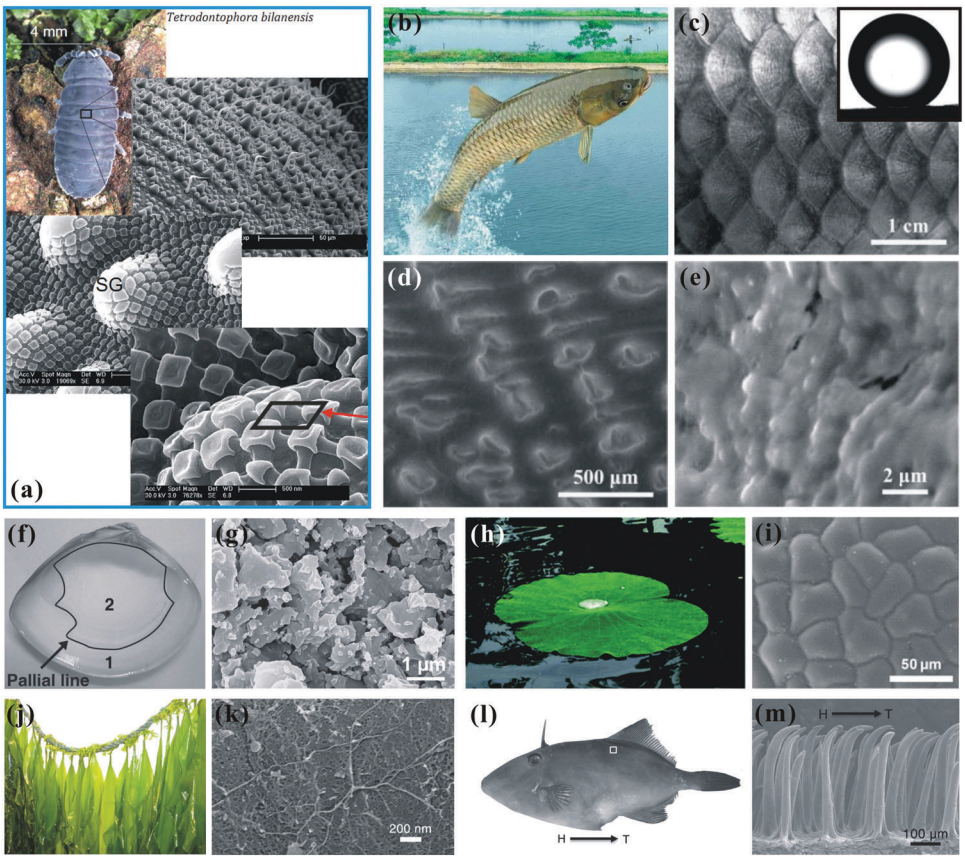

Fig. 2 Photographs and surface microstructures of natural creatures with superoleophobic surfaces: (a) springtail's skin, (b–e) fish scales, (f and g) clam's shell, (h and i) lower side of a lotus leaf, (j and k) seaweed, and (l and m) filefish skin. (a) Reproduced from ref. 167 with permission from Helbig *et al.*, copyright 2011. (c–e) Reproduced from ref. 76 with permission from Wiley, copyright 2009. (f and g) Reproduced from ref. 77 with permission from Wiley, copyright 2012. (h and i) Reproduced from ref. 170 with permission from RSC, copyright 2011. (j and k) Reproduced from ref. 116 with permission from Wiley, copyright 2015. (l and m) Reproduced from ref. 127 with permission from Wiley, copyright 2014.

is placed on the fish scale, a solid/water/oil three-phase system forms. This system is actually an underwater version of the Cassie wetting state.[94,169] Therefore, the cooperation of hydrophilic chemical composition and rough microstructures endows fish skin with underwater superoleophobicity and strong anti-oil ability.

2.1.3 Clam's shell. The internal shell of the short clam generally consists of two different areas: the relatively smooth edge region (Region-1) and the rougher central region (Region-2), as shown in Fig. 2f.[77] The chemical compositions of these two regions are much the same, while the surface microstructures have significant differences. Region-1 is featured with micrometer-scale leaf-like slices. Compared to Region-1, Region-2 looks much rougher with many microscale irregular chunks heaped in a disorderly manner (Fig. 2g), meanwhile the chunks are covered by abundant nanoscale blocks. After the clam's shell is immersed into and subsequently taken out of crude oil, Region-1 is polluted by oil whereas Region-2 keep clean all the time. The remarkable anti-oil property of Region-2 results from its underwater superoleophobicity and ultralow oil-adhesion. The hydrophilic $CaCO_3$ composition makes the shell oleophobic in water and the rough hierarchical microstructure further enhances the oleophobicity to underwater superoleophobicity.

2.1.4 Lower side of the lotus leaf. The lotus leaf is well-known for its superhydrophobicity and the self-cleaning effect of its upper surface (Fig. 2h).[20,151,152,162] Compared to the upper surface, the lower side of the lotus leaf has an inverse wettability, because the lower surface and the upper surface have different chemical coatings and microtopography.[170] There is no crystal wax layer coating on the lower surface, which is covered by a lot of tabular and slightly convex lumps, which are further decorated with nanogroove structures (Fig. 2i). The length, width, and height of the lumps are 30–50 μm, 10–30 μm, and 4 μm, respectively. In air, when a water drop is placed on the lower side of the lotus leaf, the water will completely wet the surface, exhibiting superhydrophilicity. The lower side of the lotus leaf always faces and is in contact with the water surface. Under water, an oil droplet on the lower side retains its sphere shape. The measured OCA and oil sliding angle (SA) (OSA) are 155.0° ± 1.5° and 12.1° ± 2.4° to a 1,2-dichloroethane droplet, respectively; *i.e.*, the lower surface of the lotus leaf presents superoleophobicity and low oil-adhesion in water medium.

2.1.5 Seaweed. Seaweed (*Saccharina japonica*) is one of the favorite foods in East Asia (Fig. 2j). Its surface exhibits durable underwater superoleophobicity, even in high-salinity and high-ionic-strength water.[130] The seaweed surface consistently shows an OCA larger than 150° and very low OSA in NaCl solution with different concentrations (from pure water to fully saturated water). The SEM image reveals that there are abundant porous structures on the seaweed surface (Fig. 2k). In addition, seaweed contains plenty of natural polysaccharides, such as alginate, carrageenan, and agar. The polysaccharide molecule can easily bond to water molecules, even in a high salinity solution. The combined effects of porous microstructures and salt-insensitive polysaccharide compositions endow the seaweed surface with salt-tolerant underwater superoleophobicity.

2.1.6 Filefish skin. Filefish, *N. septentrionalis*, can swim in oil-spilled sea areas freely without their skin being contaminated by oil (Fig. 2l).[127] Specifically, underwater oil droplets trend to directionally roll off its skin from head to tail, while the oil droplets are pinned in the opposite direction, exhibiting an anisotropic oil-wettability. Such novel anisotropic oil repellence gives filefish directional self-cleaning ability in oil-polluted water. The oil is prevented from gathering at the filefish's head. The filefish skin is composed of many high-surface-energy organics such as collagen, and it is also covered by oriented hook-like spines instead of common flaky scales (Fig. 2m). The close directional hook-like spines lead to a high degree of surface roughness, thereby endowing filefish skin with underwater superoleophobicity and anti-oil abilities. At the same time, the curved tips of the spines give rise to the unidirectional movement trend of oil droplets.

Among the above-mentioned animals and plants, springtails skin shows superoleophobicity in air, while fish scales, clam shells, the lower side of the lotus leaf, seaweed and filefish skin show superoleophobicity in water. Inspired by these creatures, we find that there are two different routes for designing superoleophobic surfaces: in air and in water.

2.2 Theoretical basis

When a small liquid droplet is placed onto a solid surface, one phenomenon will occur: the droplet firstly touches the substrate and forms a three-phase contact line (TPCL); then the TPCL continues to advance and finally stops when it reaches a certain radius, resulting in an approximately spherical segment of this droplet. In 1805, the English physicist Thomas Young first described the forces acting on a droplet that is placed on an ideal flat surface, as shown in Fig. 3a.[15] He considered that the contact angle (θ) of the liquid droplet was mainly dependent on the interfacial energy/tension between the solid–vapor (γ_{SV}), solid–liquid (γ_{SL}) and liquid–vapor (γ_{LV}) interfaces by the following:

$$\cos\theta = \frac{\gamma_{SV} - \gamma_{SL}}{\gamma_{LV}} \quad (1)$$

This equation is just suitable for an ideal smooth surface. As early as 1936, Wenzel realized the impact of roughness on the wettability of a material surface.[171] According to the definition of surface tension, he pointed out that actual surface area of a rough substrate was larger than its apparent surface area, and further put forward a new model (Fig. 3b) to describe the contact angle θ^* on a rough surface:

$$\cos\theta^* = \frac{r(\gamma_{SV} - \gamma_{SL})}{\gamma_{LV}} = r\cos\theta \quad (2)$$

where r is the roughness factor, which is the ratio of the actual rough surface area to the projected area, θ is the intrinsic contact angle of the liquid droplet on a flat substrate. In this state, the liquid wets the surface and completely fills all voids in

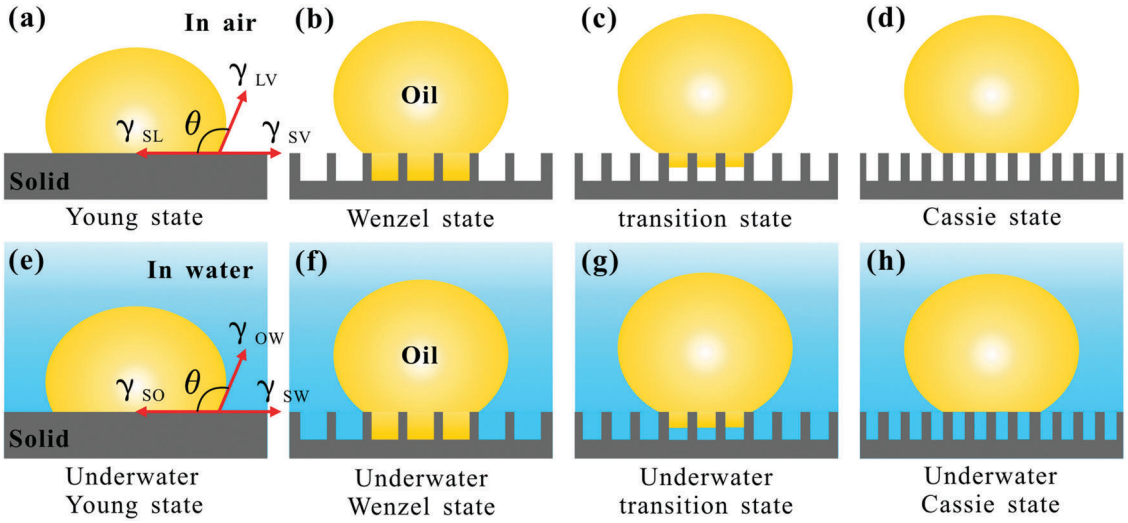

Fig. 3 (a–d) Wetting states of an oil droplet on different surfaces in air: (a) Young state, (b) Wenzel sate, (c) transition state, and (d) Cassie state. (e–h) Wetting states of an oil droplet on different surfaces under water: (e) underwater Young state, (f) underwater Wenzel sate, (g) underwater transition state, and (h) underwater Cassie state.

the rough surface. Because the r is always larger than 1, for the intrinsic hygrophilic (the prefix "hygro" comes from the Greek word for liquid) materials that the probe liquid droplet (water, oil, or other liquids) on such a smooth substrate shows a θ smaller than 90°, θ^* will decrease with increasing r. On the contrary, for the intrinsic hygrophobic materials that the probe liquid droplet on such smooth substrate shows a θ larger than 90°, θ^* will increase with increasing r. Therefore, surface roughness can make hygrophilic materials become more hygrophilic and make the hygrophobic materials become more hygrophobic; *i.e.*, rough microstructures have the function of amplifying wettability on solid surfaces.

When the surface is porous and the voids are very difficult to be wetted by liquid but are filled with air, the wettability of such an interface is very different from the Wenzel state. In 1944, Cassie and Baxter proposed an advanced model to describe the apparent contact angle θ^* of a small liquid droplet on a heterogeneous surface (Fig. 3d).[169] For example, if a surface is made up of two parts of different materials, the θ^* on such a composite surface can be expressed as follows:

$$\cos\theta^* = f_1\cos\theta_1 + f_2\cos\theta_2 \quad (3)$$

where f_1 and f_2 are the area fraction of those two parts, respectively. θ_1 and θ_2 are the corresponding intrinsic contact angles of a liquid droplet on those two materials. In general, the air, which is filled in the spaces between the rough microstructure and the liquid droplet, is ultimately a liquid-repellent, so the liquid contact angle on an air layer can be assumed to be 180°. In this case, the θ^* on a solid–air heterogeneous surface can be expressed as follows:

$$\cos\theta^* = f\cos\theta + (1-f)\cos 180^\circ = f\cos\theta + f - 1 \quad (4)$$

where θ is the intrinsic contact angle of the solid material, and f is the fraction of the surface that is in contact with the liquid.

Although both Wenzel and Cassie equations were originally put forward as semi-empirical formulas, their rigorous derivations were carried out afterwards from the point of thermodynamics.[172–175] The wetting states mentioned above were verified in the research of superhydrophobicity, which has been widely studied. The surfaces belonging to the Wenzel model usually show very high adhesion to a liquid droplet, while the surfaces belonging to the Cassie model usually show extremely low adhesion to a liquid droplet.[16,21,55,176–179] In addition, it is found that there also exists a transition state (Fig. 3c) between the Wenzel state and the Cassie state.[16,55,174,178–184] The liquid droplet may partly penetrate into the valley of the rough surface microstructures. The surfaces in this state often have a liquid adhesion between the Wenzel state and the Cassie state. Such adhesion can usually be changed from low to high, depending on the extent of the droplet penetrating into the rough microstructures.

The above-mentioned four typical wetting states (Young, Wenzel, transition, and Cassie states) are also valid for an oil droplet on flat or rough solid substrates, as shown in Fig. 3a–d. In this situation, the liquid in those models and equations refers to corresponding oils. Recently, oil-wettability of solid materials in water medium has been receiving increasing attention in research, due to its broad, promising applications.[76,79,111–116] The typical wetting states in air can be generalized to their underwater versions, *i.e.*, underwater Young state (Fig. 3e), underwater Wenzel state (Fig. 3f), underwater transition state (Fig. 3g), and underwater Cassie state (Fig. 3h).

The oil droplet on a flat solid surface in water is in the underwater Young state, resulting in a solid/water/oil three-phase interface (Fig. 3e).[76,94] The contact angle (θ_{OW}) of an oil droplet in the underwater Young state (on a flat substrate) satisfies the eqn (5).

$$\cos\theta_{OW} = \frac{\gamma_{SO} - \gamma_{SW}}{\gamma_{OW}} \quad (5)$$

where γ_{SO}, γ_{SW}, and γ_{OW} are the interfacial tensions of solid–oil, solid–water and oil–water interfaces, respectively. Consider that for the case of a water or an oil droplet on such a flat solid surface in air, the intrinsic water contact angle (θ_W) or oil contact angle (θ_O) in air can be respectively explained by the Young's equation:

$$\cos\theta_W = \frac{\gamma_{SW} - \gamma_{SA}}{\gamma_{WA}} \quad (6)$$

$$\cos\theta_O = \frac{\gamma_{SO} - \gamma_{SA}}{\gamma_{OA}} \quad (7)$$

where γ_{SA}, γ_{WA}, and γ_{OA} are the interfacial tensions of solid–air, water–air and oil–air interfaces, respectively. From eqn (6) and (7), we simply get $\gamma_{SW} = \gamma_{WA}\cos\theta_W + \gamma_{SA}$ and $\gamma_{SO} = \gamma_{OA}\cos\theta_O + \gamma_{SA}$. Then, eqn (5) can be changed as follows:

$$\cos\theta_{OW} = \frac{\gamma_{OA}\cos\theta_O - \gamma_{WA}\cos\theta_W}{\gamma_{OW}} \quad (8)$$

For a hydrophilic surface, it also shows oleophilicity in air because oils have lower surface tension than water ($\theta_O < \theta_W < 90^\circ$), so the values of $\cos\theta_O$ and $\cos\theta_W$ are all positive. Since the surface tension of oil/organic liquids are much lower than that of water ($\gamma_{OA} \ll \gamma_{WA}$), the value of $\gamma_{OA}\cos\theta_O - \gamma_{WA}\cos\theta_W$ is commonly negative. From eqn (8), it can be predicted that most hydrophilic surfaces in air show oleophobicity in water.[13,76,81] After combining with rough hierarchical microstructures, the underwater Wenzel state, underwater transition state, or underwater Cassie state may form in the solid/water/oil system. In the underwater Wenzel state (Fig. 3f), the underwater oil droplet wets the substrate and fills the valleys of the rough surface microstructures.[171] The Wenzel equation can be expressed as follows:

$$\cos\theta_{OW}^* = r\cos\theta_{OW} \quad (9)$$

where r is the roughness factor, which is the ratio of the actual rough surface area to the projected area of the surface that the oil droplet is in contact with; θ_{OW}^* and θ_{OW} are the contact angles of an underwater oil droplet setting on a rough substrate and on a flat substrate (both in water medium), respectively. There also exists a special case belonging to the underwater Wenzel wetting state. If a superhydrophobic surface is immersed in water, air can be trapped inside the surface roughness as observed on *Salvinia* plants, usually forming a silver mirror-like trapped air layer between the solid substrate and the surrounding water.[157] When an underwater oil droplet is further placed onto such a substrate, the oil will spread out along the air gap due to the capillary action and pressure, and fully wet the rough microstructures, although the microstructures repel water.[136] In the underwater transition state (Fig. 3g), which is between the underwater Wenzel and Cassie states, the underwater oil droplet may partly penetrate into the valley of the rough surface microstructures. In the underwater Cassie state (Fig. 3h), the entire interspace between the microstructures on the surfaces is prewetted by water, resulting in a trapped water layer underneath the oil droplet.[76,94,169] In fact, the underwater oil droplet sits on a solid–water composite substrate and only contacts the top part of the rough microstructures. The trapped water layer is an extremely oil-repellent medium and results in an ultrahigh oil contact angle. The apparent contact angle, θ_{OW}^*, of an oil droplet at the underwater Cassie state can be described by the underwater Cassie equation:

$$\cos\theta_{OW}^* = f\cos\theta_{OW} + f - 1 \quad (10)$$

where f is the fraction of the surface, which is in contact with oil, θ_{OW} is the underwater intrinsic oil contact angle (underwater Young's contact angle).

2.3 Terminology about super-oil-wettability

With the rapid development of the research field related to wettability, thousands of surfaces showing special wetting properties have been developed. Meanwhile, many terms are created and used to describe those special wetting phenomena. In addition to the "classical" terms, "hydrophobic" and "hydrophilic", other terms such as "oleophobic(philic)", "hygrophobic(philic)", "lyophobic(philic)", "amphiphobic", "omniphobic" have also appeared in the many recent publications. Sometimes they are preceded by a prefix "super" to express their extreme cases. Currently, the biggest problem is that the terms of wettability are not well-defined.[3,185] A same term used in different reports (by different authors) may have different meanings. For example, some people think the superhydrophobic surface must have a CA larger than 150° and a SA (or CA hysteresis) smaller than 10° with respect to a small water droplet, while the others think it is a superhydrophobic surface only when a water droplet shows a CA larger than 150° on this surface. "Superomniphobicity" is used by some people to describe the surfaces that are repellent to both high and low surface tension liquids (oils); we find that the surface wettabilities in their articles are actually the same as the definition of "superamphiphobicity", *i.e.*, superomniphobicity is confused with superamphiphobicity. Some people used "superlyophobic" to express the probe liquid showing CA $\geq$ 150° on a solid substrate, but the prefix "lyo-" comes from the word "dispersion" or "dissolution", so the "superlyophobic" is qualified as inappropriate for wettability classification. Creating uniform, clear terminology is very important to enable precise scientific and technical communication of measured and theoretical wettability results, and to establish guidelines for understanding and designing future surfaces. Recently, Marmur discussed the problem of the current terminology and attempted to classify the terminology of wettability.[185] He proposed some new terms (*e.g.*, parahydrophobic, superhygrophobic, *etc.*) and re-defined some terms with new condition (*e.g.*, "superhydrophilic", referring to only the complete wetting state with a CA of zero, *etc.*). Although his suggestions are very reasonable, those terms were rarely adopted by researchers in the next few years, probably because the step from the widely accepted terms to those suggested terminologies seems too big. The aforementioned terminology problem is still far from being solved. We believe that preserving the traditional meaning of those terms as much as possible and

making appropriate modifications are the best ways to enable the wettability classification is clear and acceptable.

As is well know, "phobic" and "philic" come from the Greek words for "fear" and "love", respectively; "hydro" (from Greek), "oleo" (from Latin), and "hygro" (from Greek) refer to "water", "oils or fats", and "liquid", respectively. The first four roots have gone deep in the brains of researchers, and the fifth root was suggested by Marmur.[185] We should build a clear terminology system for wettability on the basis of these roots. It is also worth noting that "oleo" is from Latin while "lipo" is from Greek for oils or fats. Although "lipo" should replace "oleo" in the publications, we suggest still using "oleo" rather than "lipo" because researchers have become accustomed to using "oleo". According to the classical partition, the CA of 90° is the boundary between "phobic" (>90°) and "philic" (<90°). The prefix of "hydro", "oleo", and "hygro" can be combined with "phobic" and "philic", respectively, to generate six terms: hydrophobic, hydrophilic, oleophobic, oleophilic, hygrophobic, hygrophilic. "Hydrophobic" and "hydrophilic" are used for the probe liquid of water; "oleophobic" and "oleophilic" are used for the probe liquids of low-surface-tension oils and other organic liquids; when the probe liquid is not certain, we can consider temporarily using "hygrophobic" and "hygrophilic" (for example, when we introduce different wetting states in Section 2.2, the liquid droplets in those models can be water or it can be oils, and it can also be other kind of liquids, so "hygrophobic" and "hygrophilic" are temporarily adopted for liquid-repelling and liquid-loving). When the above six properties reach their extreme cases, the terms that describe such special wetting states can be derived by prefixing the word "super" before the fundamental terms, *i.e.*, superhydrophobic, superhydrophilic, superoleophobic, superoleophilic, superhygrophobic, superhygrophilic. We suggest here that only the static wetting property is used to determine the above-mentioned terms without regard to dynamic wettability, to avoid the double standards of one term (for example, superhydrophobicity referring to both CA $\geq$ 150° and SA $\leq$ 10° or just CA $\geq$ 150°); *i.e.*, those terms just depend on the CA values of the probe liquid droplet on the material surfaces. When CA $\geq$ 150°, the surfaces are superhydrophobic, superoleophobic, and superhygrophobic. In contrast, surfaces are superhydrophilic, superoleophilic, and superhygrophilic as long as CA $\leq$ 10°. The dynamic characteristics of a small liquid droplet on a solid surface, which are usually assessed by SA, CA hysteresis, and adhesive force measurement, reflect another aspect of the surface property, *i.e.*, liquid adhesion. Some superhydrophobic surfaces show low adhesion (such as the lotus leaf), while some superhydrophobic surfaces show high adhesion (such as a rose petal) to a water droplet. These wettabilities can be expressed as "superhydrophobicity with low/high adhesion", "low/high-adhesive superhydrophobicity", "roll-down/sticky superhydrophobicity", *etc.*, to differentiate them. Such forms of expression apply to superoleophobicity as well. The surfaces simultaneously showing superhydrophobic and superoleophobic properties are generally known as the "superamphiphobic" interfaces. Sometimes "superomniphobic" is also used to describe a surface that repels various liquids from high-surface-tension water to low-surface-tension oils. However, in most current cases, "superomniphobic" is overlapped and confused with "superamphiphobic". The re-definition of "superomniphobic" and making it different from "superamphiphobic" is badly needed. Since "amphi" comes from the Greek word for "both" and "omni" comes from the Latin word for "all", there is a relation: "oleo" $\subset$ "amphi" $\subset$ "omni". Constructing a "superomniphobic" surface should be more difficult than a "superamphiphobic" surface, therefore, we suggest that superomniphobic surfaces can super-repel almost all liquids, especially very low surface tension fluids (10–20 mN m^{-1}), while superoleophobic/superamphiphobic surfaces tend to only work above this 20 mN m^{-1} limit. The superomniphobic surfaces have been fabricated by Tuteja and Kim *et al.*[73,107] The above-mentioned fourteen terms (hydrophobic, hydrophilic, oleophobic, oleophilic, hygrophobic, hygrophilic, superhydrophobic, superhydrophilic, superoleophobic, superoleophilic, superhygrophobic, superhygrophilic, superamphiphobic, and superomniphobic) are enough to describe the various wetting states. They are all adjectives, and their corresponding nouns are generated by add the suffix of "-ity". The word-building of these terms for super-wettability is summarized in Fig. 4.

3. Superoleophobicity in air

There are enormous difficulties in fabricating superoleophobic surfaces when the vast majority of organic liquids have ultralow surface tension.[12,13,72,101,112,117,186] Both the biological and theoretical backgrounds reveal that enough roughness is very important to achieve superoleophobicity in air.[167,169] In addition, materials having extremely low surface energy are preferable. Considering eqn (1), when θ = 90°, which is the boundary of hygrophilicity and hygrophobicity, γ_{SV} must be equal to γ_{SL}. The γ_{SL} can be approximated as follows:[101]

$$\gamma_{SL} = \gamma_{SV} + \gamma_{LV} - 2\sqrt{\gamma_{SV}\gamma_{LV}} \quad (11)$$

According to eqn (1) and (11), we get γ_{SV} = γ_{LV}/4 as the condition for θ = 90°. As shown in Table 1, typical surface tensions of common oils are 18–33 mN m^{-1}. To further achieve superoleophobicity, the required surface tension of material surface must be as low as a few mN m^{-1}. The –CF_3 group, almost alone, has quite low surface energy.[13,101] Therefore, to fabricate superoleophobic surfaces, most materials need be modified with a low-surface-energy layer after the formation

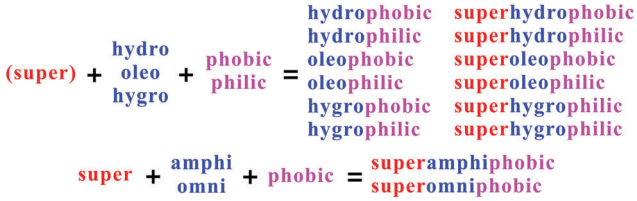

Fig. 4 Word-building of the terminology for super-wettability.

Table 2 Common fluorinated compounds used in surface modification for achieving superoleophobicity in air

Chemical compounds	CAS no.	Chemical structures	Ref.
Fluorinated polyhedral oligomeric silsesquioxane (POSS)		As shown in the inset of Fig. 5e	72, 73, 75, 108, 121, 187, 202 and 256
1*H*,1*H*,2*H*,2*H*-Perfluorodecyltrichlorosilane	78560-44-8	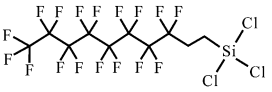	96, 120, 138, 200 and 238
1*H*,1*H*,2*H*,2*H*-Perfluorooctyltrichlorosilane	78560-45-9	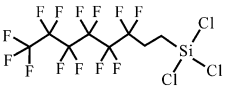	103, 105, 125, 193–195 and 203
1*H*,1*H*,2*H*,2*H*-Perfluorodecyltriethoxysilane	101947-16-4	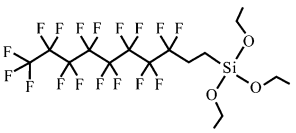	131, 204, 254 and 256
1*H*,1*H*,2*H*,2*H*-Perfluoroalkyltriethoxysilane	51851-37-7	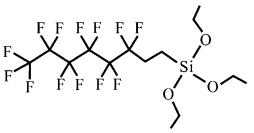	206 and 257
1*H*,1*H*,2*H*,2*H*-Perfluorodecanethiol	34143-74-3		89 and 255
Perfluorodecanoic acid	335-76-2		192
Perfluorooctanoic acid	335-67-1		130

of rough microstructures. Some of the commonly used superoleophobic chemical modifications are summarized in Table 2.

3.1 Re-entrant texture

The formation of the Cassie wetting state is crucial to achieving superoleophobicity. However, not all rough microstructures can result in a robust Cassie wetting state with the liquid droplets having extremely low surface tension (such as oils, alcohols and other organic solvents). The Young's CAs of these liquids are far less than 90° on any flat solid surface. In addition to the rough surface microstructure and low-surface-energy chemical composition, re-entrant surface curvature as the third parameter plays a very important role in designing superoleophobic surfaces.[3,12,72,73,102–108]

Fig. 5a and b shows two schematic diagrams of hypothetical solid–air–liquid situations if a liquid contacts two types of rough substrates. ψ is the local geometric angle of the texture. We presume that such two substrates are made up of the same material and therefore have the same surface free energy, so the given liquid on the two substrates shows equal intrinsic or Young's contact angle, θ. Regarding the situation of $\theta < \psi$, as shown in Fig. 5a, there is a downward net traction on the liquid–air interface. This traction can drive the liquid to penetrate into the valley of the rough microstructures and wet the solid texture, forming a fully-wetted Wenzel contact state. However, in the case of $\theta > \psi$ in Fig. 5b, the net traction is in the upward direction. The net traction tends to drive the liquid–air interface to recede to the top edge of the microstructures, resulting in a three-phase (solid/air/liquid) interface. Therefore, to form a robust Cassie state, the condition of $\theta \geq \psi$ must be met.[72,73,109] The microstructures of the material surface can be roughly divided into two types: trapezoid ($\psi > 90°$) and inverted-trapezoid ($\psi < 90°$). According to the design constraint ($\theta \geq \psi$), any liquid on these two textures in the Cassie state should be one of the situations depicted in Fig. 5c and d. Oils commonly have very low surface tension and almost all of their Young's CAs are smaller than 90°; *i.e.*, $\theta < 90°$. Consequently, oil liquids on trapezoid textures with $\psi > 90°$ are unable to be at robust Cassie states due to $\theta < \psi$, but the Cassie state can possibly be realized on inverted-trapezoid textures with $\psi < 90°$ (Fig. 5d). Such inverted-trapezoid surface microstructures ($\psi < 90°$) are usually termed re-entrant textures.[72,73,109]

The importance of re-entrant surface curvature to achieving superoleophobicity was first demonstrated by Tuteja *et al.* in 2007.[72,73] A series of fluorodecyl polyhedral oligomeric silsesquioxane (POSS) molecules were synthesized by them (inset of Fig. 5e). Then, they used POSS to modify the fiber mats, which were prepared by electrospinning (Fig. 5e).[73] Unexpectedly, the

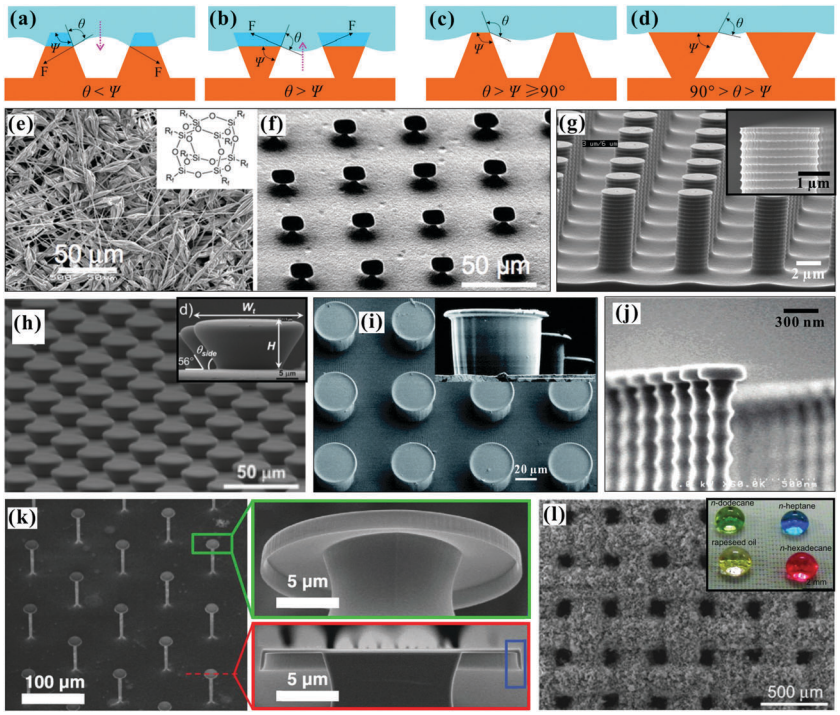

Fig. 5 The crucial role of re-entrant texture in designing superoleophobic surfaces in air. (a and b) Schematic of hypothetical solid–air–liquid interfaces on two types of rough surfaces. (c and d) Schematic of two possible robust Cassie states: (c) trapezoid texture with $\theta > \psi \geq 90^\circ$; (d) inverted-trapezoid (re-entrant) texture with $90^\circ > \theta > \psi$. (e–l) Superoleophobic surfaces with various re-entrant microstructures: (e) electrospun fibers; (f) regular micro-hoodoo surface; (g) micro-pillars with wavy vertical side walls; (h) inverse-trapezoidal microstructure; (i) T-shaped overhang microstructure; (j) silicon nanonails composed of a wavy stem and a bigger head; (k) microscale posts with nanoscale vertical overhangs (doubly re-entrant structure); (l) rough stainless steel wire meshes. The inset in (e) is the structure of POSS molecule. The insets in (g, h and i) are the magnified images of the corresponding re-entrant structures. The inset in (l) shows a variety of oils (*n*-dodecane, *n*-heptane, repeseed oil and *n*-hexadecane) on the rough metal mesh. (e and f) Reproduced from ref. 73 with permission from the National Academy of Sciences of the USA, copyright 2008. (g) Reproduced from ref. 103 with permission from ACS, copyright 2011. (h) Reproduced from ref. 104 with permission from RSC, copyright 2010. (i) Reproduced from ref. 105 with permission from RSC, copyright 2014. (j) Reproduced from ref. 106 with permission from ACS, copyright 2008. (k) Reproduced from ref. 107 with permission from AAAS, copyright 2014. (l) Reproduced from ref. 108 with permission from Wiley, copyright 2012.

composition of fluorodecyl POSS had intrinsic OCAs smaller than 90°, while the final fiber nets showing re-entrant surface curvature displayed superoleophobicity. Similarly, a regular micro-hoodoo surface was also prepared, which presented superoleophobicity in air (Fig. 5f).[73] Inspired by Tuteja's work, recently, many superoleophobic surfaces were constructed using the re-entrant surface curvature factor.[12,109] For example, Zhao *et al.* created a micro-pillar array structure on a silicon substrate through the Bosch etching process (Fig. 5g).[103] The pillars were 7 μm in height and 3 μm in diameter. The interval of the array was 6 μm. In particular, the vertical side wall of the pillars was not smooth, but consisted of a nanoscale wavy structure (~300 nm) from top to bottom. After coating with a fluorosilane molecular layer, the resultant sample exhibited superoleophobicity. The measured OCA value was 158° and the OSA was as small as 10° to a hexadecane droplet. Both the coated chemical layer and the microstructure of the pillar array were indispensable elements for achieving such superoleophobicity. Im *et al.* fabricated an inverse-trapezoidal microstructure array by using the backside three dimensional (3D) diffuser lithography and template replication method (Fig. 5h).[104] After coating a layer of Teflon, the surface became oleophobic with OCA of 135° for a methanol droplet (γ = 22.5 mN m^{-1}). Yuan *et al.* transferred T-shaped overhang microstructures from Si substrate to various curable materials (such as polydimethylsiloxane (PDMS), polymethyl methacrylate (PMMA) and glass resin) by the multiple soft replication method (Fig. 5i).[105] Both the CA values of a water droplet and a hexadecane droplet on those surfaces were larger than 150°, indicating that the fabricated surfaces had simultaneous superhydrophobicity and superoleophobicity. Ahuja *et al.* prepared a silicon nanonail array with re-entrant structure by reactive ion etching (Fig. 5j).[106] Each nanonail was composed of a stem with diameter of about 280 nm and height of 7 μm and a head with diameter of 405 nm and thickness of 125 nm. The nanonails were arranged in a square array, and the interval of the nanonails was 2 μm. The as-prepared surface displayed superoleophobicity for various liquids with surface tension ranging from 21.8 mN m^{-1} (ethanol) to 72.0 mN m^{-1} (water). By designing an opportune rough topography with overhanging microstructures, it can even make the oleophilic materials repel low-surface-energy oils and organic solvents. However, these re-entrant microstructures cannot stop being wetted by the liquids with extremely low surface tension (*i.e.*, γ < 15 mN m^{-1}), such as

fluorinated solvents, which even thoroughly wet most hydrophobic materials. Recently, Kim *et al.* pointed out that the surface with the doubly re-entrant structure is more powerful than the surface with the single re-entrant structure to repel liquids as well as achieve superomniphobicity.[107] They further fabricated an array of doubly re-entrant structures, which were composed of microscale posts with nanoscale vertical overhangs, as shown in Fig. 5k. Without any chemical modification, the as-prepared surface super-repelled all available liquids, including various oils, organic solvents, and even fluorinated solvents (for instance, perfluorohexane, $\gamma < 10$ mN m^{-1}). When a completely wetting liquid contacted the doubly re-entrant structure, the liquid first wetted the top of the micro-posts and then went downward along with the vertical overhangs. The liquid would stop advancing once it reached the vertical overhangs' bottom tip because the direction of surface tension switched to upward at this location, forming a stable liquid suspension on the rough microstructure. Therefore, the doubly re-entrant texture can provide a stronger resistance against wetting.

It is worth noting that the re-entrant texture is not limited to a microstructure with overhang. In fact, some materials such as rough metal meshes,[75,108,187] electrospun fibers,[120,188,189] fabrics,[190] and porous structures[96,118,119,124,191] can also be viewed as the analogues with re-entrant surface curvature because these microstructures have a certain degree of re-entrances. Tuteja *et al.* coated stainless steel meshes with electrospinning microbeads (PMMA + fluorodecyl POSS blend) and obtained re-entrant texture on both the macroscale and microscale (Fig. 5l).[108] The combined effect of hierarchical texture and low solid surface energy endowed the rough mesh with superoleophobicity (inset of Fig. 5l). An *n*-heptane droplet on the sample surface showed an advanced OCA of 155° and an ultralow CA hysteresis of 4°. Choi *et al.* fabricated a poly-(2,2,2-trifluoroethyl methacrylate) fiber web through the typical electrospinning method.[189] The web repelled both water and oil (hexadecane) droplets whose CAs were 153° and 154.2°, respectively. Yang *et al.* obtained a suspension of copper perfluorooctanoate based on the chemical reaction between perfluorooctanoic acid and copper acetate in water, and then sprayed the suspension onto various substrates, such as glass, copper, steel, *etc.*[191] In addition to the hierarchical textured microstructure, there were abundant protrusions and pores on the coating surface. Those protrusions and pores generated a large number of re-entrant geometries. A composite solid/air/oil interface (Cassie state) was formed when an oil droplet was put on the resultant samples, resulting in robust superoleophobicity of the uniform coatings.

Furthermore, it should be noted that although the re-entrant surface curvature is especially helpful to fabricate superoleophobic surfaces (in air), it is a necessary but insufficient condition.

3.2 Superamphiphobicity

Since Tuteja *et al.* in 2007 revealed the importance of re-entrant surface curvature for achieving superoleophobicity,[72] it is well recognized that the synergy between the chemical composition with ultralow surface energy (mainly –CF_3 compounds) and the appropriate surface roughness (including re-entrant microstructures) is the most promising route to fabricating in-air superoleophobic surfaces.[3,12,72,73,102–108] Considering the fact that most oils have smaller surface tension than water, the superoleophobic surfaces in air usually repel water also. Until now, various kinds of surfaces showing both superoleophobicity and superhydrophobicity have been reported.[12,109,117–119,192–206] The nature of such surfaces is defined by the terminology ''superamphiphobicity''.[12,14,109] All the superoleophobic surfaces with re-entrant microstructures, in Section 3.1, simultaneously exhibit superhydrophobicity in air. Therefore, those re-entrant texture-structured superoleophobic surfaces are actually superamphiphobic. The following will show some other examples of superamphiphobic surfaces.

Jiang *et al.* endowed common engineering metals (*e.g.*, zinc, iron, Zn–Fe alloy, aluminum, and nickel) with superamphiphobicity by a simple electrochemical method, as shown in Fig. 6a–c.[192] Taking pure zinc sheet as an example, the cleaned zinc plate was directly immersed into the perfluorocarboxylic acid (such as nonadecafluorodecanoic acid) in ethanol solution under ambient conditions. Zinc is a very active metal and it can be easily oxidized to Zn^{2+} ions by oxygen, especially in acidic solution. After immersing the zinc sheet in perfluorocarboxylic acid solution, the Zn^{2+} ions were released from the zinc plate. Then, the Zn^{2+} ions reacted with perfluorocarboxylic acid molecules to produce zinc perfluorocarboxylate, which could slowly adsorb on the zinc substrate. After 10 days of chemical reaction, petal-like nanosheet structures were created on the zinc sheet (Fig. 6a). The length and height of the nanosheets were in the scale of micrometers, while their thickness was only thirty to several hundred nanometers. All the petal-like nanosheets stood on the substrate. The tops of the micrometer-long sheets were interspersed with lots of fine nanostructures, forming a micro/nanoscale hierarchical rough structure. The nanosheet structured surface super-repelled both water and oil without any further surface modification (Fig. 6b). Water droplets on such a surface exhibited the WCA of 158.1° ± 5° (Fig. 6c) and could easily roll off the tilted substrate with the water SA (WSA) of 5°. As for rapeseed oil, the OCA and OSA were 155.6° ± 1° (Fig. 6c) and 10°, respectively. The superamphiphobicity was the direct result of the synergistic effect of the unique surface chemistry and petal-like microstructure. The perfluorocarboxylic acid with high content of –CF_3 and –CF_2 groups provided very low surface energy, while the rough microstructure could trap air in nanoscale concave cavities and resulted in a steady air cushion which dramatically reduced the contact area between water (oils) and the as-prepared surface, then enlarged the water- and oil-repellence.

Wong *et al.* recently fabricated flexible and transparent superamphiphobic surfaces by the large-scale omnidirectional self-assembly of nanoparticle aerosols.[193] They lit a combustible liquid solution containing hexamethyldisiloxane to generate a flame. With a substrate being placed above the flame, the tailored aerosol of nanoparticles could easily be deposited onto the substrate surface by a highly scalable flame aerosol technique. The resultant nanostructures formed by aerosol

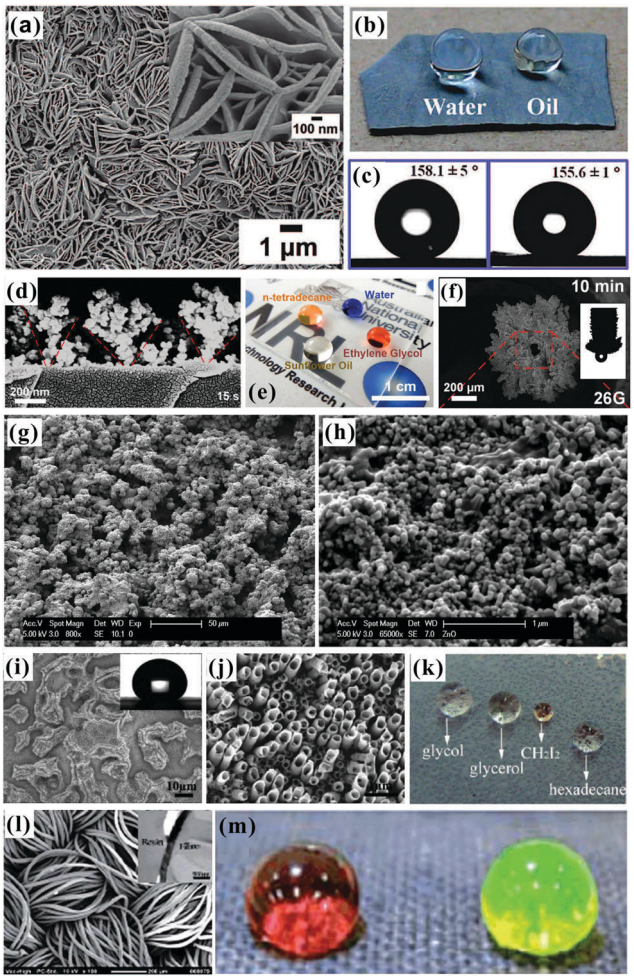

Fig. 6 Various superamphiphobic surfaces. (a) Petal-like nanosheet structures on the zinc sheet. (b) Photo of a water droplet and a rapeseed oil droplet on the rough zinc sheet. (c) Shapes of the water droplet (left) and rapeseed oil droplet (right) on the rough zinc sheet. (d) Cross-sectional SEM image and (e) superamphiphobicity of the nanoparticle aerosols self-assembled surface. (f) Textured needle after the self-assembly of nanoparticle aerosols onto its inner and outer surfaces. Inset: The superamphiphobic injector could generate and release nanoliter liquid droplets. (g and h) SEM images of nanocomposite coating. (i and j) Hierarchical rough TiO_2/Ti microstructure fabricated by double anodization: (i) low magnification, depicting the microscale structure; (j) high magnification, depicting the nanotubes on the microscale structure. (k) Photo of glycol, glycerol, CH_2I_2, and hexadecane droplets on the micro/nanostructured TiO_2 nanotube arrays. (l) SEM image of PPy–FAS coated fabrics. The inset is the cross-sectional transmission electron microscopy (TEM) image of the coated fiber. (m) Hexadecane (red, left) and water (green, right) droplets on the PPy–FAS coated fabric. (a–c) Reproduced from ref. 192 with permission from ACS, copyright 2008. (d and e) Reproduced from ref. 193 with permission from ACS, copyright 2016. (f) Reproduced from ref. 194 with permission from Wiley, copyright 2017. (g and h) Reproduced from ref. 118 with permission from ACS, copyright 2009. (i–k) Reproduced from ref. 195 with permission from ACS, copyright 2010. (l and m) Reproduced from ref. 196 with permission from RSC, copyright 2011.

deposition of SiO_2 nanoparticles looked very much like broccoli plants, having a visible re-entrant cross-section (Fig. 6d). The sample with the self-assembled deposition time of 15 s and further fluorogroup modification exhibited superamphiphobicity with OCAs above 160° for a large number of oils and low-surface-tension liquids (as low as 25 mN m^{-1}), as shown in Fig. 6e. Furthermore, the highly dewetting nanotextures could be created on an extensive set of material surfaces with complex geometries such as curved surfaces and the inner walls of tubes. For example, after the self-assembly of nanoparticle aerosols on the inner and outer surfaces of a commercial hypodermic needle, the textured needle became superamphiphobic (Fig. 6f).[194] The obtained superamphiphobic injector was capable of generating and releasing ultrasmall nanoliter droplets (down to 10 nL) of water and oils. There was no contamination of such needle during handling water and oil droplets in air or in liquid environments.

Steele *et al.* reported a spray coating method to realize superamphiphobicity on various substrates by using nanoparticle-polymer suspensions, as shown in Fig. 6g and h.[118] The ZnO particles with diameter of 50 nm were mixed with waterborne perfluoroalkyl methacrylic copolymer (PMC) (30 wt% polymer, 70 wt% water) and acetone, forming a nanocomposite solution. Among them, PMC was a low-surface-energy binder; ZnO nanoparticles were used to create nano-roughness; acetone was the cosolvent. The solutions were sprayed onto solid substrates using an airbrush atomizer, and then dried for 12 h in air. For a hexadecane droplet, the fabricated thin coatings showed OCA of 154° and CA hysteresis of 6°. The hexadecane droplet rolled almost freely on the as-prepared sample surface, as long as the substrate was slightly tilted. No oily trailing stain was left behind, and this was very similar to the process of a water droplet rolling on a lotus leaf. The coatings also exhibited excellent superhydrophobicity but not superoleophobicity. The superamphiphobicity was the result of water droplets and oil droplets on such resultant coatings all being in the Cassie state.

Wang *et al.* used two routes to build micro/nanoscale hierarchical structures on Ti substrate and successfully obtained superamphiphobic surfaces, as shown in Fig. 6i–k.[195] One route was double anodization and another was a combination of laser ablation and anodization. For the former route, a cleaned Ti plate was firstly electrochemically etched in a NaCl solution (0.1 M) at the current density of 500 mA cm^{-2} for 1 h to form microscale structures (Fig. 6i). Then, the microstructured Ti substrate served as a working electrode and was anodized in an electrolyte (0.5 wt% NH_4F, 3% hydrofluoric acid, and ethylene glycol) at 60 V for 1 h, using a graphite slice as a counter electrode. A lot of TiO_2 nanotubes were created on the top surface of the microstructure of the Ti substrate during the second anodization process (Fig. 6j). After the modification of 1*H*,1*H*,2*H*,2*H*-perfluorooctyltrichloro silane, the as-prepared surface showed both superhydrophobicity and superoleophobicity to various liquids (Fig. 6k). For example, the measured CAs and SAs are 167° and <2° for water, 167° and <2° for sea water, 162° and 3° for glycerol, 160° and 3° for liquid paraffin, 156° and 6° for crude oil, 157° and 5° for colza oil, and 155° and 7° for hexadecane, respectively. For the latter route, the only difference from the former route was that the microstructures were generated by laser ablation in the first step. In this case, the

microstructures could be designed into different patterns including the line pattern, salient pattern and pit pattern. Superamphiphobicity was also obtained through the latter route.

Wang *et al.* developed a one-step method to fabricate superhydrophobic and superoleophobic fabrics based on vapour-phase polymerization, as shown in Fig. 6l and m.[196] The fabric substrates were firstly dipped into the ethanol solution of $FeCl_3$ and fluorinated alkyl silane (FAS). After extracting the fabrics from the solution and drying them out, the fabrics were further placed into a pyrrole saturated nitrogen atmosphere to form polypyrrole (PPy). Finally, the fabrics became black, revealing that a layer of PPy–FAS was coated on the original fabric surfaces (Fig. 6l). The coated fabrics not only exhibited superamphiphobicity (Fig. 6m) with the CAs of 165° to water and 154° to hexadecane, but also had high electrical conductivity with a surface resistivity of 0.5–0.8 $k\Omega\ \square^{-1}$.

Darmanin *et al.* obtained a series of electrodeposited polymers from the pre-synthesized fluorinated 3,4-ethylenedioxypyrrole monomers.[119] The polymer film showed superoleophobicity and superhydrophobicity with ultralow adhesion to both water and oil droplets. The superamphiphobicity resulted from the nanoscale porosity of the electrodeposited polymer, which was formed during the doping process. Srinivasan *et al.* sprayed a blend of fluorodecyl POSS and PMMA on the substrate and achieved superhydrophobicity and high oleophobicity.[197] The surface microstructures could be systematically changed from randomly distributed spherical microbeads to beads-on-string structures to fibers by varying the polymer molecular weight and the solute concentration. Zhang *et al.* placed a stainless steel mesh above the flame of a candle to deposit a thin layer of soot.[100] The soot was piled with a large amount of carbon nanoparticles with the size ranging from 30 nm to 60 nm, resulting in a porous microstructure. Then, a shell of silica was further deposited on the soot layer by chemical vapor deposition (CVD) of tetraethoxysilane, using ammonia as a catalyst. The silica/soot coated mesh was hydrophilic and became superamphiphobic after tridecafluorotetrahydrooctyl trichlorosilane modification.

Superoleophobic surfaces usually super-repel water droplets as well, because the surface tension of water is much higher than that of various oils; *i.e.*, most of the superoleophobic surfaces (in air) are superamphiphobic.[12,109] However, it should be noted that not all the superoleophobic surfaces also have superhydrophobicity. There are also some superoleophobic–superhydrophilic artificial materials.[103,205]

3.3 Superoleophobic–superhydrophilic surfaces

Recently, through designing and modifying special chemical chains on the surfaces with hierarchical rough microstructures, some surfaces simultaneously showing superoleophobicity and superhydrophilicity in air have been fabricated.[103,205] Yang *et al.* reported a superoleophobic–superhydrophilic coating by the spray-casting of the nanoparticle-polymer suspension.[205] Nanoscale SiO_2 particles (0.3 g) were firstly dispersed in 100 mL of poly(diallyldimethylammonium chloride) (PDDA) aqueous solution with the concentration of 1 mg mL^{-1}. Then, 20 mL of sodium perfluorooctanoate (PFO) aqueous solution (0.1 M) was further poured in. With constant ultrasonic shaking, the PFO anions could be grafted onto the quaternary ammonium groups of PDDA (Fig. 7a). After removing the water, the dried composite material (PDDA–PFO/SiO_2) was ultrasonically dispersed in ethanol. The obtained suspension was sprayed onto various substrates using a spray gun. The PDDA–PFO/SiO_2 was tightly coated on the substrate, with the ethanol evaporating completely at room temperature. The PDDA–PFO/SiO_2 coating had both oleophobic fluorinated groups and hydrophilic carboxyl/quaternary ammonium groups, endowing the resultant polymer surface with simultaneously oleophobic and hydrophilic properties. In addition, the mixed SiO_2 nanoparticles led to a hierarchical rough structure, which significantly amplified the oleophobicity and hydrophilicity. The surface showed a textured microstructure of abundant protrusions and pores, which is a representative morphology of the sprayed coating. When a water droplet and a hexadecane droplet were put on the coated substrate, they initially showed spherical shapes. However, the water droplet slowly collapsed and spread over the sample surface within 9 min, with the WCA decreasing from $165° \pm 2°$ to 0°. This is because that water droplet resulted in a rearrangement of the surface molecular structure, and the capillary effect helped the water to fully wet the space of rough microstructures; in contrast, the oil droplet had almost no change in shape. The OCA remained larger than $155° \pm 1°$ all the time, therefore, the PDDA–PFO/SiO_2 coating exhibited simultaneous superhydrophilic and superoleophobic wetting behaviors (Fig. 7b and c). If the coating was sprayed on metal meshes, the meshes with both superhydrophilicity and superoleophobicity could be applied in separating the water/oil mixtures (Fig. 7d and e). During the separation process, water penetrated through the mesh by gravity because of the superhydrophilicity (Fig. 7b), while oils were stopped and retained on the mesh surface because of the superoleophobicity (Fig. 7c). The anti-oil property prevented the rough mesh from fouling or even being blocked by oily liquids, which extended the service life of the separation devices.

Pan *et al.* changed the intrinsically superoleophilic cotton fabric and polyester fabric surfaces to both superoleophobic and superhydrophilic by a simple fluorosilanization treatment, as shown in Fig. 7f–h.[206] (Tridecafluoro-1,1,2,2-tetrahydrooctyl)-triethoxysilane was used because this fluorosilanization had a low surface energy ($\sim$11.5 mN m^{-1}), yielding excellent oil resistance to various low-surface-tension hydrocarbons. The combined effect of the intrinsic re-entrant porous microstructure and chemistry coating with ultralow surface energy resulted in the CAs higher than 150° for various nonpolar hydrocarbons (Fig. 7h). For instance, hexane and heptane could easily bead up on the resultant fabrics and these oil droplets were at the Cassie wetting state. In a surprise twist, if a polar liquid droplet (such as water, dimethylformamide and ethanol) were dripped onto the fabric surfaces, the droplet would rapidly spread out and be absorbed by the fabrics, resulting in CAs of about 0° (Fig. 7h). In fact, the intrinsic intact cellulose chains in cotton fabrics could migrate to the outside surface, so both the fluorine and intact cellulose chain covered the surface of

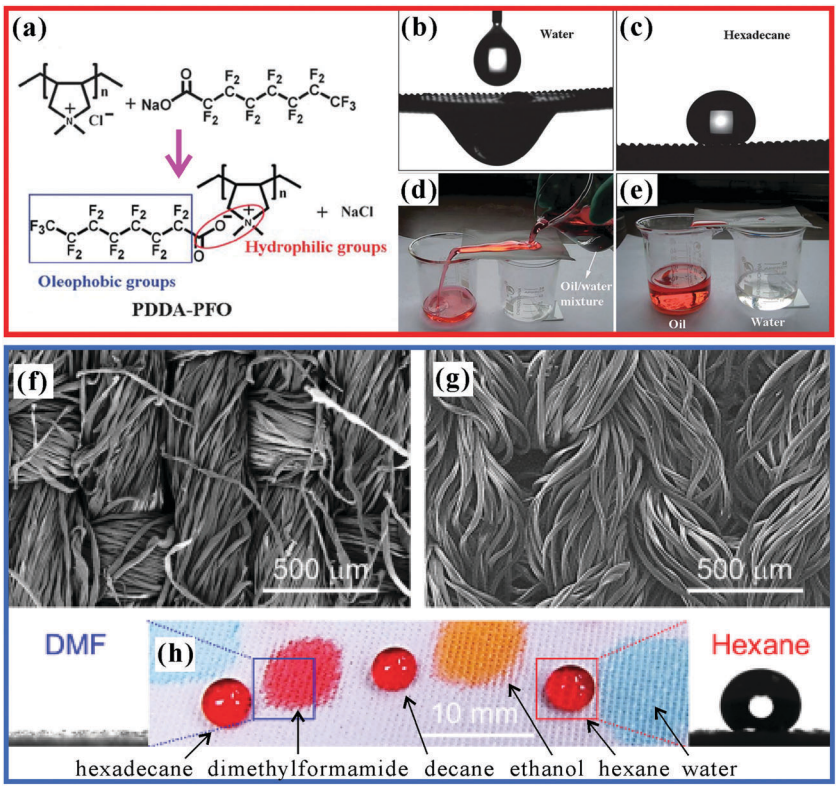

Fig. 7 Superoleophobic–superhydrophilic surfaces. (a) Chemical reaction for synthesizing PDDA–PFO. (b) Water droplet wetting and permeating the PDDA–PFO/SiO_2-coated mesh film. (c) Hexadecane droplet on the resultant mesh. (d and e) Separating the mixture of water and oil by using the PDDA–PFO/SiO_2-coated mesh. (f and g) SEM images of the superoleophobic (f) cotton fabric and (g) polyester fabric. (h) Nonpolar oils beading up and polar liquids permeating through the coated fabric. (a–e) Reproduced from ref. 205 with permission from RSC, copyright 2012. (f–h) Reproduced from ref. 206 with permission from the American Institute of Chemical Engineers, copyright 2014.

the as-prepared fabrics. According to the basic principle of "like dissolves like", the abundant intact cellulose chains promoted the contact between fabric surface and polar liquids, making the fabrics superhygrophilic for polar liquids.

It is worth noting that these superoleophobic–superhydrophilic surfaces possess both oil-repellent (*e.g.*, fluorinated chains) and hydrophilic (*e.g.*, carboxyl/quaternary ammonium groups, cellulose chains, and other polar groups) chemical compositions. The micro/nanoscale hierarchical rough structures only amplify the surface wettability to superoleophobicity and superhydrophilicity. When an oil droplet is put on the resultant surfaces, the oleophobic chemical compositions and rough microstructures play a dominant role; in contrast, when a water droplet is released onto the resultant surfaces, the hydrophilic compositions will be attracted by the polar liquid (water) and reduce the presence of the fluorinated chains at the extreme surface (surface re-arrangement), leading to superhydrophilicity.[205–207]

3.4 Slippery liquid-infused porous surfaces

Unlike the aforementioned superoleophobic surfaces, which usually use special rough microstructures to repel oil wetting,[3,12,14,109] the *Nepenthes* pitcher plant (Fig. 8a) uses microstructures to lock-in an intermediary liquid.[208] The filled liquid within the rough microstructures generates a continuous trapped liquid cushion that can act as a repellent surface (Fig. 8b). When an insect alights on the rim of a pitcher plant, the insect can hardly stand on and will slide down from the rim to the bottom, which is filled with digestive juices, because the trapped liquid cushion repels the oils on the insect's feet.[209] Inspired by the pitcher plant, Wong *et al.* recently presented a new way to create liquid slippery surfaces, named "slippery liquid-infused porous surface (SLIPS)".[208] The CAs of both oil droplets and water droplets on such surfaces were far smaller than 150° (*i.e.*, the surface was not superoleophobic), but the surface exhibited excellent liquid repellence. Therefore, we are more inclined to categorize the SLIPS into the superoleophobic materials, or we can consider that it is a broader superoleophobic interface. As shown in Fig. 8c, a surface with micro/nanoscale porous structure was pre-infused with a perfluorinated lubricating liquid, resulting in the lubricating fluid being locked in the rough microstructures to form the SLIPS. The SLIPS created a smooth, slippery, and stable interface that significantly decreased the contact line pinning effect for various liquids. The lubricating liquid layer could also resist a very high pressure, so foreign liquids would not easily lodge in the porous microstructures. The SLIPS showed very low adhesion to a variety of liquids with surface tension ranging from 17.2 mN m^{-1} (*n*-pentane) to 72.4 mN m^{-1} (water). All the droplets of various liquids could easily slide on a 5° tilted

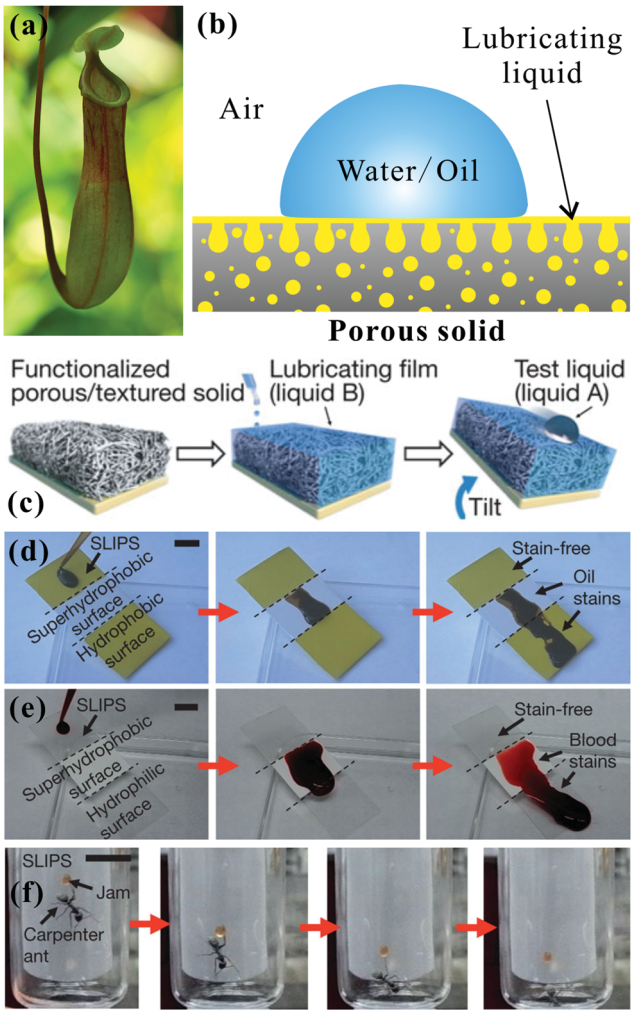

Fig. 8 Liquid repellence of slippery surface. (a) Photo of a pitcher plant. (b) Wetting schematic of a SLIPS. (c) Schematic diagram of fabricating a slippery surface. (d) Light crude oil and (e) blood sliding down a substrate composed of three different regions (from top to bottom: SLIPS, superhydrophobic porous Teflon film, and flat hydrophobic surface). A stain was left on the latter two regions. (f) Inability of an ant to stand on or adhere to the SLIPS. The scale bars in (d–f) are 1 cm. Reproduced from ref. 208 with permission from the NPG, copyright 2011.

sample, without leaving any stain. The SLIPS effectively repelled not only pure liquids, but also compound fluids, *e.g.*, crude oil (Fig. 8d) and blood (Fig. 8e); these compound liquids generally wet and contaminate most solid surfaces. In addition, the SLIPS could serve as a slippery, anti-sticking surface for insects, like pitcher plants (Fig. 8f). Other properties like self-healing and optical transparency endow the liquid-repellent SLIPS with wider application prospects, such as biomedical fluid handling, anti-fouling, fuel transport, optical devices, and self-cleaning windows.[208] To design a liquid slippery surface, attention should be paid to three criteria:[208,210–213] (1) the used materials have porous surface microstructures, which ensure that the lubricating liquid wets and is trapped in the porous microstructures; (2) the adopted lubricating liquid has a stronger ability to wet the solid substrate than the liquid we want to repel; (3) the lubricating liquid must be practically immiscible with the repelled liquids. In addition, the interconnectivity of the micro-pores is also very important to slippery surfaces, although slippery surfaces can be fabricated as long as the above-mentioned three criteria are met. Once the artificial SLIPS is damaged by cutting/abrasion, the interconnectivity of the micro-pores allows the lubricating liquid trapped in the micro-pores surrounding the damaged area to flow freely to the damaged area and re-infuse the physical voids, thereby self-repairing the damaged SLIPS. This process can be spontaneously driven by surface-energy-induced capillary action, without any external force. Therefore, if the micro-pores of the SLIPS are interconnected, the SLIPS will have self-repairing function.

Recently, Manna and Lynn fabricated slippery surface coatings by a layer-by-layer (LBL) assembly method and oil infusion.[210] Sample substrates (*e.g.*, glass, aluminum foil, wire meshes, filter paper, and so on) were firstly immersed in an acetone solution of branched poly(ethyleneimine) (PEI) (0.02 M) for 20 s. Then, the samples were taken out and dipped into two pure acetone baths for 20 s in turn. The substrates were further immersed in an acetone solution of poly(vinyl-4,4-dimethyl-azlactone) (PVDMA) (0.02 M) for 20 s. Next, the samples were rinsed again by using two pure acetone baths. The abovementioned process was repeated for many cycles to form porous PEI/PVDMA polymer multilayers. Finally, the obtained nanoporous PEI/PVDMA coatings were functionalized by the reaction between surface azlactone groups and *n*-decylamine to graft hydrophobic groups onto the coating surfaces. After the infusion of oil (*e.g.*, silicon oil) into the nanopores of the coatings, the resultant SLIPS exhibited strong liquid-repellent ability, due to the formation of liquid/liquid interfaces. A variety of chemically complex liquids, such as acidic/alkaline solutions, serum (in cell culture medium), lake water, and ketchup, could easily slide down when the substrate was slightly inclined. Even when the sample was immersed in seawater for 2 months or severely abraded by sandpaper, the slippery property was still maintained. In addition, the authors modified some regions of the original porous PEI/PVDMA multilayers with hydrophobic groups and other regions with hydrophilic groups to obtain a "sticky" patterned oil-infused SLIPS. The sticky regions did not lock silicon oil in the nanopores; thus, these regions could hinder or even stop the sliding of aqueous droplets. The patterned oil-infused SLIPS was successfully applied in extracting small liquid samples from contacting media and guiding the direction of the sliding droplets.

Endoscopes are widely used in medical examination or operations with many advantages, such as reducing the size of the required incision, shortening the surgery time, relieving patients' pain, and accelerating quick post-surgery recovery. However, current endoscopes are easily contaminated by blood and other body fluids during the operation, resulting in an obstructed vision. Nishioka *et al.* developed a facile method to prepare fluorine-free SLIPS by the self-assembly of methyl group modified silica nanoparticles.[211] Plant oil was locked into the microstructures as the lubricant because of its edible

and eco-friendly properties. The aggregation of the self-assembled hydrophobic silica nanoparticles generated a micro/nanoscale binary rough structure, which could firmly trap the lubricant even under flowing water. The plant oil SLIPS repelled not only aqueous liquids with differing pH, but also biological fluids such as blood. More specially, the as-prepared SLIPS also showed high transmittance. In addition, it was found that the SLIPS had an anti-coagulation effect. When a bare endoscope was used to observe the abdominal cavity of a mouse, the vision was easily blurred, especially around blood vessels. In contrast, when a SLIPS coated endoscope lens was applied to inspect the internal organs of a mouse, the visibility through the endoscope was very clear all the time. The comparison result was still valid for observing the inner side of the mouse stomach. The SLIPS film did not weaken the visibility after covering the endoscope lens, but it could prevent blood and other body fluids from adhering to the lens surface.

3.5 Controllable oil-adhesion

Controllable liquid adhesion endows the target surfaces with many important applications, such as microdroplet manipulation, microfluidic chips, and cell engineering.[51–53,55,80,91,112,124,150,176,214,215] Superhydrophobic surfaces showing controllable adhesion have been widely achieved by various methods.[54,99,112,155,177,179,216–220] For example, Li *et al.* fabricated distinguishing textured superhydrophobic CuO surfaces through the solution-immersion method.[177] The fluoroalkylsilane modified surfaces with different topographies exhibited different water adhesion that ranged from low to very high. Our group used the femtosecond laser selective ablation method to build superhydrophobic patterned PDMS surfaces composed of both an ultralow adhesive superhydrophobic domain and an ultrahigh adhesive weak hydrophobic domain.[53] The water adhesion could be easily controlled *via* changing the relative area fraction of laser irradiated (ultralow adhesion) and nonstructured flat (ultrahigh adhesion) domains. Around the same time, a variety of superhydrophobic surfaces with controllable water adhesion were designed using a femtosecond laser.[54,179,215,219,221] Lai *et al.* reported that the adhesion of superhydrophobic nanotube-array surfaces to a certain water droplet could be controlled by the length and diameter of the nanotubes,[216] which resulted from the strength change of the "micro-airbag effect".[221]

Compared to superhydrophobic substrates with different water adhesion, the superoleophobic surfaces showing controllable adhesion to oil droplets are much more practical because both water and oil cannot wet the surfaces;[89,124] however, so far, controllable oil-adhesive surfaces are still rarely reported. Yao *et al.* achieved controllable oil-adhesion on superoleophobic $Cu(OH)_2$ surfaces by changing the surface morphology.[89] A ribbed nanoneedle array $Cu(OH)_2$ surface was first obtained by immersing copper foil into ammonia solution (0.03 M) for 36–48 h (Fig. 9a). Then, the rough $Cu(OH)_2$ foils were dipped into the 0.01 M ethanol solution of 1*H*,1*H*,2*H*,2*H*-perfluorodecanethiol ($C_2H_4C_8F_{17}$–SH) for different times (Fig. 9b–d). The latter process not only reduced the surface free energy, but also changed the microstructures of the obtained rough

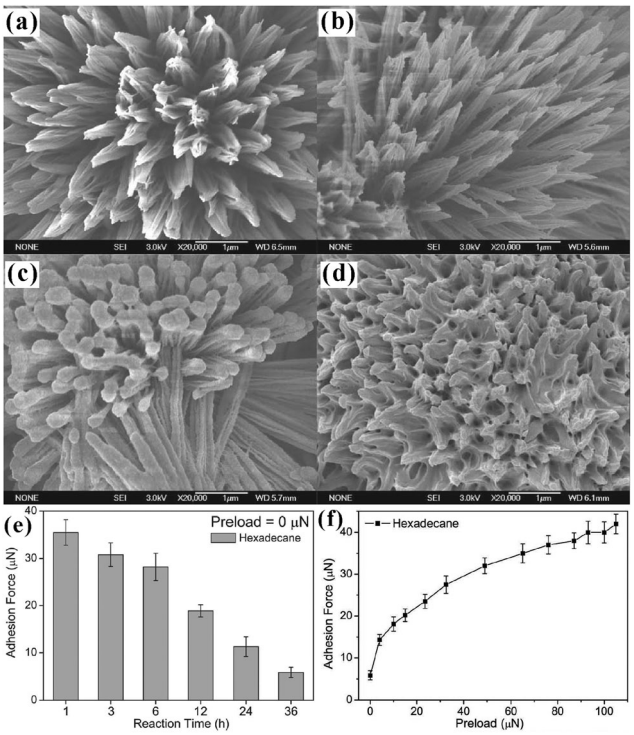

Fig. 9 Variation of the oil-adhesion of the superoleophobic $Cu(OH)_2$ nanoneedle structured surfaces with the reaction time (in $C_2H_4C_8F_{17}$–SH solution) and the applied preload force. (a) SEM image of the obtained $Cu(OH)_2$ nanoneedle structured surface at first. (b–d) SEM images of the resultant rough substrates with different reaction durations: (b) 12 h, (c) 24 h, and (d) 36 h. (e) Relationship between the oil-adhesive force and the reaction time on the resultant surfaces. (f) Oil-adhesive force for the superoleophobic surface (reaction time = 36 h) under different applied preloads. Reproduced from ref. 89 with permission from Wiley, copyright 2011.

$Cu(OH)_2$ surfaces. With increasing the reaction duration from 1 h to 36 h, the nanoneedles became shorter and denser (Fig. 9b–d). The OCA values against an oil (*n*-hexadecane) droplet were maintained above 150° for different immersing times, revealing superoleophobicity, while the adhesive force between the resultant surface and oil droplet changed from ~36 μN to 5.9 μN (Fig. 9e). The controllable oil-adhesion mainly resulted from the evolution of surface microstructures. A substrate with shorter and denser nanoneedle array had a smaller contact area with oil droplets, and thus had smaller oil-adhesion. In addition, the authors further found that the oil-adhesion also depended on the hydrostatic pressure (Fig. 9f). Using the original ultralow adhesive superoleophobic surface (reaction time = 36 h) as a study subject, the oil-adhesive force gradually increased from 5.9 μN to 42 μN as the preload force increased from 0 μN to 105 μN. The external hydrostatic pressure made the oil droplet partly penetrate into the space of rough microstructures of the resultant surface, leading to a penetrating Cassie state (transition wetting state). With the preload force increasing, the solid–oil contact area increased; thus, the oil-adhesion was greatly enhanced. Based on the controllability of oil-adhesion, an oil droplet-based

microreactor was presented *via* the superoleophobic surface (see Section 6.4 for details).[89]

Yang *et al.* fabricated superoleophobic surfaces by depositing polyelectrolyte multilayer films (PMFs) and PFO anions on rough aluminum substrates.[124] An aluminum sheet was firstly immersed in an HCl solution (2.5 M) for 10 min and subsequently dipped in boiling water for 30 min. Such treatments resulted in the formation of abundant distorted nanoflakes on the aluminum surface. The rough aluminum surface initially showed superhydrophilicity and superoleophilicity. Interestingly, it switched to superhydrophobic and superoleophobic after depositing PMF layers and PFO anions. The measured CAs of various droplets, including water, rapeseed oil, glycerol and hexadecane on the resultant surface were larger than 150°. With increasing the time of the deposition process of the PMF/PFO layer (*i.e.*, increasing the number of the polyelectrolyte bilayers), they found that the adhesion of the resultant superoleophobic surfaces to various oil droplets increased from low to high; *i.e.*, the liquid droplet changed from the rolling state to the pinned state. The enhancement of oil-adhesion was mainly caused by the change in surface microstructure. With the polyelectrolyte being continually deposited on the rough aluminum substrate, the nanoflakes began to thicken and were finally buried, and the pores were gradually filled. The decrease in surface roughness caused the wetting state to turn from the Cassie state to the transition state, and therefore, the actual solid–oil contact area expanded. As a result, the liquid adhesion gradually increased. They further demonstrated that the controllable oil-adhesive superoleophobic surfaces had the function of selecting and transporting microdroplets.

3.6 Anisotropic oil-wettability

The liquid droplet on an anisotropic textured surface exhibited clearly unequal CAs and SAs in different directions, usually named anisotropic wettability.[154,156,214,222–225] This unique property has many important practical applications, such as self-cleaning, liquid pumps, microfluidics, and smart device designs.[36–39,43,84,127] Although the anisotropic wettability of a water droplet has been successfully obtained on various textured substrates in atmosphere,[32,54,226–234] there are still significant challenges for achieving anisotropic oil-wettability because the organic liquids with lower surface tension have very different wetting behavior, compared to water. Zhao *et al.* fabricated a microgroove array on Si substrate by the Bosch deep reactive ion etching process, as shown in Fig. 10a and b.[125] The height, width and center-to-center spacing of the grooves were 4 μm, 3 μm and 6 μm, respectively. There were many side-by-side nanogrooves with the width of about 300 nm on the side wall (Fig. 10b). After etching, the sample was self-assembled with a molecular layer of tridecafluoro-1,1,2,2-tetrahydrooctyltrichlorosilane through a vapor deposition process. The resultant textured surface was found to exhibit anisotropic wettability for not only water droplets but also oil droplets (Fig. 10c). The static OCA of an oil (hexadecane) droplet on the resultant microgrooves array was 113° in the parallel direction and 162° in the perpendicular direction. The maximum OCA

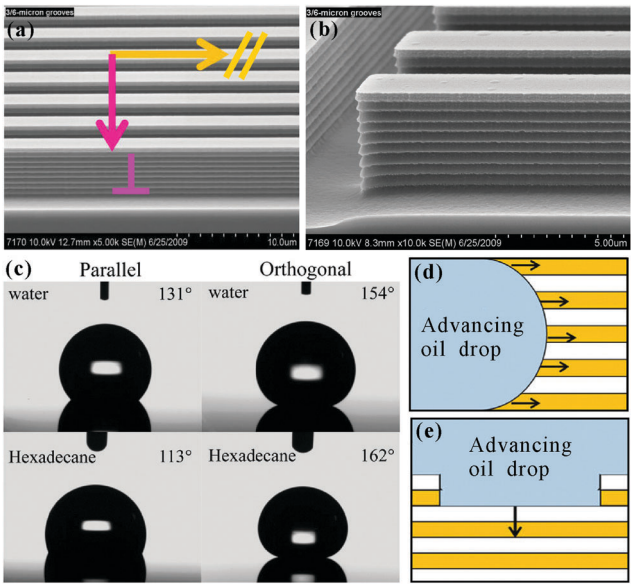

Fig. 10 Anisotropic oil-wettability of the microgroove textured Si surface. (a and b) SEM images of the microgroove array. (c) Shapes of water and oil (hexadecane) droplets on the microgroove array in the parallel direction and the perpendicular (orthogonal) direction, respectively. (d and e) Cartoon schematic of an oil droplet moving forward along the (d) parallel and (e) perpendicular directions, respectively. Reproduced from ref. 125 with permission from ACS, copyright 2012.

difference reached up to 49°, presenting obvious anisotropic oil-wetting. As for the dynamic aspect, the CA hysteresis in the parallel direction was 19°, while it increased to 66° in the perpendicular direction. The OSA was 8° in the parallel direction and 34° in the perpendicular direction. The discrepant CA hystereses and OSAs suggested that oil droplets preferred to move along the microgrooves (parallel direction).

The anisotropic wettability is the direct result of the anisotropic textured microstructures. When a liquid droplet moved forward along the parallel direction, 50% of the bottom of the droplet was in contact with the solid strips of the microgroove array and another half was held up by air, which was filled in the valley of the microgrooves (Fig. 10d). The solid strips could be wetted by oil preferentially, which reduced the energy barrier for this droplet to advance. The spread of the droplet along the strips was then enhanced. However, in the perpendicular direction, the oil droplet underwent full solid for half the time and air for half the time; that is, the oil droplet "jumped" from one strip to next one (Fig. 10e). The TPCL was generally pinned at the re-entrant microstructures in the sidewall of the microgrooves. With the oil moving forward, the TPCL should first be unpinned from the re-entrant microstructures. The unpinning process of the "stepped" TPCL caused high surface friction;[235,236] therefore, the droplet mobility in the perpendicular direction was quite difficult.

3.7 Transparency

Transparency is very important for superoleophobic materials being applied as oil-repellent optical devices, such as goggles,

self-cleaning solar panels, touch screens, difficult-to-access windows, and so on.[117,120,121,128,237,238] However, most reported superoleophobic substrates are opaque, since the required rough micro/nanoscale structures for achieving superoleophobicity usually lead to strong light scattering. How to create transparent superoleophobic interfaces has always been a great challenge. In theory, the size of the rough microstructures should be smaller than the visible wavelengths to be optically transparent.[239–247] Thus, all the length scales of microstructures for achieving transparent superoleophobicity must be less than 300 nm.

Deng *et al.* presented a simple method to obtain transparent superamphiphobic coatings based on candle soot and shell deposition technology.[117] A glass slide, as the substrate, was firstly suspended above the flame of a candle (Fig. 11a). The glass slide quickly turned black because a layer of soot was deposited on the glass surface. The soot layer was composed of abundant nanoscale spherical carbon beads. The diameter of the carbon particles was about 35 ± 5 nm. The particles chained together, forming a loose, fractal-like network. Although the soot network was rough enough to achieve superhydrophobicity, it was easily washed off due to the physical and weak particle–particle interaction. Next, the carbon network was switched to the more stable silica shell microstructure by using the soot layer as a template. The soot-coated substrates, a beaker of tetraethoxysilane (TES) and a beaker of ammonia were put in a desiccator together. After 24 hours, a silica shell with thickness of 20 ± 5 nm was coated on every soot particle through the CVD of TES under the catalyst of ammonia (Fig. 11b). The obtained compound carbon@silica network was further calcined at 600 °C for 2 hours to combust and remove the soot particles, leaving only the hollow silica shells on the substrate (Fig. 11c and d). After modifying the coating with low-surface-energy semifluorinated silane, both superhydrophobicity and superoleophobicity were obtained on the resultant surface (inset of Fig. 11e). Water droplets showed a

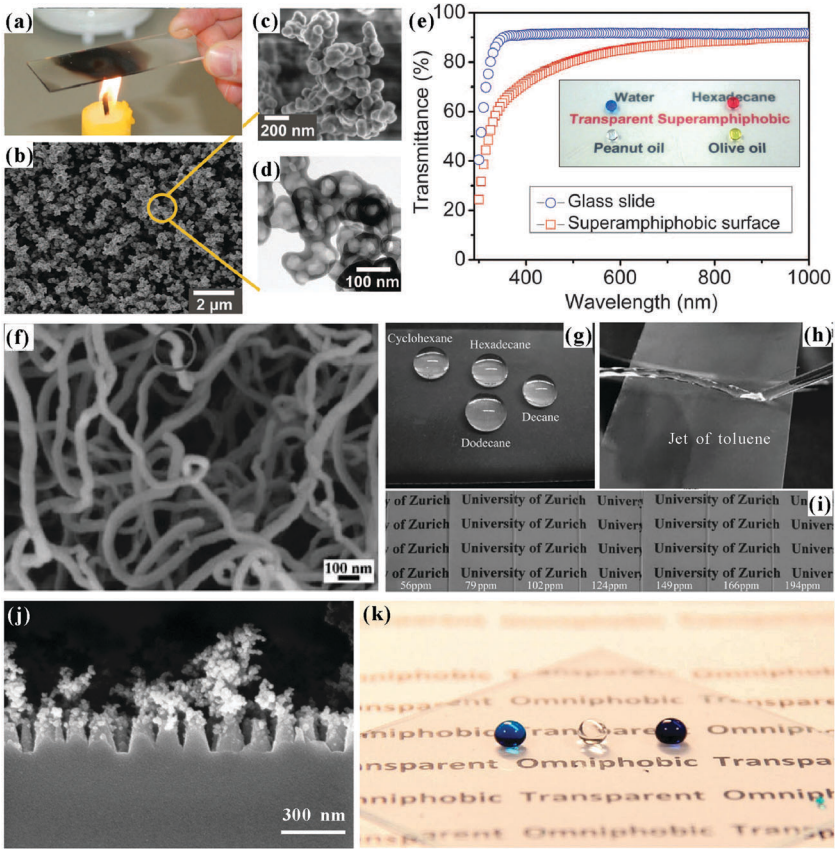

Fig. 11 Transparent, superoleophobic surfaces in the atmosphere. (a) A glass slide is held above the flame of a candle to deposit a soot layer, which is composed of abundant nanoscale spherical carbon beads. (b) SEM image of the silica shell coated nanoscale soot particles. (c) High-resolution SEM image of the hollow silica shells after removing the carbon cores (soot particles). (d) TEM image of a cluster of hollow silica shells. (e) UV-visible transmittance spectra of the as-prepared surface and its original glass substrate. The inset shows the photo of a water droplet and three oil droplets on the coated glass slide. (f) SEM image of the TCMS/PFDTS-coated silicone nanofilaments. (g) Droplets of cyclohexane, hexadecane, dodecane and decane on the TCMS/PFDTS-coated surface. (h) Jet flow of toluene bouncing off the TCMS/PFDTS-coated glass slide. (i) Good transparency of a series of TCMS/PFDTS-coated glass slides. (j) Side-view SEM image of the rough glass surface with hierarchical nanostructures (nanopillars@nanobranching). (k) Photo of three liquid droplets (from left to right: oleic acid, water, and hexadecane) on the nanopillars@nanobranching structured glass slide. (a–e) Reproduced from ref. 117 with permission from AAAS, copyright 2012. (f–i) Reproduced from ref. 120 with permission from Wiley, copyright 2011. (j and k) Reproduced from ref. 128 with permission from ACS, copyright 2014.

WCA of 165° and a WSA of about 1° on such a surface. When various organic droplets were placed on the surface, the range of the measured OCA values was from 154° (tetradecane) to 162° (diiodomethane). All the oil droplets could easily roll off as soon as the sample was slightly tilted. The measured maximal OSA was 5° for tetradecane droplet (γ = 26 mN m^{-1}). The silica network coating was also highly transparent, besides being superamphiphobic. After removing the soot core by calcination, the rest of the silica network became transparent because the shell thickness was significantly smaller than the wavelength of visible light. Taking the 3 μm-thick coating as an example, the UV-visible spectra revealed that the transmittance decreased less than 10% above 500 nm, compared with the flat bare glass slide (Fig. 11e). The letters on a white paper behind the coated glass slide were very clear (inset of Fig. 11e), revealing excellent optical transparency. Similar to, but beyond Deng's work,[117] Wong *et al.* recently reported a flame spray pyrolysis method to enable the rapid, omnidirectional synthesis of flexible and transparent superamphiphobic microstructures, as shown in Fig. 6d and e.[193] The candle was replaced by combustible liquid solutions containing hexamethyldisiloxane. Such a superamphiphobic surface with the deposition time of 15 s could exhibit up to 99.97% transparency.

Zhang *et al.* fabricated a transparent superoleophobic coating by a simple grow-form approach and subsequent chemical modification.[120] Trichloromethylsilane (TCMS) was firstly injected into toluene containing a very small amount of water (56–194 ppm). The hydrolysis of TCMS occurred due to the presence of water. Then, the dispersive TCMS quickly self-assembled into a crosslinked silicone nanofilament coating on the substrate surface (Fig. 11f). The diameters of the nanofilaments were in the range of 50–90 nm and the length reached up to several micrometers. The TCMS coating was further activated by O_2 plasma irradiation and then modified with 1*H*,1*H*,2*H*,2*H*-perfluorodecyltrichlorosilane (PFDTS). The nanofilament skeleton remained intact during plasma irradiation and chemical modification. The water concentration in toluene during the hydrolysis and condensation of TCMS had a significant effect on the surface topography, oil wettability and transparency of the nanofilament coating. The TCMS/PFDTS-coated glass slides showed superoleophobicity and ultralow oil-adhesion when the water concentration ranged from 102 ppm to 194 ppm (Fig. 11g and h). The OCAs remained larger than 150° and OSAs remained smaller than 3° for an oil (hexadecane) droplet on various resultant surfaces. The oil droplet on the sample surfaces was in the Cassie state, because such a rough nanofilament network trapped much air beneath the oil droplet. In addition, the resultant superoleophobic coating showed an antireflective function for various transparent substrates in air (Fig. 11i). The nanofilaments TCMS coating could even improve the transmittance of the glass sheet to about 94% at the wavelength of 600 nm, while that of bare glass slide was only 91.2%. Although the transmittance had a small decrease after PFDTS modification, it retained above 82% for the resultant samples with the nanofilaments growing at water concentration $<$124 ppm. The letters on a paper behind the superamphiphobic glass slides could be clearly identified. The main reason for exhibiting good transparency is that light scattering was effectively decreased by the uniform growth of the nanofilaments.

Mazumder *et al.* prepared a superamphiphobic surface made of two-level nanostructures (Fig. 11j).[128] An ultrathin layer of metal was firstly deposited on a glass surface. After the subsequent thermal annealing process, the metal film was split to disrupt nanoparticles. Next, a nanopillar structure with height of ~200 nm and diameter of ~100 nm was formed on the glass surface by ion etching, using the metal nanoparticles as a mask. The primary nanopillars were further covered with a layer of secondary branching nanostructures with length scale of 10–30 nm through the nanospray CVD method (Fig. 11j). All the samples were finally modified with fluorosilane. Water, oleic acid, and hexadecane droplets showed CAs of 113° ± 3°, 78° ± 2°, and 67 ± 2°, respectively, on the flat glass surface. Those values increased to 172° ± 4°, 163° ± 3°, and 153° ± 2° on the as-prepared rough substrate, meeting the criteria for superhydrophobicity and superoleophobicity (Fig. 11k). In addition, the surface revealed increased transmission (~93.8% for visible light) and significantly reduced reflection (<0.5%), compared to the intrinsic bare glass (Fig. 11k).

It was reported that most natural and artificial superhydrophobic surfaces are vulnerable to losing their superhydrophobicity for hot water droplets.[238,248] For example, the WCA of a hot water droplet (55 °C) on lotus leaves declined significantly to 40°, compared to 152° for a cool droplet (~25 °C).[248] This could be because (a) the condensation of water vapor between the superhydrophobic microstructures and the hot droplet increases the contact surface between liquid and solid materials; (b) the surface tension of water decreases with increasing temperature. Likewise, most of superoleophobic surfaces are also difficult to repel hot organic liquids. Recently, Li *et al.* generated a uniform silica nanotube coating on glass surfaces and obtained semitransparent superoleophobicity for hot oil droplets.[238] The dispersion of PDMS-modified multiwalled carbon nanotubes (MWCNTs) was spray-coated onto a glass slide and then the MWCNT templates were removed by calcinations, leaving a layer of silica nanotube networks covering the glass surface. After lowering the surface energy with 1*H*,1*H*,2*H*,2*H*-perfluorodecyltrichlorosilane, the resultant coatings showed superoleophobicity to various oils (*e.g.*, *n*-decane, *n*-hexadecane, toluene, *etc.*) and good transparency. Moreover, the transparent coatings still retained superoleophobicity at 75 °C.

3.8 Durability and self-healing

Most superhydrophobic or superoleophobic surfaces have poor durability so that their super-liquid-repellent ability is easily lost after physical rubbing, strong acid/alkali corrosion, strong light irradiation, oxidation in air, and so on.[60,215,249–253] The poor durability greatly limits the application areas of those superhydrophobic or superoleophobic materials. Hence, improving the durability of superoleophobic surfaces is critical to their practical applications.[117,120,128,206,238,254,255]

Chen *et al.* fabricated a kind of superamphiphobic Cu powder through a deposition method and subsequent chemical modification.[130] The Al plate was firstly immersed in the 1 mol L^{-1} $CuCl_2$ solution for 30 s, resulting in a thin Cu layer covering on the Al substrate, due to the chemical substitution reaction. The Cu-coated Al plate was washed with water to remove residual salts, and then the deposited Cu powder was peeled off by ultrasonic cleaning and collected. The separated Cu powder was further modified with perfluorooctanoic acid ($CF_3(CF_2)_6COOH$) to reduce the surface energy. The powder particles had three typical microstructures: block, dendritic, and coralline-shaped structures with size ranging from several hundred nanometers to several tens of microns. The obtained powder showed both superhydrophobicity and superoleophobicity. The powder could be coated on various kinds of substrates (such as hard Al and glass slide, soft sponge, scouring pad, filter paper and rubber) using low-cost double sided tape or spray adhesives, making those materials superamphiphobic. The superamphiphobicity had no obvious decline even though the coated substrates suffered from immersion in water/acidic/alkaline/saline solutions, falling sand abrasion, UV irradiation, or 50 cycles of stretch-release (rubber substrate), respectively.

Lin *et al.* developed a simple method to obtain durable and self-healing superamphiphobic fabrics.[121] The fluorinated-decyl POSS (FD-POSS, left in Fig. 12a) was firstly dissolved in FAS (right in Fig. 12a) (wt% : wt% = 1 : 5). The viscous solution was further dissolved in ethanol. After ultrasonic treatment for 30 min, they obtained a homogeneous suspension that could be easily coated on a variety of fabrics by coating techniques (*e.g.*, spraying or dip-coating), as show in Fig. 12b and c. The CAs of water, hexadecane, and tetradecane droplets on the FD-POSS/FAS coated fabrics were 171°, 155°, and 152°, respectively, showing both superhydrophobicity and superoleophobicity (Fig. 12d). When the coated fabric was irradiated by plasma to cause artificial damage, its wettability would switch from superamphiphobicity to both superhydrophilicity and superoleophilicity (Fig. 12e). Both water, hexadecane and tetradecane droplets presented CAs of 0° on the sample surface. Fortunately, the original super-liquid-repellency could recover after heating the plasma-irradiated fabrics at 135 °C for 3 min (Fig. 12f). The resultant fabrics could maintain the superoleophobicity even after 40 cycles of alternate plasma irradiation and heating, and maintain the superhydrophobicity for 100 cycles, demonstrating strong self-healing ability. Likewise, the superamphiphobicity would be lost if the coated fabrics were etched by strong alkali (*e.g.*, KOH solution with pH = 14) and would be re-obtained by heat treatment. On the other hand, the FD-POSS/FAS coated fabrics presented no obvious change in WCAs and OCAs (hexadecane) after being damaged through (a) immersion in H_2SO_4 solution (pH = 1) for 24 h, (b) UV irradiation for 24 h, (c) 200 cycles of standard machine laundry, and (d) 6000 cycles of abrasion damage at the pressure of 12 kPa, respectively. The result revealed that the coating was durable enough to resist most of damage; even though some treatments (*i.e.*, plasma irradiation and strong base corrosion) turned the wettability of the coated fabric into hydrophilic/oleophilic, the

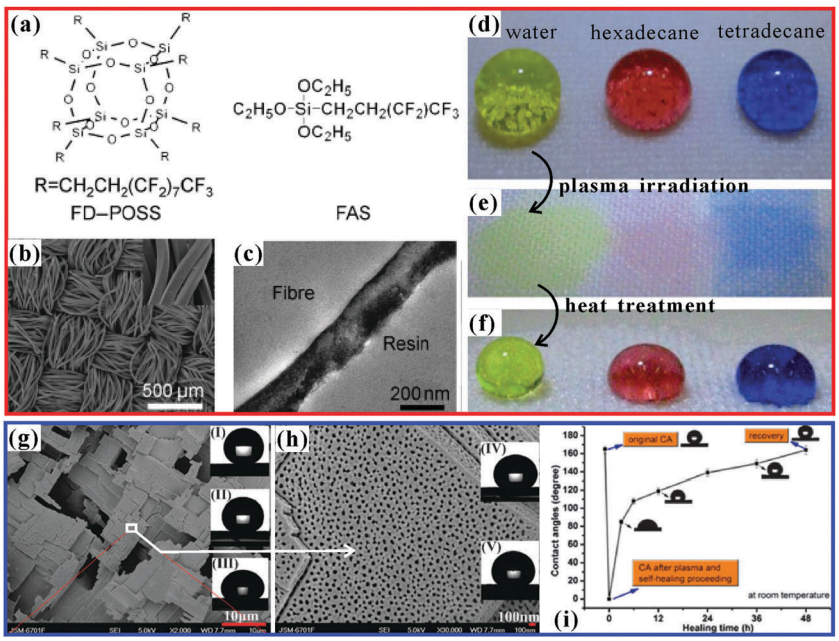

Fig. 12 Durable and self-healing superoleophobic surfaces. (a) Molecular structure of the used FD-POSS and FAS. (b) SEM image of the FD-POSS/FAS coated polyester fabric. (c) Cross-sectional TEM image of the coating layer. (d) Water, hexadecane, and tetradecane droplets on the resultant fabric. (e) Liquid droplets wetting the plasma irradiated FD-POSS/FAS coated fabric. (f) Liquid droplets on the damaged FD-POSS/FAS coated fabric after 100 cycles of alternate plasma irradiation and heating. (g and h) SEM images of the anodized alumina after double anodizations. The insets depict the shapes of water, glycerol, CH_2I_2, hexadecane, and rapeseed oil droplets (from I to V) on the fluorinated anodized alumina surface. (i) Variation of the contact angle of a water droplet on the plasma-damaged surface with the healing time at room temperature. (a–f) Reproduced from ref. 121 with permission from Wiley, copyright 2011. (g–i) Reproduced from ref. 132 with permission from RSC, copyright 2011.

damaged fabric could self-heal and re-obtain both superhydrophobicity and superoleophobicity by heating. During the process of damaging the surface composition, polar groups that usually had a high surface free energy were normally introduced. As a result, the surface hydrophobicity/oleophobicity declined. In contrast, heat treatment could enhance the mobility of the FD-POSS molecule. With the molecules rotating and moving, the damage-introduced polar groups are more inclined to be hidden inside the coating layer; meanwhile, the low-surface-energy fluorinated alkyl chain is still exposed to the outside. Therefore, the heat treatment could self-heal the damaged surface chemistry and re-endow the FD-POSS/FAS coated fabrics with superamphiphobicity.

From the same research group mentioned above, Lin *et al.* further found a new coating system that could endow the coated fabrics with robust, self-healing superamphiphobicity through a double dip-coating process.[131] The coating was made up of modified silica nanoparticles, poly(vinylidene fluoride-*co*-hexafluoropropylene), and 1*H*,1*H*,2*H*,2*H*-perfluorodecyltriethoxysilane ($C_{16}H_{19}F_{17}O_3Si$). The coated fabrics maintained their superhydrophobicity and superoleophobicity even after respectively suffering from 600 cycles of standard laundry, 8000 cycles of abrasion, strong acid/base corrosion, storing under ozone environment, and boiling treatment. Although the coated fabrics became hydrophilic and oleophilic after plasma irradiation, they re-obtained excellent liquid repellence just by being heated for a few minutes or being stored at room temperature. Based on the same design principle, this research group also developed several other self-healing superamphiphobic coatings.[256–258]

Li *et al.* fabricated robust superamphiphobic coatings by combining palygorskite (PAL), tetraethoxysilane (TEOS) and 1*H*,1*H*,2*H*,2*H*-perfluorodecyltriethoxysilane (PFDTES).[254] First, PFDTES and TEOS were dissolved in an ethanol–water solution containing abundant nanoscale rod-like PAL. The PFDTES and TEOS were gradually deposited onto the PAL surface, catalyzed by ammonia, forming a fluorinated polysiloxane (POS) modified PAL microstructure (PAL@fluoroPOS) through a hydrolytic co-condensation process. Next, the PAL@fluoroPOS was mixed with PFDTES, and the obtained homogeneous suspensions were spray-coated onto various substrates, forming a superamphiphobic PAL@fluoroPOS/PFDTES coating. The resultant surfaces super-repelled not only cool liquids, but also hot liquids. Furthermore, the superamphiphobic coatings had high mechanical and chemical stability. The only method that resulted in the degeneration of liquid-repellence was plasma treatment, but the damaged coatings could spontaneously repair themselves under a room temperature environment for 24 h and become superamphiphobic again, showing great self-healing ability. The mechanism of self-healing is analogous to Lin's work.[121]

The self-healing ability of the aforementioned superoleophobic coatings are based on the fluorine migrating from the inside to the outside of the coatings. In addition to such polymer coatings, nanoscale porous structures are also conducive to making the superoleophobic materials have self-healing functions. Wang *et al.* prepared anodized alumina with micro/nanoscale hierarchical morphology by double anodizations.[132] The first anodization endowed the alumina plate with microscale blocks (Fig. 12g), and dense nanopores were further formed on the top surface of the micro-blocks by the second anodization (Fig. 12h). Finally, the perfluorooctyl acid with low surface energy was filled into the nanopores, assisting with a vacuum pump. The fluorinated, rough, anodized alumina showed superamphiphobicity with the CAs of 165° (water), 162° (glycerol), 150° (CH_2I_2), 155° (rapeseed oil), and 153° (hexadecane), as shown in the insets of Fig. 12g and h. If the sample was irradiated by O_2 plasma for 10 s, it would switch to superamphiphilic; *i.e.*, both water droplet and oil droplet would spontaneously wet and spread on the treated surface. This result was caused by the damage of the perfluorooctyl acid on the top surface. However, the WCA and OCA of the plasma treated surface increased to above 160° and above 150° again, respectively, just after being placed at room temperature for two days (Fig. 12i). The self-healing mechanism is similar to Lin's work, but is slightly different.[121] Although the low-surface-energy composition (*i.e.*, fluorine) on the top surface was removed by plasma treatment, new perfluorooctyl acid would migrate to the top surface at room temperature, which was thermodynamically derived by minimizing the surface tension. The new introduced fluorinated alkyl chains were not from the inner material but from the nanopores, which looked like the nanoreservoirs of perfluorooctyl acid. The underlying perfluorooctyl acid inside the nanopores was not damaged by short time exposure to O_2 plasma. As more and more low-surface-energy fluoride-chains gradually moved to the top, the superamphiphobicity of the resultant sample was finally restored. The abundant nanopores on the anodized alumina substrate were indispensable to endowing the superamphiphobic surface with self-healing ability. For the anodized alumina with only microscale roughness (no nanopores in this case), which was fabricated by just first anodization and perfluorooctyl acid infusion, its superhydrophobicity was not able to recover after plasma irradiation. The better microstructures for achieving self-healing are the microvascular networks that connect the outside surface.

4. Underwater superoleophobicity

Fabricating a superoleophobic surface is harder than the fabrication of a superhydrophobic surface, mainly because the surface tensions of oils are much lower, compared to that of water.[12,13,72,102,112,117,186] To produce a superoleophobic surface in air, sufficient rough hierarchical micro/nano-structure and re-entrant surface curvature are needed, in addition to the further lowering of the surface free energy by rigorous chemical modification.[3,12,72,73,102–108] Recently, inspired by fish scales, an alternative approach to achieving superoleophobicity in an aqueous environment was proposed by Jiang's group.[76] It is well-known that fish can swim freely in oil-polluted water without their scales being soiled because of the underwater superoleophobicity of the scales. Such a unique characteristic of fish scales is ascribed to the synergy between the hydrophilic chemical composition and the hierarchical rough surface

topography. It has been proved that a surface exhibiting superhydrophilicity in air generally shows superoleophobicity once immersed in water.[76,79,94,113,114,129,136,144]

4.1 From superhydrophilicity to underwater superoleophobicity

Inspired by fish scales and followed the design principle of "from superhydrophilicity to underwater superoleophobicity", many microfabrication methods have been used to build hierarchical rough microstructures on intrinsic hydrophilic materials to obtain superhydrophilicity in air and then to achieve underwater superoleophobicity; these include laser ablation,[7,78,90,94,95,126,129,136] chemical etching,[76,77,99,111,113,141,259] electrochemical deposition,[80,135,144,145,260,261] self-assembly,[91,112,262] spray/dip coating,[133,134,263–265] the template method,[76,127,170] lithography,[76,79,111] electrochemical anodization[266] and the hydrothermal method.[137]

Jiang *et al.* obtained a hydrogel replica of fish scales by a double template replication process.[76] The reason for using the hydrogel was that this material is hydrophilic and can retain water molecules. In water, the hydrogel film with fish-scale structures exhibited superoleophobicity, with an OCA of 162.6° ± 1.8°. They further designed three different samples on silicon substrates: smooth silicon surface, microstructured silicon surface, and micro/nanoscale hierarchical rough silicon surface.[76] All three samples showed hydrophilicity in an air environment. The microstructured surface and the micro/nanoscale hierarchical rough surface were even superhydrophilic with WCAs being less than 5°. In air, oil droplets such as 1,2-dichloroethane easily spread out on all kinds of silicon surfaces, which demonstrated the superoleophilicity of these samples. However, when the samples were immersed in water, the smooth silicon surface switched to oleophobic with an OCA of 134.8° ± 1.6°, and the microstructured surface and the micro/nanoscale hierarchical rough surface exhibited superoleophobicity with OCAs of 151.5° ± 1.8° and 174.8° ± 2.3°, respectively. Unlike the underwater oleophobicity or even superoleophobicity, these artificial surfaces exhibited significantly different adhesive behaviors. The adhesive force of the smooth surface on an underwater oil droplet was greater than 24.7 ± 1.7 μN. For the microstructured silicon surface, the measured oil-adhesive force was about 10.2 ± 2.4 μN underwater. Interestingly, the adhesive force of the micro/nanoscale hierarchical rough surface was smaller than 1 μN so that the oil droplet could retain its spherical shape without any volume loss during the whole process of being in contact with and leaving the sample surface.

Wang *et al.* fabricated an inorganic copper oxide coating with underwater low oil-adhesive superoleophobicity.[77] A copper sheet was immersed in aqueous ammonia (pH = 10.5) for about 24 h at room temperature until its color changed from bright yellow to black, resulting in a layer of rough CuO microstructure covering the substrate. As a result, there were many microscale cauliflower-like clusters with the size of 1–10 μm forming on the copper sheet. The clusters were decorated with abundant nano-branches (about 100 nm). The resultant rough surface showed superhydrophilicity in air with a WCA of 1.6° ± 0.8°. After immersing in water, the sample became superoleophobic. An oil droplet on the surface (in water) looked like a sphere with OCA of 163.0° ± 4.5°, and easily rolled off when the sample was slightly tilted. The underwater superoleophobic surface also had a very low adhesive force (<1 μN) on various oil droplets.

Our group reported an efficient, one-step method to realize underwater superoleophobicity on a silicon surface by femtosecond laser ablation, as shown in Fig. 13.[94] A flat Si wafer showed intrinsic hydrophilicity in air with the WCA of 60° ± 2° (Fig. 13c) and therefore presented oleophobicity under water. The underwater oil droplet (1,2-dichloroethane) on the Si wafer had an almost half-sphere shape with the OCA of 124.6° ± 1° (Fig. 13e). After irradiation by femtosecond laser pulses, an aligned micro-mountain array with the interval of 10 μm was formed on the Si substrate (Fig. 13a).[223,267] The rough micro-mountains had a diameter of approximately 6 μm and a height of 2.9 μm. There were abundant protrusions with the size of

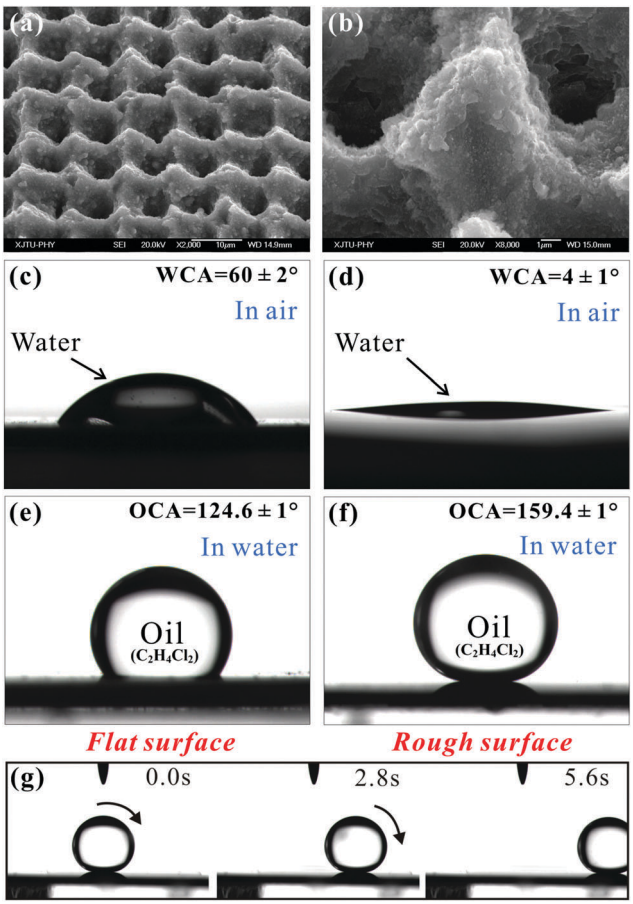

Fig. 13 Femtosecond laser ablated underwater superoleophobic Si surface. (a and b) SEM images of the rough Si surface irradiated by femtosecond laser. (c and d) Water wettability on the (c) flat and (d) laser-induced rough Si surfaces in air environment. (e and f) Oil wettability on the (e) flat and (f) laser-induced rough Si surfaces in a water environment. (g) Underwater oil droplet rolling on a femtosecond laser ablated surface with tilt angle of 0.5°. Reproduced from ref. 94 with permission from RSC, copyright 2014.

tens to a few hundreds of nanometers decorating every micro-mountain (Fig. 13b). The surface roughness was about 2.46 μm. The micro/nanoscale hierarchical structure was able to largely enhance the wettability of the silicon surface. In an air environment, the as-prepared rough surface was transformed from ordinary hydrophilic into superhydrophilic. When a 7 μL water droplet was lowered to touch the sample, the droplet spread out within one second, resulting in a very small WCA of only 4° (Fig. 13d). In contrast, when the resultant rough silicon surface was submerged in water, an underwater oil droplet on the surface could retain a spherical shape with OCA reaching up to 159.4° ± 1°, showing underwater superoleophobicity (Fig. 13f). The surface also exhibited ultralow oil-adhesion underwater, with the result that the oil droplet could easily roll down when the surface was slightly inclined at 0.5° (Fig. 13g). The superoleophobicity in water and ultralow oil-adhesion of the as-prepared surface mentioned above can be explained by the underwater version of the Cassie contact state (Fig. 3h). Once the fabricated sample was immersed in water, the valley of the hierarchical micro/nanoscale rough structures was filled by water due to the superhydrophilicity. When an underwater oil microdroplet was placed on this rough surface, there existed a layer of water trapped in the hierarchical microstructures. The trapped water cushion was just between the oil microdroplet and the surface, preventing oil from penetrating into the rough microstructures because water naturally repels oil. In fact, the underwater oil droplet only touched the peaks of the micro-mountain array structures, resulting in a greatly reduced contact area between the underwater oil droplet and the rough substrate. The trapped water endowed the femtosecond laser ablated silicon surface with underwater superoleophobicity, and the small contact area further caused ultralow oil-adhesion. It was tested that the hydrophilicity of the flat silicon surface in air turned into oleophobicity in water, and the oleophobicity was greatly increased to underwater superoleophobicity by femtosecond laser ablated hierarchical rough microstructures.

Inspired by fish scales, Lin *et al.* fabricated a robust underwater superoleophobic surface of hierarchical macromolecule-nanoclay hydrogels.[111] The interaction of flexible macromolecules and rigid nanoclays made the trapped water layer on the rough surface microstructures very stable, thereby endowing the as-prepared material with robust underwater superoleophobicity. Wang *et al.* used the *in situ* alternating-current deposition method to prepare flower-like conversion films composed of amorphous iron phosphate on carbon steel.[260] The hierarchical micro/nanostructured conversion films were superhydrophilic in air and superoleophobic in water. Xu *et al.* obtained an ion-induced organic/inorganic hybrid film using the typical LBL assembly method.[268] The hybrid film was superoleophobic and showed ultralow oil-adhesion even in artificial seawater. Zhang *et al.* coated sodium silicate and TiO_2 nanoparticles on the stainless steel mesh through a LBL assembly method.[269] The obtained mesh showed underwater superoleophobicity and had the function of separating water/oil mixtures. Once the separating mesh was polluted, the TiO_2 composition would break down and remove the contaminants by UV irradiation and make the contaminated mesh regain the separation ability. Ma *et al.* reported a novel strategy for realizing substrate-independent underwater superoleophobicity.[270] A catechol bearing polymer was synthesized and then coated on various substrates. Next, a nanostructure was formed on the polymer coated substrate by the LBL assembly method. The resultant surfaces exhibited stable superoleophobicity in water. In addition, sticky or rolling underwater superoleophobic surfaces could be prepared by using spin-assisted or dip-assisted LBL processes, respectively. Lai *et al.* prepared a large scale, pine-cone-like TiO_2 particle film, based on the one-step electrochemical anodizing method.[271] With the film shifting from air atmosphere to underwater, its wettability changed from superhydrophilicity and superoleophilicity to excellent superoleophobicity. Liu *et al.* fabricated underwater superoleophobic copper wires whose surfaces were covered by hierarchical copper oxide microstructures through an alkali-corrosion process.[99] Zhu *et al.* used a surface-initiated atom transfer radical polymerization process to prepare a superhydrophilic and underwater superoleophobic zwitterionic polyelectrolyte brush–poly(3-(*N*-2-methacryloxyethyl-*N*,*N*-dimethyl)ammonato-propanesultone) grafted poly(vinylidene fluoride) membrane for separating oil from water.[272]

4.2 Controllable oil-adhesion

Superoleophobic surfaces with very low oil-adhesion have strong anti-oil ability.[75,77,94,260,270] In contrast, when the oil-adhesion of a superoleophobic surface is not ultralow, but ultrahigh, that oil droplet can stick to the substrate at any tilted angle; such a surface can be used in no-loss micro-oil-droplet transportation.[78,91,144] Currently, multifunctional superoleophobic surfaces with differing oil-adhesion (from low to high) have attracted tremendous attention because these surfaces allow the manipulation of oil droplets on the target materials.[78,80,91,112]

Huang *et al.* prepared three latex particles (with spherical, cauliflower-like, and single-cavity structures) by emulsion polymerization, as shown in Fig. 14a–f.[112] The shape of the latex particles was controlled by the feeding modes of divinylbenzene into the polymerization system. They further obtained three typical films assembled with these three kinds of latex particles. All three resultant films showed superoleophobicity in water. The underwater OCAs of a silicon oil droplet were 146.5° ± 1.6°, 159.5° ± 1.3° and 160.5° ± 2.1° on the substrates assembled from spherical, cauliflower-like, and single-cavity latex particles, respectively. In addition, these films exhibited adjustable underwater oil-adhesion (Fig. 14g–i). The film with spherical latex particles had an ultrahigh adhesive force to an oil droplet (>69.6 μN) (Fig. 14g). After approaching and just contacting the sample surface, an underwater oil droplet had a large shape distortion and finally broke into two parts when it was carried off the film. The film assembled from cauliflower-like latex particles showed a moderate oil-adhesion in water (Fig. 14h). The adhesive force was 43.1 μN. For the surface covered with single-cavity latex particles, the adhesive force to an underwater oil droplet was as low as 9.8 μN (Fig. 14i). The oil

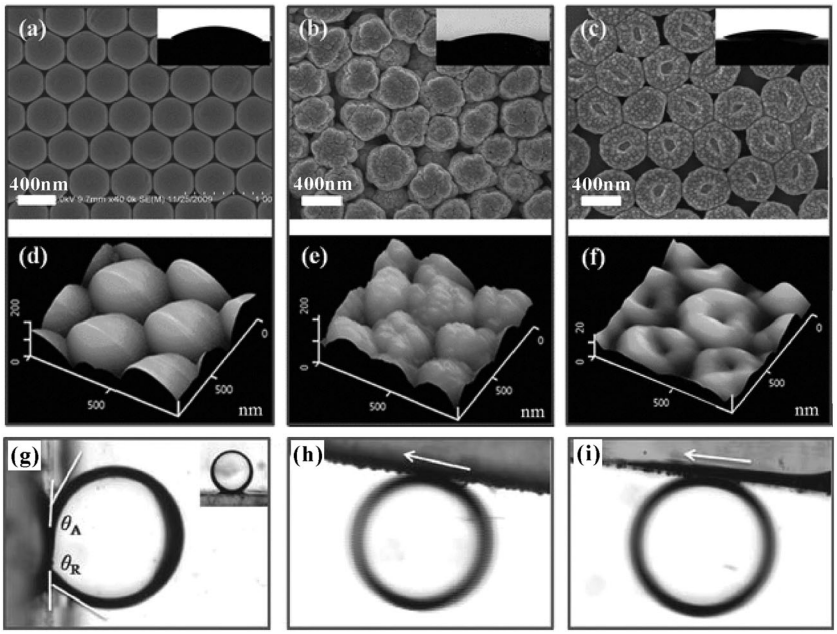

Fig. 14 (a–c) SEM and (d–f) AFM images of the films assembled with three different kinds of latex particles: (a and d) spherical, (b and e) cauliflower-like, and (c and f) single-cavity latex structures. The insets in (a–c) show the shapes of a water droplet on the corresponding films in air. (g–i) An underwater oil droplet sticking or rolling on the three films assembled from (g) spherical, (h) cauliflower-like, and (i) single-cavity latexes. Reproduced from ref. 112 with permission from Wiley, copyright 2011.

droplet hardly adhered to the resultant surface and had almost no shape deformation during the whole process of approaching, contacting, and leaving. The controllable oil-adhesion was ascribed to the continuous change in the wetting state/contact model from underwater Wenzel, to Wenzel–Cassie transitional, to the Cassie regime.

The spherical latex particles looked relatively smooth. The underwater oil droplet could wet the rough microstructures of the sample surface assembled from spherical latex particles. The large contact area between the oil droplet and the substrate formed a continuous solid/water/oil TPCL, resulting in a very high CA hysteresis and oil-adhesion.[156,218] The oil droplet stuck on the film even through the sample was vertical or turned upside-down (Fig. 14g). The oil droplet on the film was in the underwater Wenzel state. For the film with cauliflower-like latex particles, the underwater oil droplet partly penetrated the space of the irregular nanostructures. The decreased contact area between the oil droplet and the sample surface gave rise to a decrease in oil-adhesion (Fig. 14h). This contact model belonged to the underwater version of the transition state. In comparison, the underwater oil droplet could easily roll off the film covered with single-cavity latex particles, with almost no CA hysteresis (Fig. 14i). This result agreed well with the characteristics of the underwater Cassie state. A water layer was trapped in the cavity, which prevented the oil droplet from fully touching the latex particles. Consequently, the underwater oil microdroplet only contacted the protruding point of the latex cavity, decreasing the oil contact area. The discontinuous TPCL led to an ultralow oil-adhesive force.[156,218]

Zhang *et al.* fabricated different microstructured Ni/NiO surfaces showing underwater superoleophobicity by combining electro-deposition and heating techniques.[80] The surface microstructures as well as the oil-adhesion could be simply controlled by the annealing temperature. There were many micropores with diameter of 4–11 μm, with close and disorderly distribution on the Ni sample surface, which were electrodeposited for 30 s and subsequently annealed at 500 °C for 5 h. With the annealing temperature increasing to 900 °C and further to 1100 °C, the porous structure gradually degenerated, and a lot of irregular blocks and smooth microscale crystals appeared instead. The adhesive force of the resultant surface on an underwater oil droplet was tuned from ultralow to ultrahigh (1–60 μN), with the contact model regulating from the underwater Cassie state to the underwater transition state and then to the underwater Wenzel state.

Similarly, our group obtained underwater superoleophobic glass surfaces with different micro/nanoscale hierarchical rough structures, induced by femtosecond laser.[78] When the average distance (AD, which was determined by the laser scanning speed and the shift of scanning lines) of the laser-pulse-ablation points was relatively small (*e.g.*, AD = 2 μm), a self-organized micro-island array, decorated with abundant nanoscale porous structures and protrusions, was formed on the substrate surface (Fig. 15a–c). There were no typical femtosecond-laser-pulse-induced microcrater-like structures in this case, due to the strong overlap of the adjacent laser pulse irradiated areas. With AD increasing to 4 μm, the laser pulse ablated craters were partly overlapping and connected with each other, resulting in a wave-like pattern (Fig. 15d and e).

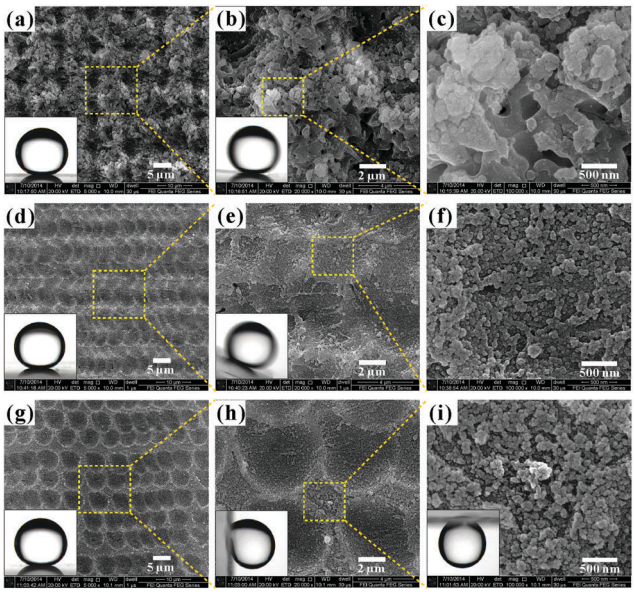

Fig. 15 Topography and underwater oil-wettability of the femtosecond laser ablated glass slide surfaces fabricated at different average distances of laser-pulse-ablation points: (a–c) AD = 2 μm, (d–f) AD = 4 μm, and (g–i) AD = 6 μm. Insets in (a, d and g) are the shapes of 8 μL underwater oil droplets on the corresponding surfaces. Insets in (b, e, h and i) reveal an underwater oil droplet rolling or being pinned on the corresponding surfaces. Reproduced from ref. 78 with permission from Springer, copyright 2015.

Apart from the micro-waves, a layer of nanoparticles with diameter of just a few tens of nanometers uniformly covered the whole surface (Fig. 15f). For the as-prepared sample with AD of 6 μm, the surface was covered by nearly complete micro-craters decorated with nanoparticles (Fig. 15g–i). All the underwater oil droplets on these surfaces presented almost spherical shapes, revealing underwater superoleophobicity (inset of Fig. 15a, d and g). The corresponding OCAs were as large as $160.5^\circ \pm 2^\circ$ (AD = 2 μm), $158^\circ \pm 2.5^\circ$ (AD = 4 μm), and $154^\circ \pm 1.5^\circ$ (AD = 6 μm), respectively. In contrast, the oil-adhesive properties of the laser ablated surfaces with different parameters varied greatly, compared to the similar underwater superoleophobicity, which could be tuned from very low to ultrahigh by increasing the parameter AD. When the AD increased from 2 μm to 4 μm and then to 6 μm, the underwater OSA increased from 3.5° (inset in Fig. 15b) to 25.5° (inset in Fig. 15e) and then to 90° (insets in Fig. 15h and i). The OSA of 90° expressed that the oil droplet was firmly pinned on the substrate, even when the substrate was vertical or turned upside down. The controllability of oil-adhesion was ascribed to the surface topography variation, which resulted in the wetting behavior changing from the underwater Cassie state to the transition state, and even to the underwater Wenzel state. The femtosecond laser induced underwater superoleophobic surfaces with ultralow oil-adhesion have strong capability for oil resistance in water, while the high oil-adhesive surfaces can be used to transfer small oil droplets, like a ''mechanical hand'' (see Section 6.4 for details).

Besides varying surface microstructures, the oil-adhesion can also be adjusted by regulating the surface chemical composition of underwater superoleophobic materials. Cheng *et al.* obtained tunable oil-adhesive superoleophobic surfaces underwater, based on a two-step sputtering and self-assembled monolayer process.[91] A layer of nanoscale copper particles was firstly covered on the glass substrate *via* a simple sputtering process. The samples were further modified with an *n*-alkanoic monolayer by immersion into the ethanol solution containing different *n*-alkanoic acids (0.001 M) for about 12 h. By simply increasing the chain length of the *n*-alkanoic acids, the adhesive force of the resultant surfaces on an underwater oil droplet increased from less than 1 μN to larger than 58 μN, revealing that the underwater oil-adhesion was controlled from low to very high.

Chen *et al.* prepared a thermal-responsive poly(*N*-isopropylacrylamide) (PNIPAAm) hydrogel whose underwater oil wettability could be reversibly switched between ultralow adhesive superoleophobicity and high adhesive oleophobicity by changing the ambient temperature.[142] Ding *et al.* synthesized an underwater superoleophobic aligned polyaniline (PANI) nanowire film through electrochemical polymerization.[144] With the applied potential changing from 0.43 V to −0.2 V or 0.8 V, the 1,2-dibromoethane droplet reversibly switched from the rolling state to the pinned state in water. Cheng *et al.* grafted the pH-responsive poly(acrylic acid) (PAA) onto a glass substrate by means of plasma polymerization.[140] The adhesive force between the resultant film and the underwater oil droplet changed from 21.6 ± 5.0 μN to zero as the pH of the surrounding water medium increased from 1 to 12. Heng *et al.* fabricated different porous films, which were made up of montmorillonite clay/PAA.[273] The underwater oil-adhesion could be controlled by the montmorillonite arrangement in the pore wall.

4.3 Underwater anisotropic oil-wettability

The anisotropic wettability can be realized not only in air, but also in water medium.[92,126,127] Recently, our group reported a kind of microgroove array structure on Si substrate through a simple line-by-line femtosecond laser serial scanning process, as shown in Fig. 16a.[126] The width and depth of the rough periodic microgrooves were about 8 μm and 5 μm, respectively. The period of the microgroove array could be adjusted by the interval of the scanning lines. Every microgroove was formed by many consecutive micro-craters, which were generated by laser pulse ablation (top inset of Fig. 16a).[222,267,274,275] There were abundant irregular particles, with size ranging from tens to several hundreds of nanometers, densely decorating the inner wall and outer rim of the microgrooves. Underwater anisotropic oil-wetting was exhibited after immersing the resultant sample in water. For the underwater microgroove array with the period of 450 μm, the OCA perpendicular to the grooves reached up to $155.5^\circ \pm 1.6^\circ$ (Fig. 16c), while the OCA parallel to the grooves was only $135.7^\circ \pm 1.5^\circ$ (Fig. 16b). The OCA difference revealed that the underwater oil microdroplet preferred to spread along the microgrooves. In addition, the anisotropic oil-wetting could be easily tuned by just changing the interval of the microgroove

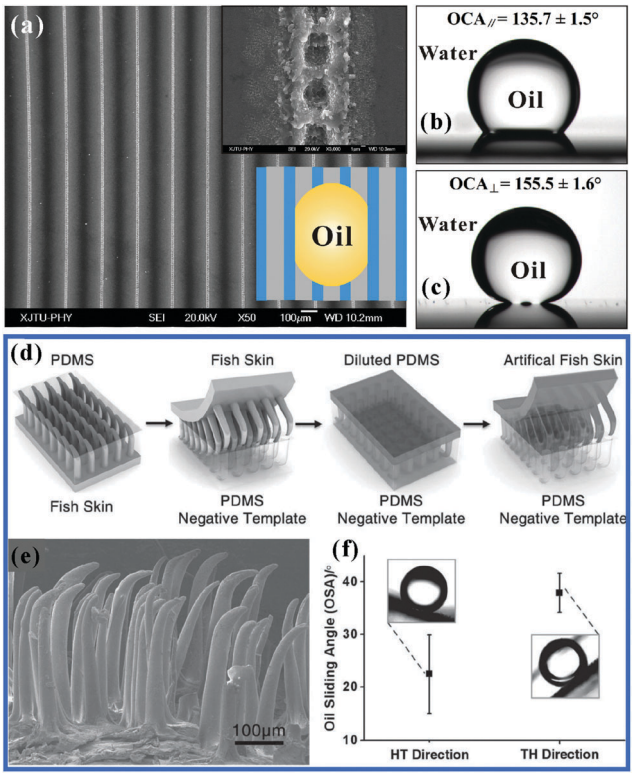

Fig. 16 Underwater anisotropic oil-wettability on a femtosecond laser induced Si microgroove array and a PDMS replica of filefish skin. (a) SEM image of the microgroove array fabricated through the line-by-line femtosecond laser scanning method. The top inset shows the SEM image of a single microgroove at high magnification. The bottom inset reveals the restricting effect of the microgroove array on an underwater oil droplet. The energy barrier at the boundary between the untreated flat domain and laser ablated microgrooves prevents the oil droplet from spreading in the perpendicular direction. (b and c) Shapes of an underwater oil droplet on the microgroove structured surface in the (b) parallel and (c) perpendicular directions, respectively. (d) Schematic diagram of obtaining a PDMS replica from filefish skin. (e) Microstructures of the PDMS replica surface. (f) Sliding behavior of an underwater oil droplet on the replica surface. (a–c) Reproduced from ref. 126 with permission from AIP, copyright 2014. (d–f) Reproduced from ref. 127 with permission from Wiley, copyright 2014.

arrays, with the degree of the wetting anisotropy being changed from 0° to ~20°. The femtosecond laser ablated rough Si surface exhibited underwater superoleophobicity and ultralow oil-adhesion because water filled in the microgrooves, thus preventing the oil droplet from effectively touching the rough microstructures.[94] The contact model of the underwater oil droplet and the laser-induced microgrooves domain could be considered as an underwater Cassie state.[76] On the contrary, the oil droplet would be fully in contact with the non-irradiated flat part, which was between two adjacent microgrooves, belonging to the underwater Young state. An energy barrier usually exists between adjacent domains with dissimilar wettabilities, according to Gibbs' criterion.[223,233] For the rough microgroove-array surfaces, the energy barrier between the flat domain and the trapped water in the laser-ablated microgrooves prevented the oil droplet from spreading in the perpendicular direction (bottom inset of Fig. 16a), while there was no energy barrier in the parallel direction. The oil was elongated along the microgrooves, so the OCAs along the parallel direction were smaller than those along the perpendicular direction, exhibiting a controllable anisotropy.

Compared to the two-dimensional anisotropic oil-wettability of the microgroove array structure, directional oil-adhesion (at the one-dimensional level) was also achieved on the asymmetric microstructures. Cai *et al.* prepared an artificial filefish surface by replicating the *N. septentrionalis* skin.[127] The cleaned filefish skin was first gradient dehydrated by ethanol solution to promote its hardness. Using the pre-treated filefish skin as the template, its PDMS replica was obtained by two rounds of replication (Fig. 16d). The obtained PDMS replica had a very similar surface microstructure to filefish skin (Fig. 16e). Hydrophilic surface composition is necessary to achieve underwater oleophobicity, but PDMS is a typical hydrophobic material with low surface energy.[53,54,71,179,221,226] To address this limitation, the artificial PDMS "fish skin" was irradiated by oxygen plasma. With the silanol group (–SiOH) forming on the PDMS surface, the artificial skin switched from hydrophobic to hydrophilic.[79,127] When the PDMS fish skin was immersed in water, it showed quasi-superoleophobicity with an OCA of 143° ± 2.1°. Like the natural filefish, the artificial PDMS fish skin also exhibited an anisotropic underwater oleophobicity. Along the direction of the oriented hook-like spines, the OSA was 22.5° ± 7.3°, but the underwater oil droplet stayed on the sample surface until the artificial skin was tilted at 37.9° ± 3.7° in the opposite direction, as shown in Fig. 16f. It was demonstrated that the oil droplet in water was more inclined to move in a certain direction. This kind of anisotropic wettability is usually called unidirectional adhesion/rolling, which was initially observed from butterfly wings.[156,226] They further achieved the unidirectional oil-adhesion on commercial cloth corduroy through unidirectional ironing and subsequent hydrophilic polymer modification. The OCA difference along two opposite directions could reach up to 20°. If an oil droplet was sandwiched between two resultant samples exhibiting unidirectional oil-adhesion in water medium, the continuous directional oil transportation would be achieved by repeating the cycles of pressing together and release.

In general, two criteria play a very important role in constructuring underwater anisotropic oleophobic surfaces: high surface energy and anisotropic microtextures. The former ensures that the rough microstructure is fully wetted by water and repels oil after immersion in water. The latter results in the anisotropic static or dynamic oil-wettability on the microtextured substrates. The underwater anisotropic oil-wetting surfaces have many potential applications, such as movement guiding of underwater organic liquids, oil collection, oil transportation, and self-cleaning coatings for marine equipment.[92,126,127,160,214]

4.4 Transparency

Transparency is very important for the application of underwater superoleophobic materials in underwater optics, such as diving goggles, oil-proof windows of underwater cameras, and even imageable substrates for biologically active cells or tissue.

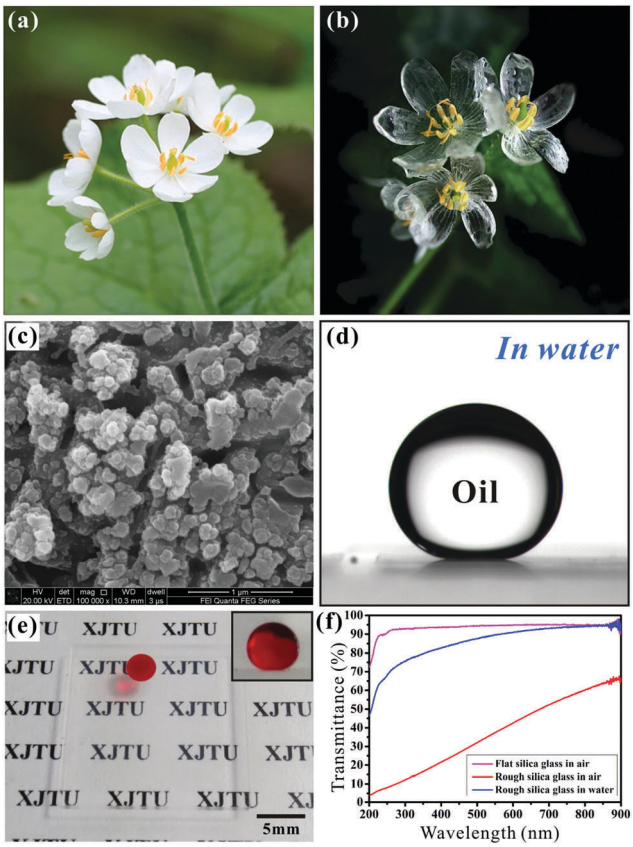

Fig. 17 Transparent underwater superoleophobic silica glass surface. (a and b) Petals of *Diphylleia grayi* (a) on a sunny day and (b) in the rain. (c) SEM image of the femtosecond laser ablated microstructure on a silica glass surface. (d) Oil droplet on the rough silica glass surface in water. (e) Underwater high transparency of the femtosecond laser ablated glass surface. (f) UV-vis spectra of different silica glass: purple line, bare flat silica glass in air; red line, rough silica glass in air; blue line, rough silica glass in water. Reproduced from ref. 129 with permission from RSC, copyright 2015.

Our group obtained a rough silica glass sheet with both underwater superoleophobicity and good transparent property through a femtosecond laser ablation process.[129] Fabrication of the underwater superoleophobic microstructure was inspired by fish scales,[76] while the achievement of transparency was inspired by *Diphylleia grayi*. As shown in Fig. 17a and b, the *Diphylleia grayi*'s petals change from white to transparent if the weather shifts from a sunny day to a rainy day; the cell structure of the petal is very loose. On a sunny day, the intercellular space is filled with air. The diffuse reflection at the interface between the colorless cytolymph and the trapped air results in a white color. Water can displace the trapped air and enter into the intercellular spaces in the rain. The transparent property is improved by the newly generated water–cytolymph (liquid–liquid) interface, so the petals become transparent. We used the femtosecond laser ablation method to form a layer of irregular nanoparticles on silica glass surface (Fig. 17c). After immersing the sample in water, superoleophobicity and very low adhesion to an oil droplet were exhibited. This oil droplet maintained a spherical shape and could easily roll on the surface (Fig. 17d). The measured OCA and OSA were $160.2^\circ \pm 1^\circ$ and 1°.

The original laser ablated surface was white and looked opaque in air. Nothing could be seen behind the glass sheet. Interestingly, it became transparent just through being shifted into water medium. The letters "XJTU" in a paper behind the resultant sample could be clearly observed, demonstrating that the rough silica glass in water had high transparency (Fig. 17e). The UV-vis spectra further indicated that the transmittance of the underwater rough glass was very close to that of the bare flat silica glass in the visible region (Fig. 17f). When a He–Ne laser beam with the wavelength of 633 nm and the power of 0.96 mW passed through the underwater sample, the transmittance reached to 91.6%. The excellent transparency resulted from the existence of the surrounding water environment. The reflectance, R_{12}, at the interface of two different media (1 and 2) can be expressed as follows:

$$R_{12} = \left(\frac{n_1 - n_2}{n_1 + n_2}\right)^2 \quad (12)$$

where n_1 and n_2 are the refractive indexes of medium-1 and medium-2, respectively. This equation reveals that the smaller the difference in the refractive indexes of both media, the smaller is the reflectance generated at the interface.[211] The laser-induced nanoscale rough structure was wetted by water with immersion of the silica glass in water. A glass-water interface was formed, replacing the glass-air interface. The Mie scattering and the reflectance were significantly weakened due to the closer refractive index of water (n = 1.33) and silica glass ($n \approx 1.46$).[117,241] Therefore, the rough superoleophobic silica glass sheet became transparent in water, like the *Diphylleia grayi*'s petals becoming transparent in the rain.

4.5 Durability

Chemical and physical durability are essential to the applications of the underwater superoleophobic surfaces in harsh environments, which will provide the surfaces with important opportunities in different kinds of industrial production and our daily life, such as industrial waste oil cleanup and cell engineering.[129,133–135]

Li *et al.* fabricated a rough mesh with robust superoleophobicity in water through spraying the mixture of palygorskite powders and polyurethane onto a copper mesh substrate.[133] Palygorskite consists of hydrated octahedral layered magnesium aluminum silicate with reactive –OH groups on the surface. It is a typical hydrophilic crystal and has great water-absorbing and water-retaining ability. Waterborne polyurethane was used to enhance the binding force between the substrates and the palygorskite powders coating. The palygorskite powder (0.3 g) was firstly pre-activated with 4 M HCl solution, and then was dispersed in 20 mL of acetone solution of waterborne polyurethane (0.05 g), forming a homogeneous suspension after magnetic stirring. The suspension was coated on a copper mesh with pore diameter of ~75 μm (200 mesh size) by a spray method and subsequently dried in air. As a result, abundant palygorskite was densely and randomly

coated on the copper mesh. The large magnification SEM image revealed that the palygorskite coating was the aggregate of a lot of single fibrils with length of several hundreds of nanometers and diameter of 100 nm. Due to the existence of many hydroxyl groups and hierarchical rough microstructures on the coating surface, the as-prepared rough mesh showed superhydrophilicity and superoleophilicity in air. After immersing in water, the coated mesh became superoleophobic. The OCAs of various oil droplets (*e.g.*, chloroform, kerosene, petroleum ether, rapeseed oil, toluene, and hexane) were greater than 150°. The palygorskite coated mesh surface also exhibited ultralow oil-adhesion in water. For example, an underwater oil droplet of chloroform could easily roll off the inclined sample surface when the tilted angle of the surface was just 8°. Furthermore, it was also found that the coated mesh also super-repelled underwater oils when the mesh was immersed in different corrosive solutions (1 M HCl, 1 M NaOH and 1 M NaCl) and hot water, showing stable underwater superoleophobicity. The advantage of chemical resistance to harsh environments endowed the underwater superoleophobic rough meshes with the ability to efficiently separate the mixtures of oil and various corrosive aqueous solutions.

Waste potato residue is made up of superhydrophilic and superoleophilic starch, cellulose and pectin. In addition, it is a very low-cost material and can easily be obtained. Li *et al.* also prepared a potato residue powder-coated metal mesh by the spraying method, which is the same as mentioned above.[134] The resultant meshes exhibited durable underwater superoleophobicity, even when the sample was immersed in a series of corrosive solutions (1 mol L^{-1} HCl, 1 mol L^{-1} NaOH, and 10 wt% NaCl). Our group found that the femtosecond laser induced rough silica glass could maintain superoleophobicity and low oil-adhesion not only in water, but also in strong acid or alkaline aqueous solutions.[129] The OCAs remained larger than 150° and the OSAs were smaller than 10° in all cases, with the pH of environmental liquids ranging from 1 to 13. Zhang *et al.* fabricated a beautiful porous structured copper mesh film by electrodeposition technology.[135] The copper mesh substrate was used as the cathode, and a Pt plate (2×2 cm^2) was the anode. The electrodeposition process was performed in an electrolyte solution of 0.1 M $CuSO_4$ and 1 M H_2SO_4 at the constant current density of 6 A cm^{-2} and lasted 5 to 15 s. After electrodeposition, there were abundant porous structures coving the copper wires. The pores were $\sim$23 μm in size and their sidewalls were decorated with massive nanoparticles. The as-prepared films were superhydrophilic in air and showed superoleophobicity and very low oil-adhesion in water. When the film was immersed in acidic, basic or salt solutions for 24 h, it was found that the underwater low-adhesive superoleophobicity was still there. The underwater superoleophobic films with excellent environmental stability are promising for use in more complex applications.

5. Smart oil-wettability

In recent years, triggered by the peculiar properties and promising functions, various ''smart'' surfaces that can respond to external stimulation (*e.g.*, light,[87,102,136,137,276–282] pH,[88,139–141,283,284] temperature,[97,143,217,285–288] electrical potential,[144,145,289–291] magnetic field,[292–294] surface curvature,[295] density of surroundings,[90] applied force[296]) to reversibly switch their static or dynamic wettability have been increasingly investigated.[16,297] The smart superhydrophobic or superoleophobic surfaces are the most complicated and subtle interfaces in the research field of wettability, which are usually hailed as ''the bright pearl on the imperial crown''. The surfaces showing smart wettability are usually obtained by forming rough microstructures on stimuli-responsive material surfaces or modifying rough solid surfaces with stimuli-responsive molecular layers.[16,285,298–300] Although many smart superhydrophobic surfaces have been developed,[217,276,284,285,292,295] the realization of smart oil-wettability on superoleophobic surface is still in its early stages and further research is needed.

5.1 Light response

Our group fabricated a novel wettability-switchable hierarchical rough titanium dioxide (TiO_2) layer on a titanium substrate using the one-step femtosecond laser ablation method.[136] The synchronicity of microstructure formation and oxidization during femtosecond laser ablation constructed a stratum of rough TiO_2 layer on the original substrate (Fig. 18a, b and g). The rough TiO_2 surface looked like a micro-mountain array decorated with randomly distributed nanoscale protrusions. Initially, the laser-induced hierarchical rough TiO_2 surface showed superhydrophobicity with the WCA of 154.5° ± 2.5° (Fig. 18c). Once immersed in water, the as-prepared TiO_2 region can reflect homogeneous light just like a silver mirror. This mirror forms by virtue of the trapped air between water and the substrate, which demonstrated that the contact state between the sample and water belonged to the Cassie model.[48,163,164,301,302] If an oil droplet is in contact with the rough surface submerged in water, the underwater oil will rapidly spread out on the sample surface. The OCA of only 4° was measured, indicating the underwater superoleophilicity of the laser-induced TiO_2 surface without any treatment (Fig. 18e). Surprisingly, when the sample was irradiated with UV light for 40 min, the WCA in air sharply decreased to 2.5°, which revealed that the wettability of the resultant surface in air was transformed from superhydrophobicity to superhydrophilicity (Fig. 18d). The silver mirror-like reflectance disappeared when the sample was submerged in water because water wetted and filled the interspace of the rough micro/nanoscale structures. The rough surface showed underwater superoleophobicity with the OCA reaching up to 160.5° ± 2°, due to the intrinsic oil-repellency of the filled water (Fig. 18f). The underwater oil droplet easily rolled off as soon as the substrate was slightly inclined. It was found that the underwater oil-wettability showed an opposite switching trend to water-wettability in air. Interestingly, if the sample was further stored in the dark for two days, the original wettabilities such as superhydrophobicity and underwater superoleophilicity would recover (Fig. 18c and e). The above-mentioned wettability switching process could be repeated for many cycles.

The internal mechanism of the switchable wettability is based on the fact that TiO_2 is an excellent photo-responsive material.[276,277]

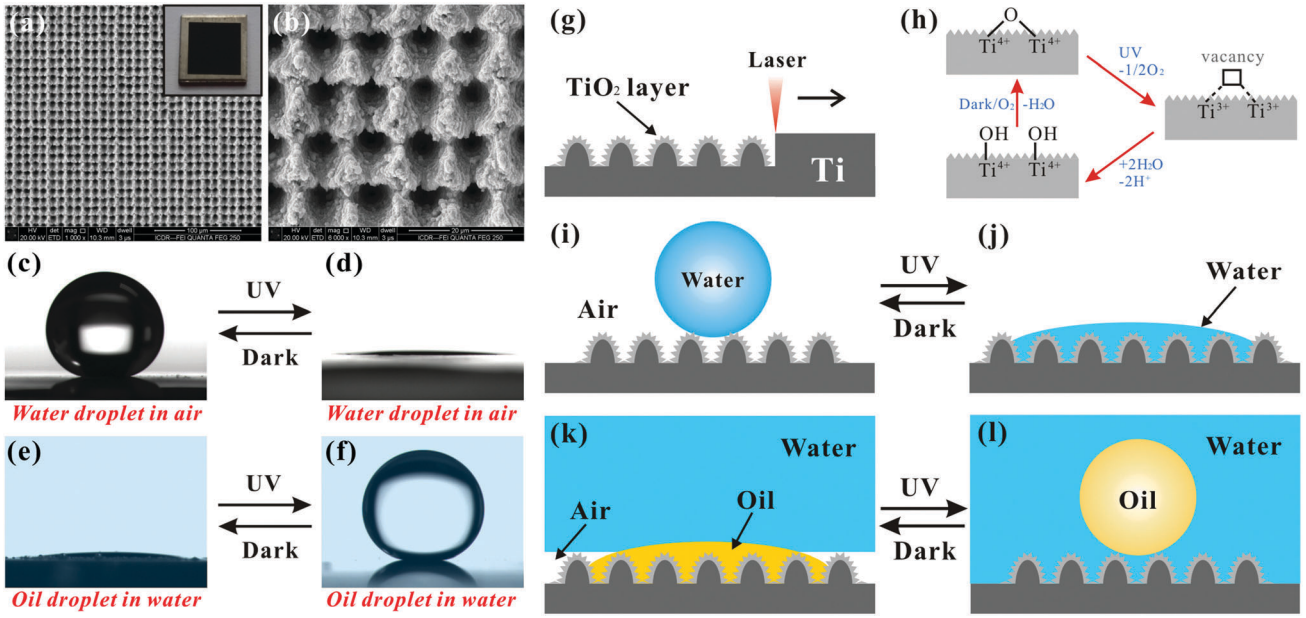

Fig. 18 Light-induced switching of underwater superoleophobic–superoleophilic states. (a and b) SEM images of the rough Ti surface after femtosecond laser ablation. (c and d) Water droplet on the rough sample surface after (c) storing in the dark and (d) irradiation with UV light, respectively, in air environment. (e and f) Underwater oil droplet on the rough sample surface after (e) storing in the dark and (f) irradiation with UV light, respectively. (g–l) Schematic illustration of the switchable wettability. Reproduced from ref. 136 with permission from RSC, copyright 2015.

The laser induced rough TiO_2 layer initially exhibits superhydrophobicity and ultralow water adhesion in air, agreeing well with the Cassie state (Fig. 18i). According to the Cassie wetting state, a trapped air cushion was generated between water and rough microstructures after immersing the sample in water. At this point, if an underwater oil droplet was put on the sample surface, the oil would spread along with the air cushion and displace the trapped air due to the capillary action and water pressure. Therefore, the surface showed underwater superoleophilicity (Fig. 18k). As shown in Fig. 18h, UV light irradiation created pairs of electrons and holes on the rough TiO_2 surface.[276,277,281,303,304] The photogenerated holes immediately united with lattice oxygen to form highly unstable oxygen vacancies. These oxygen vacancies were inclined to absorb the atmospheric water by dissociation, generating two adjacent Ti–OH groups per vacancy. On account of the high surface energy of the –OH groups, the UV-irradiated rough TiO_2 surface was superhydrophilic in air (Fig. 18j). Water could fully wet the rough microstructures of the TiO_2 surface when the metal sheet was dipped into water. An underwater oil droplet on such rough TiO_2 microstructures is in the underwater Cassie state, so the surface shows underwater superoleophobicity (Fig. 18l). When the substrate was further stored in the dark, the implanted hydroxyl moieties were more easily replaced by ambient oxygen (Fig. 18h), causing the sample to recover its original superhydrophobicity and underwater superoleophilicity (Fig. 18i and k).[276,277,281,303,304]

The reversible transition of underwater oleophilicity-superoleophobicity on the rough TiO_2 surface can also be realized by alternating contamination treatment and UV irradiation. Wang *et al.* used a simple one-step hydrothermal method to form hierarchical rutile TiO_2 flowers on a fluorine-doped tin oxide substrate.[137] There were many uniform TiO_2 flowers with diameter of ~6 μm on the resultant surface. Every microscale flower was composed of many tetragonal pillar-liked petals with a rough top and smooth side wall. The submicron petal was an aggregation of many ultrathin nanoneedles. The just prepared surface showed superhydrophilicity and superoleophilicity in air. The CAs were 0° to both water and oil (trichloromethane) droplets. Similar to fish scales, the resultant surface became superoleophobic after immersion in water with an underwater OCA of 155°. This good underwater anti-oil capability was caused by the formation of a three phase (solid/water/oil) system. In this wetting state, a water layer underneath the oil droplet was trapped in the rough TiO_2 microstructures. However, when the sample was contaminated with oleic acid (in *n*-pentane, 0.5 wt%) for 5 s, the as-prepared TiO_2 coating would lose its underwater superoleophobicity, with the OCA directly decreasing to 64°. In this case, the oil droplet on the contaminated TiO_2 surface was at a heterogeneous wetting state, since some oleic acid spots were also trapped in the hierarchical rough microstructures. The trapped oleic acid spots resulted in a decrease in the contact area between the trapped water and oil droplet as well as the apparent underwater OCA. Interestingly, the oil-wettability could recover to the original underwater superoleophobicity upon UV light (wavelength = 365 ± 10 nm) irradiation for 2 h. TiO_2 is a photosensitive material.[276,277] The electron–hole pairs were generated and migrated to the TiO_2 surface during UV light irradiation. These holes preferred to react with OH^- or to adsorb surrounding water molecule to generate highly reactive hydroxyl radicals. The hydroxyl radicals were able to further

oxidize and decompose most organic compounds, such as oleic acid, re-endowing the TiO_2 surface with underwater superoleophobicity. Furthermore, the rough TiO_2 surface still maintained the responsivity after four cycles of oleic acid contamination and UV irradiation recovery.

Zhang *et al.* prepared TiO_2/single-walled carbon nanotube (SWNT) composite coatings through a modified liquid phase deposition process.[138] Then, the TiO_2/SWNT coatings were modified with 1*H*,1*H*,2*H*,2*H*-perfluorodecyltrichlorosilane (FDTS) to chemically lower the surface energy. The treated rough coating displayed superoleophobicity with an OCA of 160.4° and an OSA of 5.9° to a silicon oil (γ = 21.5 mN m^{-1}) droplet in air. When the surface was irradiated with UV light (wavelength = 365 nm, intensity = 21 mW cm^{-2}) for 13 h, the composite coatings were thoroughly converted from superoleophobic to superoleophilic. This conversion was ascribed to the FDTS monolayer being decomposed by the photocatalytic action of the TiO_2 component.[305–312] As the UV illumination time went on, the atomic percent of C–F chemical bond decreased almost linearly and tended to zero after 12 hours. This result revealed that the FDTS monolayer could be completely decomposed. The UV-induced conversion from superoleophobicity to superoleophilicity was also valid for various liquids, such as hexadecane, glycerol, 40% ethanol in water (γ = 30.2 mN m^{-1}), 11.1% ethanol (γ = 46.0 mN m^{-1}), and water. The OCA would sharply reduce to almost zero once the UV illumination time exceeded a threshold. Interestingly, the critical values were different for different liquids. The liquid with higher surface tension needed more irradiation time to become superoleophilic on the resultant surface. As a result, there was a state where the sample surface showed superoleophobicity to one oil droplet but superoleophilicity to another with lower surface tension, by precisely controlling the exposure time of UV light. The distinguishable difference in the surface tensions of these two liquids was even lower than 5 mN m^{-1}. Based on the inverse oil-wettability, the separation of two organic liquids with different surface tensions using a TiO_2/SWNT coated metal mesh was demonstrated.

5.2 pH response

Cheng *et al.* prepared a pH-responsive surface showing switchable oil wettability.[139] The surface was superoleophilic in acidic aqueous solutions, but superoleophobic in basic aqueous solutions. The hierarchical microstructures were firstly formed on the copper foil substrates by immersing the samples into the solution of NaOH (2.5 M) and $(NH_4)_2S_2O_8$ (0.1 M), and subsequent heat treatment. As shown in Fig. 19a and b, the treated surface was composed of abundant microflowers with the size of ~4 μm and nanowires of about 20–80 nm in diameter; all the microflowers stood on the nanowires. The sample was then dipped into a mixed thiol solution of $HS(CH_2)_9CH_3$ and $HS(CH_2)_{10}COOH$ to graft both carboxylic acid and alkyl groups. In water, the OCAs of an underwater oil droplet (octane, 4 μL) on the resultant surface remained constant at about 0° in neutral and even acidic water (pH ≤ 7), showing underwater superoleophilicity (Fig. 19c). However, the OCAs increased with increasing pH in basic water. The OCA reached up to 162° at the

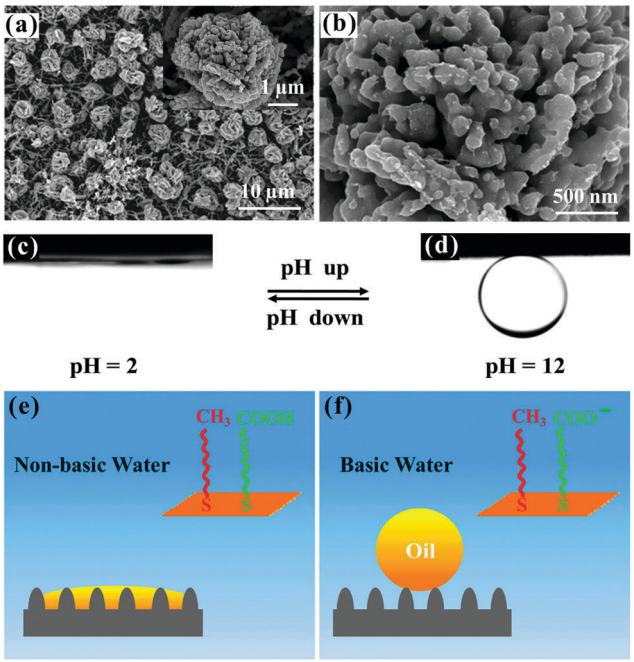

Fig. 19 pH-induced switching of underwater superoleophobic–superoleophilic states. (a and b) SEM images of the hierarchical-structured surface at (a) low and (b) high magnification. (c and d) Oil (octane) droplets on the resultant surface in acidic (c, pH = 2) and basic (d, pH = 12) solutions. (e and f) Schematic illustration of the mechanism of the pH-dependent switchable oil-wettability. Reproduced from ref. 139 with permission from ACS, copyright 2013.

water pH of about 12, indicating that the surface switched to underwater superoleophobic (Fig. 19d). After the sample was taken out of the basic water and instantly washed with pure water, it would recover to superoleophilic after immersion into acidic liquid again. Such a reversible transition between underwater superoleophilic and superoleophobic states could be repeated many times. Both carboxylic acid and alkyl groups were grafted on the sample surface during the preparation process. Generally, the carboxylic acid groups are protonated in nonbasic aqueous solutions and deprotonated in basic aqueous solutions. In the neutral or acidic water (pH ≤ 7), the alkyl groups on the sample surface were dominant, resulting in the low surface free energy of the surface (Fig. 19e). The surface showed intrinsic oleophilicity in water. The oil-wettability was further magnified to underwater superoleophilicity by the rough microstructures. In contrast, the surface carboxylic acid groups were deprotonated in basic water (Fig. 19f). The deprotonated state was hydrophilic, since hydrogen bonding generally occurred between the deprotonated carboxylic acid groups and water molecules. As a result, water wetted the sample surface and was trapped among the rough microstructures. Higher pH led to more deprotonated carboxylic acid groups as well as more trapped water. Particularly at pH ≥ 12, the trapped water layer was thick enough, which led to the underwater superoleophobicity due to the formation of a stable solid/water/oil three-phase system (underwater Cassie state). Based on the above, it can be found that the switching ability of

underwater oil-wettability was caused by the cooperation between the surface chemistry variation and hierarchical structures on the surface.

Cheng *et al.* used the plasma polymerization method to graft a layer of pH-responsive PAA on a glass substrate (PAA-G).[140] The PAA film exhibited rough nanostructures with thickness of about 64.5 nm. The underwater adhesion of the sample surface to an oil droplet could be reversibly switched by the environmental pH values. As the pH changed from 1.0 to 4.6, 5.0, 8.0 and then to 12.0, the adhesive force on a underwater oil droplet decreased from 21.6 ± 5.0 μN to 15.0 ± 2.9 μN, 2.0 ± 0.6 μN, 1.5 ± 0.4 μN and then to 0 μN. The PAA-G surface would recover high oil-adhesion once the sample was again placed in solutions with low pH value. The switch between high-oil-adhesion and low-oil-adhesion states could cycle at least 10 times. This switchability of oil-adhesion was caused by the pH-dependent chemical composition and surface roughness. When the pH was smaller than the threshold of 4.7, the neighboring carboxylic acid groups on PAA branched chains formed intramolecular hydrogen bonds, resulting in a dehydrated coiled state and a rough surface. The low water content was not enough to fully prevent the oil from wetting the PAA-G substrate. The oil droplet penetrated into and contacted with the rough microstructures of the PAA-G surface, belonging to the underwater Wenzel state. In this case, the resultant surface presented an OCA below 150° and ultrahigh adhesion to an oil droplet in water. When the pH was higher than 4.7, the intermolecular hydrogen bonds between the carboxylic acid groups on the PAA branched chains and water molecules were easier to form on the PAA surface than intramolecular hydrogen bonds. The conformation of PAA became a hydrated stretched state instead of a coiled state. The intermolecular hydrogen bonds gave rise to a high ratio of water content. As a result, a water layer was trapped between the PAA-G surface and the oil droplet, which provided a repulsive force to the oil. This underwater Cassie wetting state exhibited ultralow oil-adhesive superoleophobicity in water.

5.3 Temperature response

Chen *et al.* prepared a thermal-responsive PNIPAAm hydrogel.[142] When the resultant sample was immersed in water, its surface wettability and adhesion to an oil droplet was found to be in response to the temperature of the surrounding water solution. When the temperature was below the LCST (~32 °C) of PNIPAAm, the as-prepared hydrogel surface showed underwater superoleophobicity and very low oil-adhesion. The OCA and adhesive force to an underwater oil droplet at the solid/water interface were measured to be 151.7° ± 1.6° and 5.8 μN. If the environment temperature increased above the LCST, the wettability state would switch to a weak oleophobicity with high oil-adhesion in water. In this case, the OCA decreased to 127.0° ± 4.6°, while the adhesive force increased to 23.1 μN. These two different wetting states could be reversibly switched for many cycles. There is a balance between hydrophobicity and hydrophilicity in the PNIPAAm hydrogel network, *i.e.*, hydrophobic –CH(CH_3)$_2$ and hydrophilic –CONH– groups on the side chains. In general, N–H/C═O groups on the PNIPAAm branched chain and water molecules formed intermolecular hydrogen bonds at room temperature (<LCST), resulting in a hydrated, swollen state of the gel. The repulsive action between trapped water (polar) and oil (nonpolar) molecules endowed the hydrogel with underwater superoleophobicity and low oil-adhesive force. Above the LCST, the N–H and C═O groups formed intramolecular hydrogen bonds with those on neighboring branched chains, resulting in a dehydrated collapsed hydrogel. Such sample surface with low water content exhibited weaker oleophobicity and higher oil-adhesion because of the higher affinity between the hydrophobic molecular structure of PNIPAAm and oil.

The thermal-responsive underwater oil-wettability was successfully realized by the cooperation of single PNIPAAm molecules and rough surface topography. However, the switching range of the oil-wettability of the above-mentioned smart surfaces is very limited. Liu *et al.* recently reported a surface that could switch between underwater superoleophobic and superoleophilic states by adjusting the water temperature.[143] Both the underwater oleophilic heptadecafluorodecyltrimethoxysilane (HFMS) and the thermo-responsive PNIPAAm were modified on the surface with silicon nanowire arrays microstructure. A 2 μL underwater oil droplet (1,2-dichloroethane) on the resultant surface showed an OCA of 157° at 20 °C (Fig. 20a). However, the OCA was only about 3° at 60 °C (Fig. 20b). This switching between underwater superoleophobicity (at 20 °C) and underwater superoleophilicity (at 60 °C) could be reversibly repeated for many cycles (Fig. 20c). The grafted PNIPAAm chains were able to conceal or expose the oleophilic HFMS component through a thermo-responsive change in molecular configuration. At room temperature, the PNIPAAm chains preferred to bond with water molecules, forming intermolecular hydrogen bonding (Fig. 20d). The hydrated PNIPAAm chains extend outward and the HFMS was hidden, leading to an underwater superoleophobic surface. With the temperature increasing to 60 °C, the intramolecular hydrogen bonding of PNIPAAm chains was dominant (Fig. 20e). The grafted PNIPAAm chains thereby shrinked and became dehydrated. Therefore, the exposed HFMS chains led to an underwater superoleophilic surface.

5.4 Electrical potential response

PANI is a novel conducting polymer. All of its color, conductivity and wettability show a big difference between the electrochemically reduced state and oxidized state.[144] In general, there are three stable oxidation states of the PANI surface: the half-oxidized emeraldine base (EB), the fully oxidized pernigraniline form (PNB), and the fully reduced leucoemeraldine form (LEB). The EB form could be doped into the conducting state of the emeraldine salt form (ES) by a proton. Ding *et al.* prepared a PANI nanowire film through a galvanostatic deposition process.[144] The aligned PANI nanowires were very uniform, with the length of 141.3 ± 5.0 nm and the diameter of 45.7 ± 1.7 nm (Fig. 21a). When a voltage of 0.43 V was applied to the PANI nanowire film, the sample surface showed superoleophobicity and ultralow oil-adhesion in 0.1 mol L^{-1} $HClO_4$ solution (pH = 1.2). The measured OCA of the 1,2-dichloroethane droplet was

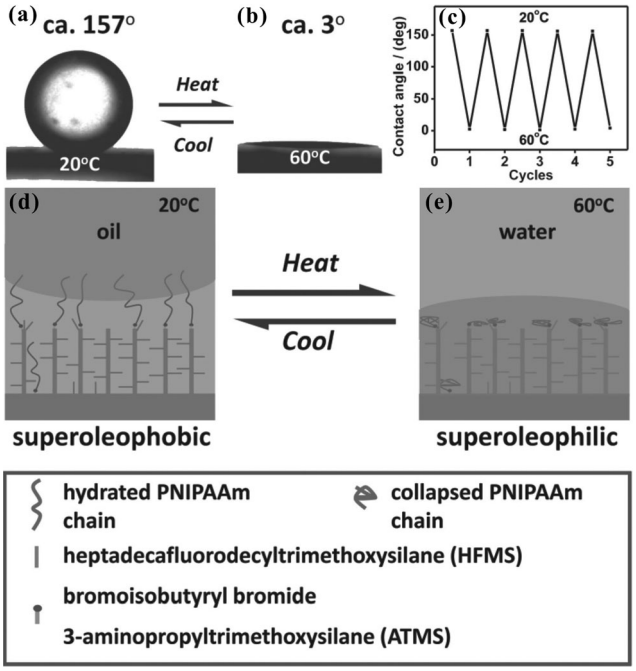

Fig. 20 Temperature-induced switching of underwater superoleophobic–superoleophilic states. (a and b) Underwater oil droplet on the resultant substrate at (a) 20 °C and (b) 60 °C. (c) Repeatability of the switchable oil-wettability in water. (d and e) Schematic illustration of the mechanism of the temperature-dependent switchable oil-wettability. Reproduced from ref. 143 with permission from Wiley, copyright 2015.

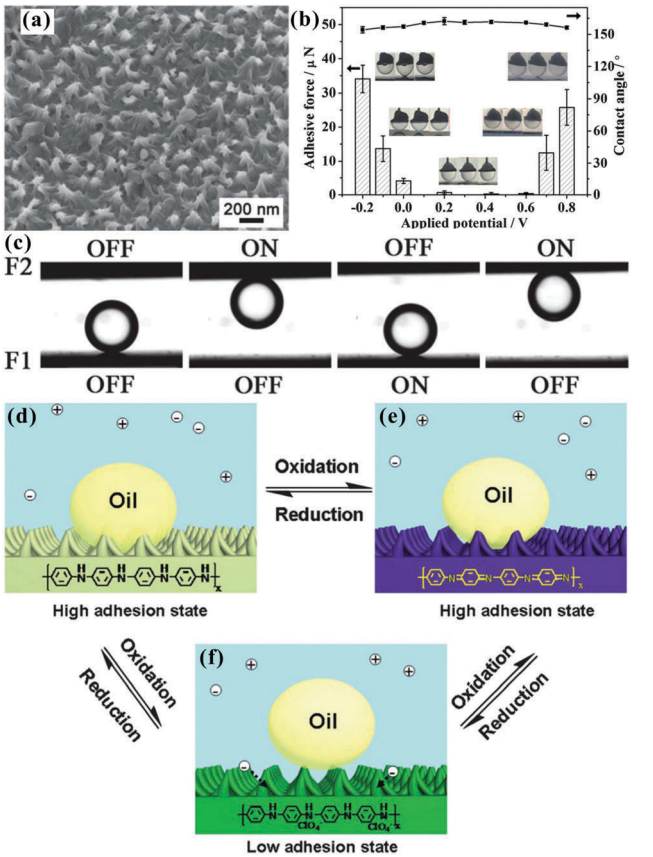

Fig. 21 Applied electrical potential induced switchable oil-adhesion between very low and ultrahigh on the underwater superoleophobic PANI nanowire films. (a) SEM image of the PANI nanowire microstructure. (b) OCA and oil-adhesive force on the PANI nanowire film in 0.1 mol L^{-1} $HClO_4$ solution, with the applied potential ranging from −0.2 V to 0.8 V. (c) Circularly transferring an underwater oil droplet between two PANI nanowire substrates by alternately turning off and on the applied potential (−0.2 V). (d–f) Schematic diagram of the switching mechanism of the oil-adhesion on the PANI nanowire film: (d) LEB state, (e) PNB state, and (f) ES state. Reproduced from ref. 144 with permission from RSC, copyright 2012.

161.6° ± 1.5°, while the OSA was less than 3°. As the voltage was tuned to −0.2 V, the sample still maintained underwater superoleophobicity with the OCA of 154.2° ± 2.9°, while the oil droplet stuck tightly to the PANI nanowire film, even though the sample was tilted to any angle. The resultant surface presented a strong oil-adhesive superoleophobic state in aqueous solution. Similarly, the underwater superoleophobicity and ultrahigh oil-adhesion were also achieved at the applied potential of 0.8 V. Therefore, the oil-adhesion of the underwater superoleophobic PANI films could be controlled by adjusting the electrochemical potential (Fig. 21b). By alternately turning off and on the applied potential (−0.2 V), an underwater oil droplet could be circularly passed between two parallel PANI nanowire surfaces, as shown in Fig. 21c.

It was found that the state of the PANI nanowire film could transform from ES (Fig. 21f) to LEB (Fig. 21d) or PNB (Fig. 21e) with the electrical potential switching from 0.43 V to −0.2 V or 0.8 V, respectively. The electrochemical change usually results in a flux ion into the PANI backbone. For the PANI nanowire film at the ES state, protonation occurred at the imine nitrogen sites to yield polysemiquinone. As a result, the polaron became unrestricted and left the PANI chains. The anion species (ClO_4^-) had to act as counter-ions to the N^+ sites to maintain charge neutrality. The molecular interaction between the PANI surface and water was enhanced. Therefore, the rough microstructures of the PANI nanowire film were fully wetted by electrolyte solution. An electrolyte solution cushion was trapped in the microstructures of the substrate surface and underneath the placed oil droplet. This underwater Cassie contact state endowed the resultant surface with a high OCA and low oil-adhesion (Fig. 21f). As the potential decreased to −0.2 V or increased to 0.8 V, the PANI form was turned from the ES state to the LEB or PNB state. With the dopant ions (ClO_4^-) moving out of the PANI backbone, the interaction between the PANI and water molecules was weakened, while the attraction between PANI and oil molecules was strengthened. Therefore, oil partly penetrated into the rough microstructure of the PANI nanowire films (Fig. 21d and e). An underwater transition state formed in the solid/liquid/oil system, giving rise to a high oil-adhesion.

Tian *et al.* developed a method to directionally drive the motion of underwater oil droplets by the combined action of electric field and gradient microstructure.[313] A gradient-structured porous polystyrene film was pre-fabricated based on the breath figure process under a humidity field gradient. There were lots of micro-pores forming on the resultant surface. Their size decreased gradually from one edge to another edge on the same sample surface, arranging as a gradient distribution.

The WCA of a water droplet on such a surface declined from 120° in the area with larger pores to 98° in the area with smaller pores, while the corresponding OCA of an underwater oil droplet on the surface increased from 34° to 45°. When an oil droplet (liquid paraffin) was put on the gradient-structured film in water, an unbalanced pressure was generated on both ends of the droplet due to the gradient of the porous structured film. Such an unbalanced pressure endowed the oil droplet with an asymmetrical shape and the motion trended toward a certain direction. When an electric field was added, the contact area between the underwater oil droplet and the gradient-structured porous film was decreased. Meanwhile, the viscous drag on the as-prepared surface was efficiently overcome. Once the applied voltage exceeded a threshold, the underwater oil droplet could directionally move from the large pore area to the small pore area on the sample surface. In their experiment, the driving distance of the oil droplet reached up to 5 cm.

5.5 Magnetic field response

Recently, Feng *et al.* demonstrated a facile method for magnetic-field-driven manipulation and transport of oil-based magnetic fluids.[146] A ZnO nanorod array was grown on a glass substrate by a low-temperature hydrothermal method. The as-prepared ZnO nanoarrays consist of uniformly aligned nanorods with diameter of 150–250 nm and length of ~6 μm. After UV treatment, the resultant ZnO nanoarrays showed superhydrophilicity and superoleophilicity in air with the WCA of 6° and OCA of 9°, respectively. When the surface was placed in water, it became superoleophobic (OCA = 156°) and could easily roll down (OSA < 5°). Two underwater superoleophobic ZnO nanoarrays were then applied to manipulate and transfer oil droplets in water medium. One substrate (top) was suspended above another one (down), allowing them to be face-to-face with an appropriate space. A magnetic fluid droplet (silicon oil of Fe_3O_4 nanoparticles) was injected onto the down substrate. With a periodic external magnetic field being applied to this system as the actuating force, the oil droplet could quickly respond to the magnetic stimuli and be reversibly transferred between two substrates. There was no adhesion of magnetic oil droplet during the transport process because the ZnO nanorod arrays exhibited ultralow oil-adhesive force to the magnetic oil. In contrast, if two smooth ZnO film coated substrates were used to perform the same transport experiment, an obvious delay in the movement and loss of magnetic oil would be observed.

5.6 Density of surrounding water solution response

Based on the underwater superoleophobic surfaces, our group reported a simple way to achieve *in situ* oil droplet transportation in an aqueous environment just by switching the density of the water solution.[90] Fig. 22a depicts the setup for transferring the position of an oil droplet in water. It was mainly composed of a water-filled glass container and two parallel underwater superoleophobic sheets (laser ablated Si substrates). The lower sheet was fixed while the upper one could be continuously moved up and down inside the container. Fig. 22b shows the whole transportation process. At the outset, an oil droplet with the volume of 15 μL and the density of 1.26 g cm^{-3} was located on the surface of the lower sheet (step 1). The underwater oil droplet presented a spherical shape, due to the underwater superoleophobicity of the substrate. Then, the upper sheet was lowered slowly until it touched the top of the oil droplet (step 2). At that moment, we started to increase the density of the aqueous solution in the container by slowly adding sugar water with density of 1.52 g cm^{-3} into the container. After some time, the oil density was switched from higher than to lower than the surrounding water solution (step 3). With the upper sheet being lifted up, the oil droplet moved upward along with the upper sheet, just like being grappled up by a hand because the buoyancy force of the oil droplet in water was large enough to resist its gravity (step 4). Interestingly, this oil droplet could also be put back on the lower sheet. The upper sheet was moved down until the bottom of the hanging oil droplet just touched the lower sheet (step 5), and deionized water was subsequently added to the container to dilute the aqueous solution (step 6). As the density of the aqueous solution decreased and switched to be much smaller than that of oil, the water solution became clear and transparent once again. Finally, when the upper sheet was lifted again, the oil droplet was released and stayed on the lower sheet successfully (step 7). During the entire process of oil transportation, the upper underwater superoleophobic sheet was employed as a ''mechanical hand'' for ''picking up'' the underwater oil droplet from the lower sheet and then ''putting it back'' just through reversibly regulating the density of the surrounding water solution (Fig. 22c). This simple reversible transportation could be achieved circularly without any oil loss (Fig. 22d).

6. Applications

As the demand for multi-functional materials with special wettability is increasing, currently, many researchers and engineers are interested in designing and fabricating superoleophobic surfaces that have a broad range of applications. This section mainly focuses on the new and typical functions of superoleophobic surfaces, both in air and in water, including anti-oil ability,[75–78] self-cleaning,[79,80] oil/water separation,[56,81,83–88] oil droplet manipulation,[79,80,89–93] chemical shielding,[75] anti-blocking,[79,94] liquid microlens array,[95] oil capture,[96] bioadhesion,[97] guiding the movement of oil droplet,[92,98] and floating on oil.[99,100]

6.1 Anti-oil coatings

Pan *et al.* prepared a compound coating that was made up of cross-linked PDMS and 50 wt% fluorodecyl POSS.[75] After coating the compound onto stainless steel wire meshes by an electrospinning method, the metal meshes showed a rough hierarchical surface structure that had re-entrant curvature at both the macro-level (Fig. 23a) and on the micrometer scale (Fig. 23b). The interaction among the re-entrant curvature, the hierarchical rough microstructure and the low surface energy endowed the coated meshes with excellent superamphiphobicity (Fig. 23c and d). The coated surface virtually repelled all

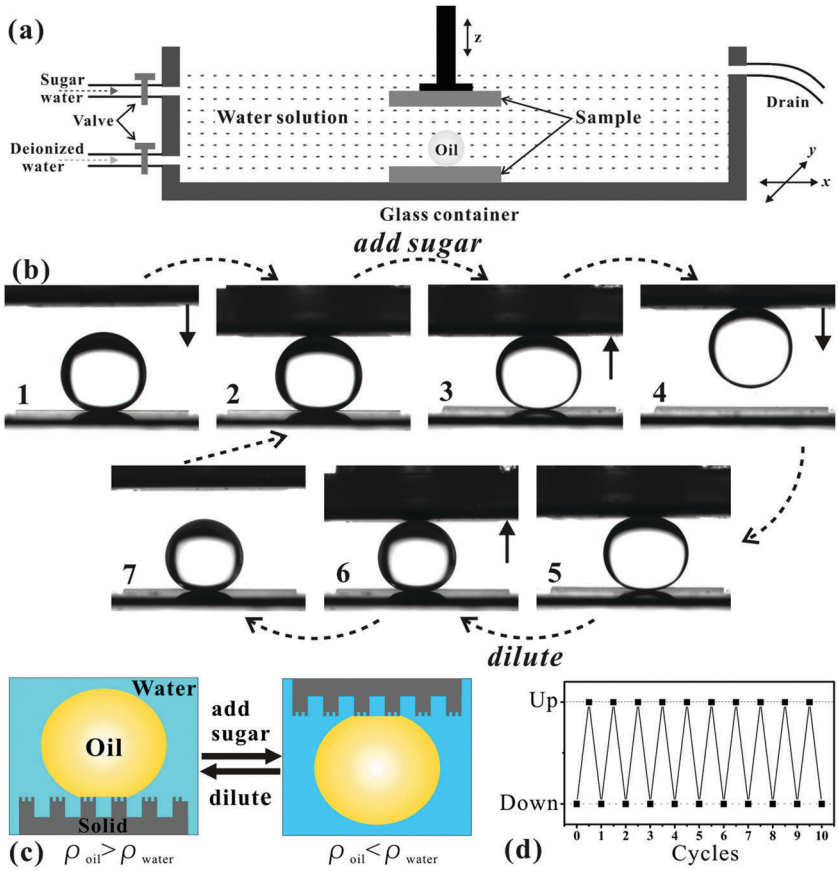

Fig. 22 Reversible transportation of underwater oil droplet by underwater superoleophobic surfaces and reversibly switching the density of the surrounding water solution. (a) Schematic of the setup. (b) Operational process of "picking up" and "putting down" an oil droplet. The underwater oil droplet could be picked up by the mechanical hand when the density of oil was lower than that of the aqueous solution, and could also be put down when the density of the oil became higher than that of the aqueous solution again. (c and d) The repeatability of the no-loss transportation of the oil droplet in water. Reproduced from ref. 90 with permission from Wiley, copyright 2014.

organic and inorganic liquids, including solvents and various acids/bases. In addition, the resultant surface showed low CA hysteresis and ultralow adhesion to essentially all Newtonian liquids. A series of jets of different liquids (*e.g.*, dimethylformamide, toluene, acetic acid, hexadecane, hexylamine, PDMS) could easily bounce on the sample surface, demonstrating excellent anti-oil properties, as shown in Fig. 23d.

The underwater superoleophobic surfaces with ultralow oil-adhesion have great anti-oil ability in water.[76,77] For example, the anti-oil-contamination performance of the femtosecond laser induced rough glass slide (AD = 2 μm, Fig. 15a–c) with ultralow oil-adhesive superoleophobicity underwater was investigated by our group.[78] The glass slide was first dipped into a water filled beaker. Then, the dyed oil with red color was deliberately dripped on the sample surface. After taking the treated glass slide out of the beaker, we used an optical microscope to qualitatively analyze the degree of pollution; the non-structured flat region was seriously polluted. It was found that a lot of red spots and patterns firmly adhered to this area. However, the laser structured rough region remained its initial color. There was no red imprint on the underwater superoleophobic area. The comparison result demonstrated that the laser structured underwater superoleophobic surfaces had the strong ability to repel oil contamination in water.

6.2 Self-cleaning

Since most in-air superoleophobic surfaces usually have superhydrophobicity, so such superamphiphobic surfaces also have self-cleaning ability like ordinary superhydrophobic surfaces. Fig. 24 shows the concept of the self-cleaning behavior of superamphiphobic surfaces with low liquid adhesion. Compared with a general surface, the water/oil droplet on a superamphiphobic surface shows a quasi-spherical shape. If a water/oil droplet is placed on a slightly tilted superamphiphobic surface, the droplet can easily roll away. Similar to the lotus leaf having self-cleaning ability,[20,22,54,151,152,162,264] during the rolling process, the droplet will adhere and remove the foreign dirt particles on the material surface because it is easier for dust particles to stick to the liquid droplet than to the solid substrate (Fig. 24b). In this way, superamphiphobic surfaces can be kept clean. In contrast, liquid droplets just pass over the dust on the normal flat surface, leaving the dust particles behind (Fig. 24a).

Underwater superoleophobic materials with ultralow oil-adhesion also have an excellent self-cleaning function.[79,80]

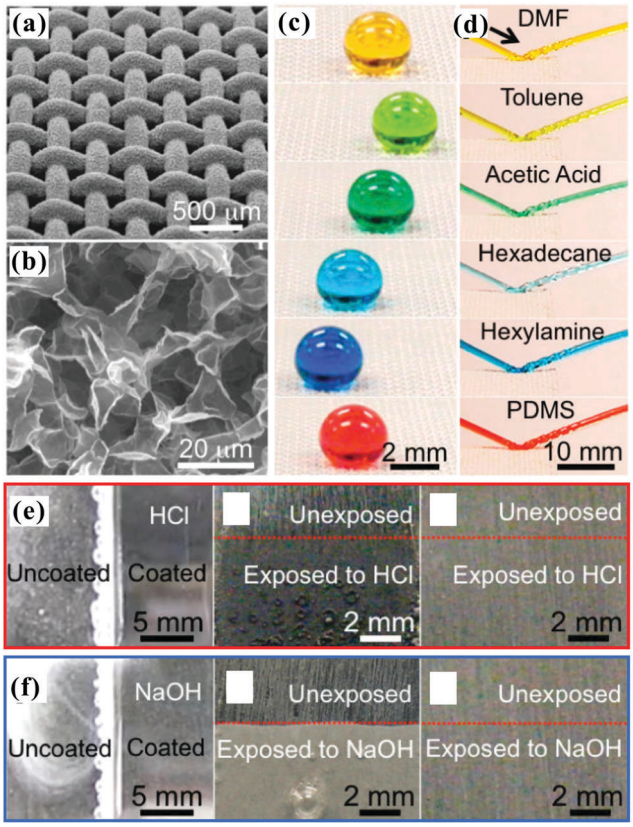

Fig. 23 Anti-oil and chemical shielding of the superamphiphobic coating. (a) SEM image of the rough coated metal mesh. (b) SEM image of the electrospun coating on the mesh surface, showing the existence of the re-entrant curvature. (c) Various oil droplets with very high contact angles on the resultant surface. (d) Jets of various liquids bouncing on the resultant surface. (e and f) Immersion of an aluminum plate composed of half untreated domain and half coated domain into the (e) concentrated HCl and (f) concentrated NaOH solutions. Reproduced from ref. 75 with permission from ACS, copyright 2012.

Sun *et al.* prepared gecko foot-like hierarchical microstructures made of PDMS by combining photolithography and soft lithography.[79] After subsequent oxygen plasma treatment, the rough surface showed extreme underwater superoleophobicity, with an OCA larger than 170° and an OSA less than 1°. A soya-bean oil droplet was deliberately put onto the surface as a pollutant in an air environment. The oil quickly adhered and wetted the sample surface. Interestingly, just by immersing the polluted sample into water, the oil was completely removed (Fig. 25), whereas the oil on the untreated flat region was still retained; *i.e.*, the oil was not washed away. This result revealed that underwater superoleophobic surfaces have strong self-cleaning ability. Although both the underwater superoleophobic surface and superhydrophobic lotus leaf have self-cleaning functions, their self-cleaning abilities are caused by different physical mechanisms. Water droplets can easily roll away on a lotus leaf, while taking away the dust particles on the leaf.[20,54,128,151,162,267] However, the self-cleaning effect of underwater superoleophobic surface originates from its intrinsic superhydrophilicity, since oil can be removed by the water

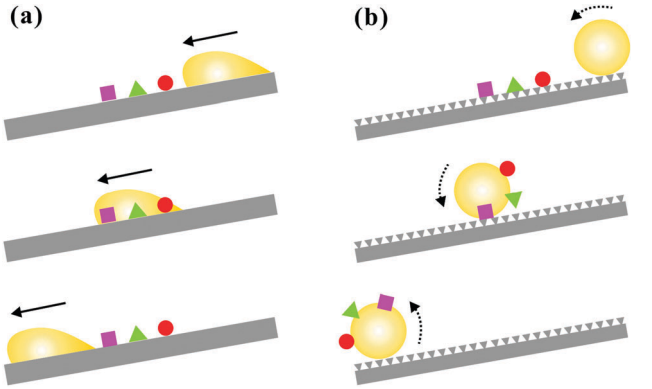

Fig. 24 Schematic illustration of the self-cleaning mechanism. (a) Water/oil droplet sliding down a normal flat surface and leaving the dust particles behind. (b) Water/oil droplet rolling down a superamphiphobic surface and taking away the dust particles.

injection (Fig. 25a).[22] Besides the surface tension of the water/oil/air interface, there is another main hydrophilic force to push the oil contamination out of the solid microstructures.[79] A higher level of hydrophilicity usually results in a stronger hydrophilic force. Once the oil-polluted sample is gradually immersed in water, the water is injected into the rough microstructures and pushes the oil out, resulting in the oil impurity being cleared, as shown in Fig. 25a.

6.3 Oil/water separation

With the global energy demand growing, the amount of industrial oily sewage discharge continues to increase and oil spill accidents occur frequently.[56,81–83] Nowadays, oil/water separation technology has become a hot research field to protect the environment and reduce economic loss. Recently, meshes or porous materials showing superhydrophobicity–superoleophilicity or superoleophobicity–superhydrophilicity have been successfully applied in oil/water separation devices because water and oil have different interface effects.[56,81,84–88] In 2004, Feng *et al.* first separated the mixtures of water and oil by using a superhydrophobic–superoleophilic mesh film.[57] Water was intercepted by the mesh for the superhydrophobicity, but oil fully wetted and quickly permeated through the resultant mesh because of the superoleophilicity, so as to achieve a separation; in fact, oil was removed from the mixture, therefore, the mesh is an "oil removing" material.[56–60,301,314–319] However, the oils easily adhere to the mesh and further block it, which significantly decreases the efficiency of the separating materials.[114,133,135,139,259,261,266,280,320–322] In addition, such superhydrophobic mesh films are not suited for removing light oils, which have a lower density than water, from the mixed solution.[83] This is because water will sink below the light oil, generating a thick water layer underneath the oil and above the rough mesh. The water layer prevents the oil from continuing to touch and pass through the mesh film. Unfortunately, the densities of most of oils are smaller than that of water. In order to overcome the above-mentioned multiple deficiencies, in 2011, Xue *et al.* developed an underwater superoleophobic mesh and

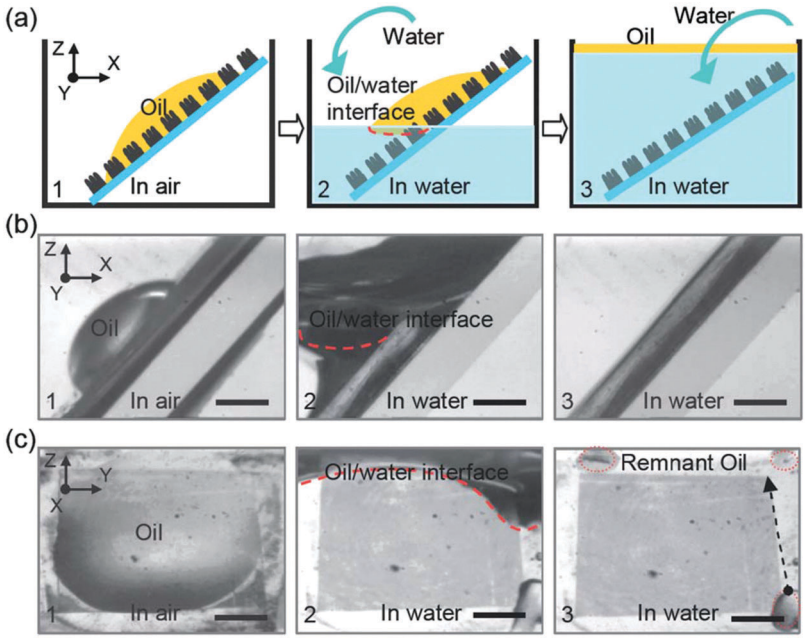

Fig. 25 Self-cleaning ability of underwater superoleophobic surfaces. (a) Schematic diagram describing the process of removing oil contamination when a polluted underwater superoleophobic film is dipped into water. (b and c) A series of optical microscopy photos of experimental self-cleaning results observed from (b) side and (c) top-down views, respectively. Reproduced from ref. 79 with permission from RSC, copyright 2011.

also achieved the function of oil/water separation.[321] Nanostructured hydrogel was simply coated on a rough porous stainless steel mesh. The obtained rough mesh exhibited underwater superoleophobicity and had great ability to remove water from the mixture of water and oil. Because oil was repelled by water in rough microstructures and was difficult to really touch the mesh, the hydrogel-coated mesh could not be fouled by oil during the whole oil/water separation process. Such mesh is usually called "water removing" material because water is removed from the mixture.[56] Following this strategy, a lot of underwater superoleophobic meshes or porous films were developed and successfully used to separate mixtures of water and oil.[113,115,133,135,226,261,266,272,280,282,320,322–328] For example, Sun *et al.* prepared a graphene oxide (GO) coated rough metal mesh that finally presented underwater superoleophobicity.[265] The GO-coated mesh could separate the mixture of bean oil and water that imitated culinary sewage. Jin *et al.* fabricated a rough $Cu(OH)_2$ copper mesh with both superhydrophilicity and underwater superoleophobicity.[113] There were abundant nanowire-hairs covering the mesh surface. Both water-rich immiscible mixtures and dispersed oil–water mixtures were separated by the rough mesh. Zhang *et al.* prepared a rough nitrocellulose film with microscale and nanoscale multiple pores, which showed superoleophobicity in water.[114] The film could even efficiently separate the mixtures of various oils and corrosive liquids. Wen *et al.* obtained a zeolite-coated metal mesh that exhibited excellent superhydrophilicity and underwater superoleophobicity.[328] The mixtures of various oils and water were efficiently separated by the zeolite-coated mesh. Furthermore, the underwater superoleophobicity was very stable, even in harsh environments such as acid and concentrated salt, *etc.* The stability made the mesh an ideal candidate in practical applications of oil/water separation.

Deserts occupy a large area on the earth's surface (Fig. 26a), but are not suited for human beings. Rain droplets can instantly percolate through the sand, revealing the remarkable water absorbing ability of the sand layer. Such superhydrophilicity can possibly endow the sand layer with underwater superoleophobicity; thus, the sand is a promising candidate for application in oil/water separation. Our group found that the surface of sand particles is not smooth, but covered by macro/micro/nano-scale hierarchical rough structures (Fig. 26c–e).[83] After immersion in water, the wetted sand layer exhibited underwater quasi-superoleophobicity and ultralow oil-adhesion to both heavy and light oil droplets (Fig. 26b, f and g). The measured oils included 1,2-dichloroethane, chloroform, petroleum ether, paraffin liquid, hexadecane, dodecane, decane, crude oil, diesel, sesame oil, and so on. Based on the underwater superoleophobicity of sand, we designed an oil/water separation device by using a sand layer as a separating membrane. As shown in Fig. 26h, the sand layer was fixed between two plastic tubes. A piece of cloth was put below the sand layer to avoid the loss of sand particles. Before the separation process, there was an essential step that the sand layer needed to be pre-wetted with a little water. Then, the mixture of oil (petroleum ether) and water was poured into the designed device (Fig. 26h). It was found that only the water (dyed blue) quickly permeated through the pre-wetted sand layer, whereas the oil (dyed red) was prevented and remained in the upper tube (Fig. 26i). The experimental results clearly indicate that the oil/water mixture was successfully separated by the pre-wetted sand layer. This separating process was driven by just gravity without any other

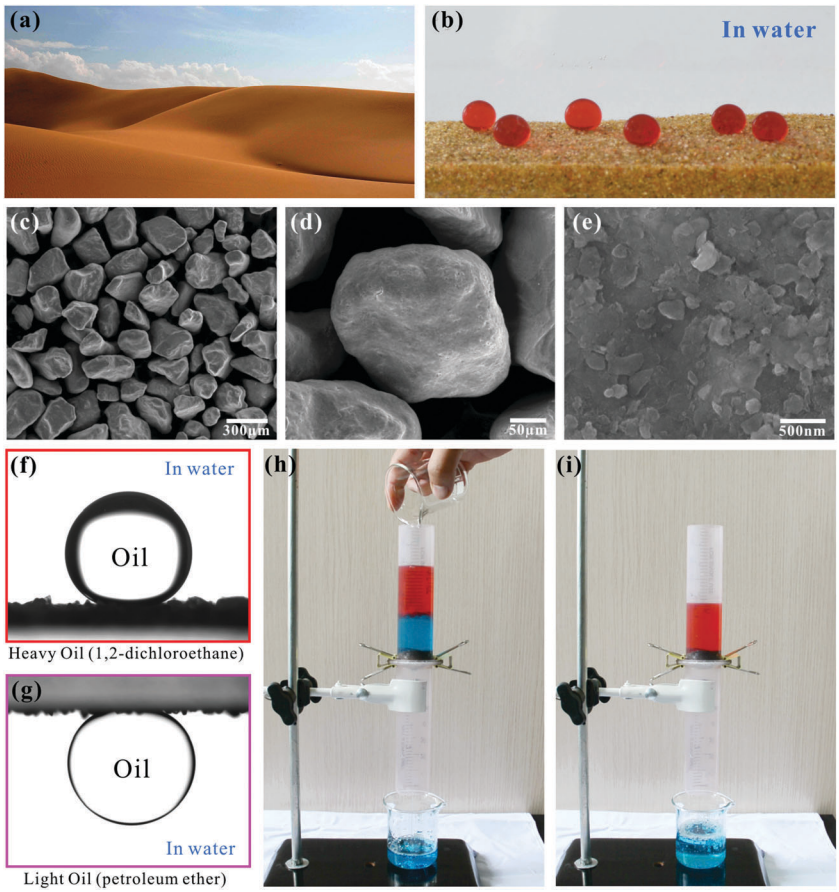

Fig. 26 Oil/water separation based on a pre-wetted sand layer. (a) Photo of the desert. (b) Photo of underwater oil droplets on the sand layer. (c–e) SEM images of the sand particles. Shapes of (f) heavy and (g) light oil droplets on the sand layer in water. (h) Pouring the mixture of oil (dyed red) and water (dyed blue) into the designed separation device. (i) After separating the mixture of water and oil. Reproduced from ref. 83 with permission from Wiley, copyright 2016.

external force acting on the device. In addition, the separation process could be repeated for many cycles and the designed system could work continuously. The used sand was directly obtained from the desert without any further treatment. This simple, green, almost free, large-scale, highly efficient way for oil–water separation offers a bright prospect for practically solving the pollution problems caused by oily industrial wastewater and oil spills.

6.4 Oil droplet manipulation

Microdroplet manipulation technology has attracted remarkable interest because of its potential applications in liquid transportation, *in situ* analysis, droplet based microreactors, droplet positioning, and labs-on-chips.[16,90,93,162,295,299] In most cases, liquid droplets are controlled and transported by expensive and precision mechanical micro-components, such as micropumps, microvalves, and microchannels.[40,64,144] The operational process is very complex and usually causes much droplet loss, due to droplet wetting and pinning.[144] The emergence of controllable adhesive superhydrophobic/superoleophobic surfaces provides an alternative solution to manipulating microdroplets.[53,78,80,89,91,92,294]

Yao *et al.* demonstrated an oil-based microreactor, taking advantage of the controllable oil-adhesive superoleophobic surfaces.[89] An oil droplet (10 μL) containing styrene was first put on a substrate that showed superoleophobicity and very low oil-adhesion, while another brown oil droplet containing Br_2 was placed on a high oil-adhesive superoleophobic substrate. The droplet containing styrene was then dragged from the substrate by a metal cap and transported to touch the Br_2 droplet. These two droplets coalesced as soon as they came in contact with each other. The color of the new merged droplet gradually faded, due to the reaction between Br_2 and styrene. The combined droplet was left on the sample surface with high oil-adhesion. The droplet-based microreactor systems will play an important role in enzymatic kinetics, protein crystallization, or other biochemical reactions.[329]

Our group prepared different hierarchical rough microstructures on glass slide surfaces by femtosecond laser ablation.[78] The laser ablated surfaces showed not only superoleophobicity, but also controllable oil-adhesion that ranged from ultralow to ultrahigh in water medium. Underwater no-loss transportation of oil droplets was performed by using the underwater superoleophobic glass with very high oil-adhesion as a "mechanical

hand'', as shown in Fig. 27a. A small oil droplet (8 μL) was firstly deposited on an ultralow oil-adhesive superoleophobic substrate in water (step-1), then lowered down a sticky superoleophobic surface (mechanical hand) to touch the oil droplet (step-2). After the mechanical hand just contacted the oil, we started to lift the mechanical hand up. The oil droplet left the original substrate and completely adhered to the mechanical hand for a stronger oil-adhesive force (step-3). The mechanical hand was shifted, which made the suspended oil droplet contact the other flat glass surface that had the highest oil-adhesion (step-4 and step-5). The oil droplet was released and remained on the flat glass surface when the mechanical hand was removed (step-6). The result demonstrated that the oil droplet was successfully transported from a low adhesive substrate to an ultrahigh adhesive surface. Interestingly, the whole transfer process had no oil volume loss due to the very small contact area between the oil droplet and underwater superoleophobic mechanical hand. The fusion of two oil/organic microdroplets was further realized, based on the above-mentioned droplet transfer method (Fig. 27b). No-loss oil transportation can also be carried out by other underwater superoleophobic materials, such as Ni/NiO microstructures,[80] copper films,[91] and silicon surfaces.[92]

It should be noted that the underwater superoleophobic surface with ultrahigh adhesion can only shift an oil droplet from an ultralow oil-adhesive substrate to the target surface with higher oil-adhesion. The transportation process is irreversible. The smart switchable underwater superoleophobic surfaces make it possible to manipulate an oil droplet *in situ*.[90,144]

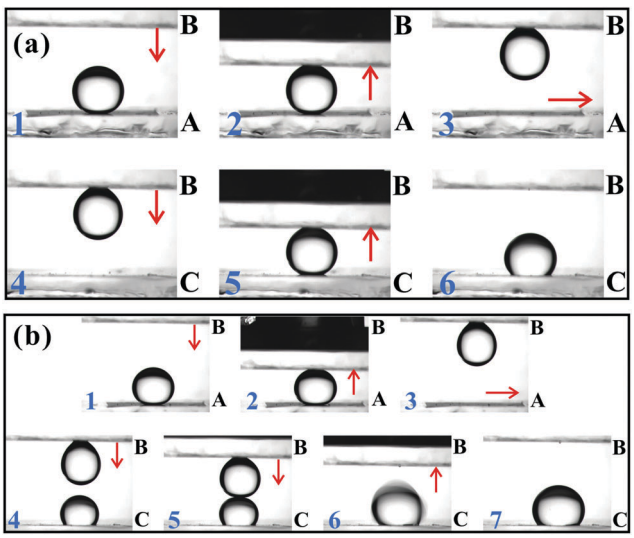

Fig. 27 Manipulating oil droplets in a water environment by using underwater superoleophobic surfaces with different oil-adhesion properties. (a) No-loss oil droplet transportation. (b) Fusion of two small oil/organic droplets. Sample A: ultralow oil-adhesive superoleophobic surface in water. Sample B: underwater superoleophobic glass with very high oil-adhesion, which was used as a ''mechanical hand''. Sample C: flat glass slide with highest oil-adhesion. The red arrows indicate the direction of movement of corresponding substrates. Reproduced from ref. 78 with permission from Springer, copyright 2015.

For example, our group used two underwater superoleophobic Si sheets to simply achieve the *in situ* transportation of small oil droplets in water by switching the density of the water solution (Fig. 22).[90] The underwater oil droplet could be ''picked up'' when the density of oil was smaller than that of the water solution, and be ''put down/back'' when the density of oil was larger than that of the water solution.

6.5 Chemical shielding (chemical resistance)

Interestingly, the superamphiphobic coating in Fig. 23a that was prepared by Pan *et al.* exhibited not only great anti-oil ability, but also exceptional chemical shielding function.[75] For example, when an aluminum plate composed of half untreated domain and half coated domain was immersed in 12 M concentrated hydrochloric acid (Fig. 23e) and 19 M concentrated sodium hydroxide (Fig. 23f), respectively, the uncoated aluminum surface immediately reacted with the surrounding solution and released gas bubbles, while the coated domain remained calm with no perceivable chemical reactions. After immersion in concentrated HCl or concentrated NaOH for a few minutes, the uncoated aluminum surface was badly damaged. In contrast, the surface topography of the coated aluminum showed no changes on either the microscale or the nanoscale, revealing effective chemical shielding.

Vahabi *et al.* fabricated a free-standing, flexible, superamphiphobic film, which was composed of a polyurethane layer and a layer of fluorinated silica particles.[200] The film could be wrapped around spools of different sizes and delivered to the end-users, who can easily paste the film on virtually any substrate (even irregular shapes) and endow those materials surfaces with liquid-repellent ability. The chemical resistance of the as-prepared superamphiphobic film was verified by immersing two aluminum samples into concentrated sulfuric acid. One aluminum sample was covered with the flexible superamphiphobic film and another was covered with just a polyurethane layer (not superamphiphobic). The latter sample turned black quickly, as soon as it came in contact with the sulfuric acid, while the superamphiphobic film coated sample remained unaffected. It was found that the superamphiphobic film showed excellent chemical resistance in a wide variety of aqueous and organic acids and bases.

6.6 Anti-blocking

Pipe blockage, caused by discharging water with a small amount of oily impurities, usually happens both in household kitchens and in industry. The ultralow oil-adhesive underwater superoleophobic surface provides a desirable way to deal with this issue, due to its anti-blocking ability.[94] Fig. 28a presents a situation where water with oil impurity is flowing in a conventional pipe. The oil impurity droplets in the water flow are prone to sticking to the inside wall of the pipe because the oil droplet can fully touch the flat pipe surface. The adherent oil impurity on the inner wall will hinder water from flowing through the pipe, because the flow tendency of water is disrupted by the adherent oil impurity. The disorganized flow route slows the speed of water flow down, and reduces the

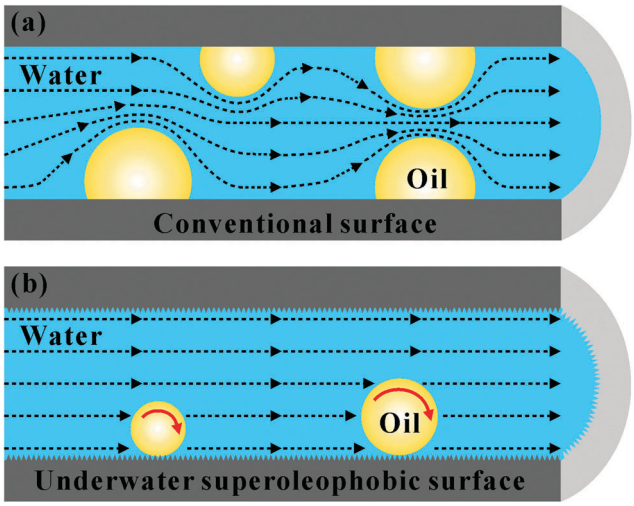

Fig. 28 Working principle diagram of the anti-blocking function of the underwater superoleophobic drainage pipe. Water with oil impurity flows in (a) a conventional water pipe; (b) a water pipe with underwater superoleophobic inner wall. The water flow trend is indicated by black dotted lines. The red arrows in (b) show that the oil impurity droplets roll forward with water flow. Reproduced from ref. 94 with permission from RSC, copyright 2014.

efficiency of this drainage system. On the other hand, with the drainage volume of the water–oil mixture increasing, more and more free oil impurities will attach to and merge with the adherent oil droplet. After a while, the adherent oil will accumulate enough and will block the pipe. Fortunately, the blockage can be prevented by using underwater superoleophobic and ultralow oil-adhesive pipes, as shown in Fig. 28b. The inner wall of these pipes allows the oil impurity to maintain a spherical shape and roll forward along with the fluxion of water. Consequently, the flow speed of water will not be impeded or slowed down, and pipe blockage will not increase, due to the timely cleanup of the oil impurity. These drainage pipes can work in a highly effective manner for ages. Such anti-blocking ability of underwater channels can also be broadly applied in other fields. For example, if an artificial blood vessel wall possesses underwater superoleophobicity, the risk of potential fatal thrombosis and blood clots will greatly decrease.

6.7 Liquid microlens array

As a basic optical device, lenses play a very important role in eyes, light convergence/divergence, photography, optical communication, microscopy, laser microfabrication, *etc.*[330–333] Liquid lenses are one important form of lenses, which take advantage of the surface tension of the liquid droplet (*e.g.*, water) to form a partial-sphere lens shape.[334–336] The liquid lens has many advantages such as economical material, simple preparation process and the easy adjusting of focal length.[334–338] Our group developed a novel strategy to prepare an underwater oil microlens array based on an underwater superoleophobic–oleophobic pattern, as shown in Fig. 29.[95] A circle array pattern was firstly formed on a glass surface by selective femtosecond laser ablation (Fig. 29b). The pattern was composed of an untreated flat

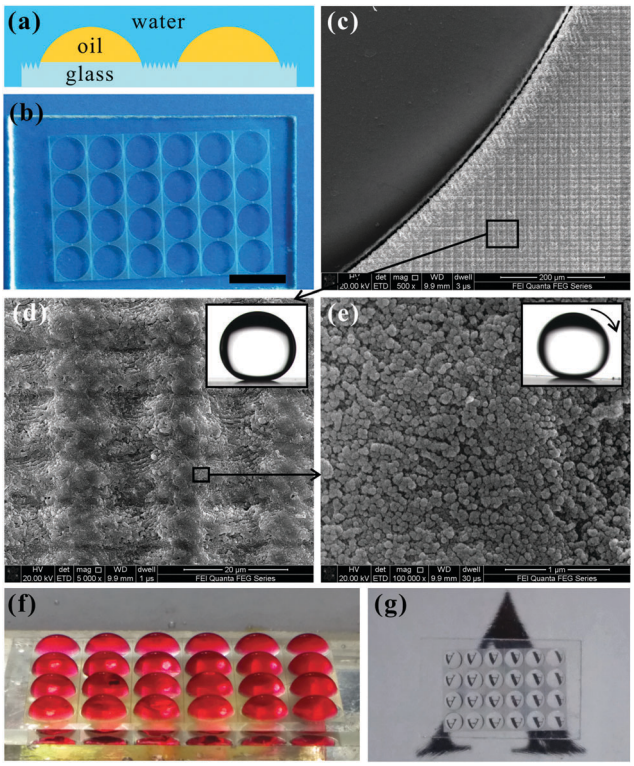

Fig. 29 Liquid lens array fabricated by an underwater superoleophobic-oleophobic pattern. (a) Design principle. (b) Photo of a circle array pattern fabricated by the selective femtosecond laser ablation. Scale bar: 5 mm. (c) SEM image of the boundary between the untreated flat domain and the laser-induced rough domain. (d and e) SEM images of the femtosecond laser ablated rough glass slide surface. The insets reveal the static shape and rolling of an underwater oil droplet on the entire laser ablated glass slide surface. (f) Side view of the as-prepared oil lens array. (g) Imaging ability of the designed microlens array. Reproduced from ref. 95 with permission from RSC, copyright 2015.

circle array and surrounding laser-induced rough microstructures (Fig. 29c–e). The femtosecond laser induced rough microstructures presented low adhesive superoleophobicity to oil droplets in water, with the OCA of $160.5^\circ \pm 2^\circ$ (inset in Fig. 29d) and the OSA of 1° (inset in Fig. 29e). In contrast, the untreated bare domain only showed intrinsic weak oleophobicity with OCA of $121^\circ \pm 3^\circ$ in water. The designed circle array was indeed a typical heterogeneous topography, composed of both weak underwater oleophobic circular domains and surrounding underwater superoleophobic domains. Next, the resultant sample was immersed in water, and oil droplets were placed on every circular area. An energy barrier generally exists at the boundary between the centric underwater ordinary oleophobic domain and the circumambient underwater superoleophobic domain.[54,126] The energy barrier is able to prevent the oil droplet from spreading to the laser-induced region, so the oil droplets are restricted to the untreated circles (Fig. 29a). Surface tension drove the oil droplet to self-form a partial-sphere shape that could act as a lens (Fig. 29f). Since the oil droplet was immersed in water, the underwater oil lens overcame the evaporation problem, which is a common defect of liquid lenses. Moreover, the shape as well as

the optical parameters of the oil lens could be simply designed by the diameter of the untreated circles and the oil volume. A uniformly arranged microlens array was further fabricated (Fig. 29f). On account of the great isolation effect of laser-induced superoleophobic domain, the oil lenses could be located very close to each other. The liquid microlens array possessed good imaging ability. When a paper with a letter "A" was put behind the microlens array plane, an array of inverted real images was clearly captured (Fig. 29g).

6.8 Oil capture

One of the paths for removing oil from water is using oleophilic materials to absorb oil pollution.[339–344] However, such materials cannot be reused after the first oil capture, due to the enormous difficulty in removing absorbed oil, which causes a huge waste of oil and oleophilic materials. It is thus desirable to develop new oil absorbing materials that can repeatedly capture and release the oil droplet/layer. Jin *et al.* fabricated a superamphiphobic organosilane network surface through the phase separation reaction and subsequent 1*H*,1*H*,2*H*,2*H*-perfluorodecyltrichlorosilane grafting.[96] Interestingly, the resultant surface exhibited superoleophilicity in water, which was the opposite of superoleophobicity in air. Once an underwater oil droplet contacts the surface, the oil spreads out quickly, resulting in a flat and ultrathin oil film. The as-prepared materials were applied in a designer "oil capture system". A lot of 1,2-dichloroethane droplets with density larger than that of water were pre-sprayed on the bottom of a water-filled glass container. Next, they moved an organosilane network coated glass tube to absorb the oil droplets. These droplets were gathered and spontaneously ran into the glass tube. The underwater oil droplets were finally captured and collected. Taking advantage of the superamphiphobicity (in air) of the tube wall, the captured oil could be pushed out easily after shifting the tube to the air environment. If a superhydrophobic/superoleophilic surface was used to perform the oil capture experiment, the surface would be totally wetted and polluted by oil. Therefore, it was the integration of superoleophobicity in air and underwater superoleophilicity that endows the resultant materials with repeatable oil capture function.

6.9 Bioadhesion

Previously, the surface of blood vessels was thought to be smooth; otherwise, the platelets would firmly adhere to the inner walls of the blood vessels and cause serious thrombosis problems.[345] Recently, a study from Han *et al.* demonstrated that the inner walls of arterial vessels of rats were composed of massive amounts of aligned nanoscale grooves.[346] The nanostructures not only optimize the blood fluid dynamics and thereby weaken the turbulence of blood flow, but also prevent platelets from adhering to the blood vessel wall. Furthermore, they found that the vessel surface was superhydrophilic with a WCA of about 0°. Although the underwater oil-wettability was not investigated by them, we assume that there is a strong possibility that the vessel surface will show superoleophobicity in water. The superhydrophilicity and underwater superoleophobicity of blood vessel walls are quite conducive to inhibiting protein adsorption, and thus further inhibiting the adhesion of platelets.

Blood-compatible materials and devices are very important in implantation and many other medical treatments.[299,345,347,348] However, most implanted materials easily absorb blood proteins and cause platelet activation and adhesion. As a result, blood coagulation and thrombosis usually occur in the repaired human and animal body. The blood compatibility of materials is determined by many factors, *e.g.*, chemical composition, surface morphology, charge, and wettability.[44,48,50,349] Particularly, wettability has a significant effect on protein adsorption, platelet activation/adhesion, and blood coagulation.[4,24,46,47,49,350] Chen *et al.* investigated the platelet adhesion on PNIPAAm modified silicon nanowire array (SiNWAs) surfaces (SiNWA-PNIPAAm) *in vitro*.[97] The SiNWA was obtained by chemical etching of the silicon wafer in $AgNO_3$/HF aqueous solution. The PNIPAAm molecular layer was then coated on SiNWA using a surface-initiated atom transfer radical polymerization method. There were many silicon nanoclusters made up of several nanowires on the resultant surface. The average diameter of the nanowires was 67.9 ± 4.3 nm and the length was 25 ± 3.3 μm. The PNIPAAm coating was about 32.3 nm thick. It was found that the resultant SiNWA-PNIPAAm surface had a strong inhibition effect on the activation and adhesion of platelets. The platelet adhesion test was performed *in vitro via* the platelet-suspension method and inspected by SEM imaging, as shown in Fig. 30a–i. Only a few platelets adhered to the as-prepared surface, both above (37 °C) and below (20 °C) the LCST (~32 °C) of PNIPAAm (Fig. 30e and i). In contrast, lots of platelets adhered to other surfaces, including smooth silicon wafer (Fig. 30b and f), non-grafted bare SiNWA (Fig. 30c and g), and 37 °C PNIPAAm-grafted smooth silicon wafer (Fig. 30h). When the SiNWA-PNIPAAm sample was immersed in water, its surface showed quasi-superoleophobicity, regardless of whether the temperature was lower or higher than the LCST. The oil-adhesive force was measured to be only 4.6 μN at 20 °C and 3.2 μN at 37 °C, revealing that the oil-adhesion is very low in water. The underwater quasi-superoleophobicity and ultralow oil-adhesion implied that water filled, and was trapped in, the rough microstructures of the SiNWA-PNIPAAm surface after immersion in water. Therefore, the SiNWA-PNIPAAm had a high ratio of water content. In general, the high water content in the hydration layer of the polymer outer chains could prevent the protein or cells from adsorbing (Fig. 30j and k). Therefore, the adhesion of platelets was significantly reduced on the underwater superoleophobic SiNWA-PNIPAAm surfaces.

6.10 Guiding the movement of oil droplets

Wu *et al.* used the femtosecond laser to ablate a nickel substrate in sucrose solution and fabricated hierarchical microcone arrays on the nickel surface.[98] The ablated surface showed superhydrophilicity and superoleophilicity in air, and superoleophobicity in water. A hollow "Y" shaped path that was like a flat canal was designed. The middle part of the path was a bare flat nickel surface without any treatment. The untreated nickel was weakly oleophobic underwater. Both sides of the path were irradiated by femtosecond laser, forming two underwater

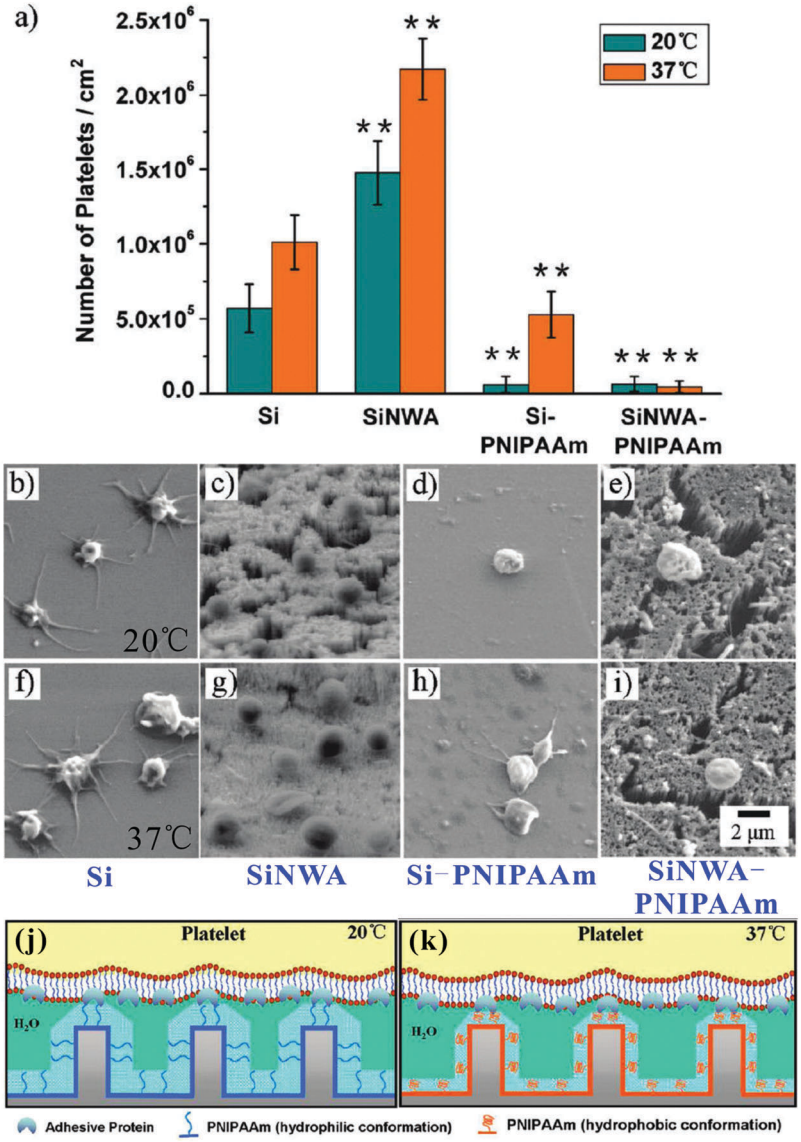

Fig. 30 Anti-platelet ability of the underwater superoleophobic substrate. (a) Statistical number of adhered platelets on different surfaces at 20 °C and 37 °C, respectively. Si: flat bare silicon; SiNWA: silicon nanowire array; Si-PNIPAAm: PNIPAAm modified smooth silicon; SiNWA-PNIPAAm: PNIPAAm modified silicon nanowire array. (b–i) SEM images of the adhered platelets on different substrates: (b and f) Si, (c and g) SiNWA, (d and h) Si-PNIPAAm, and (e and i) SiNWA-PNIPAAm. The platelets in (b–e) were cultured at 20 °C, while the platelets in (f–i) were cultured at 37 °C. (j and k) Schematic illustration of the anti-platelet ability of the underwater quasi-superoleophobic SiNWA-PNIPAAm surfaces at (j) 20 °C and (k) 37 °C. Reproduced from ref. 97 with permission from ACS, copyright 2009.

superoleophobic thick lines. In water, oil droplets were limited to the middle path and were only able to slide along the set path between two laser induced lines on both sides. The remarkable underwater superoleophobicity of the two side lines provided enough energy barrier to avoid the oil droplet derailment. When two oil droplets were placed on the two ends of the "Y" shaped path, respectively, the droplets could travel along the "Y" shaped line, and finally mixed together with the sheet being slightly inclined.

6.11 Floating on oil

Most of the earth's surface is covered by liquid, such as oceans, lakes and rivers, and humans constantly think about how to float and travel on the liquid surface. In ancient times, our ancestors mastered the shipbuilding technology. They used the fabricated boats for long-distance travel, transportation, and fishing. The boats generally had a large volume and were made from lightweight materials like wood. In recent years, miniaturization has led to new advantages over past bulky devices, such as low cost, occupying less space, easy portability, and so on. Therefore, the micro-devices that can float and move on liquid surfaces have many significant potential applications such as in water environment monitoring, sensing pollution, supporting the feet of aquatic microrobots.[71,99,100,351,352] In nature, the lotus leaf can float stably on the water surface, even with a heavy frog resting on it (Fig. 31a). Our recent experiment

revealed that the superhydrophobicity of the upper surface not only gives the lotus leaf self-cleaning ability, but also enhances its loading capacity; *i.e.*, it is the superhydrophobicity of the upper surface that endows the lotus leaf with very large loading capacity.[71] The former keeps the lotus leaf clean, while the latter lets the lotus leaf float on the water surface and its upper surface always faces the sky. Both effects benefit its growth by allowing it to receive more sunlight and maximizing photosynthesis. Unlike the leaf-like micro-boat of the lotus leaf, the water strider can also float and even jump on the water surface without sinking, but it has only six superhydrophobic legs (Fig. 31c).[158,159] In addition, it is found that even the small objects whose densities are higher than that of water can float on the surface of water. Fig. 31b and d show the photos of a metal coin and a needle floating on the water surface, respectively.

Our group has made an artificial planar superhydrophobic PDMS micro-boat that has a superhydrophobic upper surface like a lotus leaf.[71] The upper surface of a PDMS wafer (with the thickness of 0.73 mm and the diameter of 4 cm) was fully ablated by femtosecond laser to form hierarchical rough microstructures (Fig. 31e). A water droplet on such a rough surface showed a WCA of $156^\circ \pm 2^\circ$ (inset of Fig. 31e) and a small WSA ($<4^\circ$). The micro-boat could float on the water surface effortlessly, even though it was loaded with some heavy objects, demonstrating a strong loading capacity (Fig. 31f). Although the maximum buoyancy force estimated from the same water volume of the micro-boat was only 0.92 g, the micro-boat could load 5.58 g weights. Interestingly, the micro-boat kept floating even if its top was below the water level, with a curved side water surface (Fig. 31g). Such a water/air meniscus has been also observed by other research groups.[100,353] The curved convex water surface was caused by the water surface tension and the superhydrophobicity of the laser-induced rough PDMS surface. Therefore, the loading capacity was greatly increased because the curved water surface resulted in a very large total displacement. To reveal the underlying mechanism of the superhydrophobic micro-boat's loading capacity, we designed five different types of leaf-like micro-boats and compared their loading capacity. Experimental results demonstrated that the wettability of the micro-boat's lower surface had little impact on its loading capacity, while the superhydrophobicity of its upper surface, especially the superhydrophobicity at the edge of its upper surface, was responsible for the micro-boat's large loading capacity on the water surface. This effect is called the "superhydrophobic edge effect".

As shown in Fig. 31h, the lifting forces exerted on the superhydrophobic micro-boat include the surface tension (F_σ) and the buoyancy force (F_b) acting on the boat's bottom. The maximum total lifting force is equal to the following:[351,352]

$$\begin{aligned} F &= F_\sigma \sin\varphi + F_b = 2\pi\alpha r \sin\varphi + \rho g(z + h_0)S \\ &\approx 2\pi\alpha r \sin\varphi + \rho g\left(z + 2\sqrt{\frac{\alpha}{\rho g}}\sin\frac{\varphi}{2}\right)S \end{aligned} \tag{13}$$

where φ is the bending angle of the curved water profile at the TPCL; α and ρ are the surface tension and density of water,

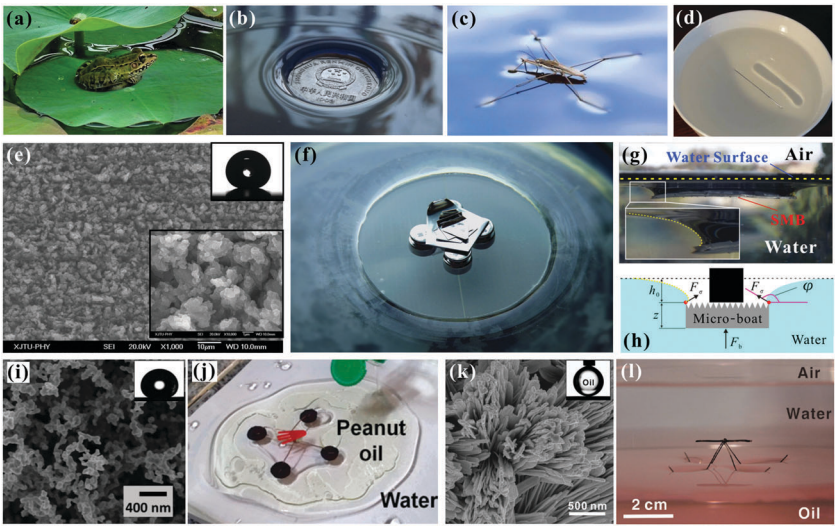

Fig. 31 Superhydrophobic or superoleophobic micro-boats floating on water or oil surfaces. (a–d) Small objects floating on water surface: (a) lotus leaf with a frog resting on it, (b) a metal coin, (c) a water strider, and (d) a metal needle. (e) Femtosecond laser induced microstructure of the upper surface of the artificial superhydrophobic PDMS micro-boat. Upper inset: a water droplet on the micro-boat surface; bottom inset: the high-magnification SEM image of the rough microstructure. (f) Artificial PDMS micro-boat floating on water surface with 5.58 g weights on its surface. (g) Cross-sectional profile of the micro-boat on the water surface. The boundary between the water surface and air is highlighted by yellow dotted lines. (h) Schematic diagram of a loaded superhydrophobic micro-boat on the water surface. (i and j) Artificial micro-boat ("oil strider") with four superoleophobic feet floating on the oil-contaminated water surface: (i) the microstructure of the pan-shaped feet surface, (j) the photo of the oil strider. The inset shows a peanut oil droplet on the superoleophobic feet surface. (k and l) Artificial micro-boat ("oil strider") with four underwater superoleophobic legs floating on the water/oil interface: (k) the microstructure of the wire legs, (l) the photo of the oil strider. The inset shows an oil droplet (1,2-dichloroethane) on the as-prepared copper wires. (a, b and e–h) Reproduced from ref. 71 with permission from IOP, copyright 2014. (i and j) Reproduced from ref. 100 with permission from ACS, copyright 2014. (k and l) Reproduced from ref. 99 with permission from ACS, copyright 2012.

respectively; r and z are the radius and thickness of the circular micro-boat, respectively; g is the gravitational acceleration; h_0 is the distance from the TPCL to the horizontal water level $\left(h_0 \approx 2\sqrt{\frac{\alpha}{\rho g}}\sin\frac{\varphi}{2}\right)$,[351,352] and S is the bottom area of the superhydrophobic micro-boat. For the wire-like micro-boats, the F_b can be neglected because of the small surface area. The lifting force that makes such a micro-boat float on water mainly comes from the surface tension. For example, surface tension endows the water strider with the ability to move on the water surface, since its legs are pretty thin.[158] In contrast, for the planar leaf-like micro-boats, the perimeter $2\pi r \ll 1$ m, F_σ is negligible compared to F_b. Higher CA usually signifies higher φ because both of them describe the surface wettability. Therefore, the above formula reveals that the higher the hydrophobicity of the upper surface of planar micro-boats is, the larger the loading capacity that can be obtained. Superhydrophobicity of the upper surface can make φ large enough and greatly improve the loading capacity of the artificial micro-boat. Our study clarifies the buoyancy generation mechanism of the leaf-like superhydrophobic micro-boat, and is helpful in the design and manufacture of super-buoyant aquatic devices.

Like the superhydrophobic micro-boat floating on water surface, superoleophobicity enables some micro-boats and micro-devices to float and work on oil surfaces. For example, Zhang *et al.* coated stainless steel meshes with a superamphiphobic layer by the processes of burning in a candle flame, silica shell deposition and then fluoroalkylsilane modification.[100] The deposited soot nanoparticles with carbon cores and silica shells formed a loose network on the mesh wire surface (Fig. 31i). The resultant rough mesh showed the OCAs of $155^\circ \pm 3^\circ$ to an *n*-hexadecane droplet and $165^\circ \pm 4^\circ$ to a peanut oil droplet (inset of Fig. 31i). Both those oil droplets had OSAs less than 10° on the mesh. The disk-like superamphiphobic mesh could float on various organic liquid surfaces. The loading capacity of the artificial mesh micro-boat exceeded 15 times its weight on the *n*-hexadecane surface. They further designed a model device using four pan-shaped superamphiphobic meshes as feet, like an "oil strider". The artificial oil strider not only floated on an oil-polluted surface, but also moved freely on the oil surface, guided by applying a permanent magnet (Fig. 31j). Inspired by the unique ability of the water strider to walk and jump on the surface of water, Liu *et al.* made an artificial "oil strider" that had four underwater superoleophobic metal "legs".[99] The legs were copper wires, which were coated by hierarchical rough copper oxide microstructures (Fig. 31k). The rough wires were fabricated through an alkali-corrosion process and exhibited underwater superoleophobicity (inset of Fig. 31k). The metal oil strider could freely float on the oil/water interface; *i.e.*, the oil strider was underwater but on the oil surface (Fig. 31l).

7. Conclusions and future perspectives

This review systematically summarizes the recent developments of superoleophobic surfaces. Much attention is focused on the design principles, fabrication, characteristics, functions, and important applications of various superoleophobic surfaces. The deepening understanding and the constant breakthroughs of such surfaces are very meaningful for most fundamental research and a great number of commercial applications. In the past decade, many important achievements on superoleophobicity have been accomplished, such as presenting the concept of re-entrant surface curvature and opening the branch of underwater superoleophobicity. However, there are still many challenges that need to be addressed. First and foremost, more research is required to further understand the forming principle of the superoleophobic system. The fundamental theory plays a very important guiding role in fabrication and applications of superoleophobic surfaces. Secondly, the current fabrication technologies still need to be improved and perfected because most of the methods are only limited to the laboratory and are difficult to industrialize. Simple, rapid, efficient, low-cost technologies for constructuring superoleophobic interfaces are eagerly awaited. Thirdly, the poor mechanical and chemical durability severely restricts the wide applications of fabricated superoleophobic surfaces. Many surfaces easily lose their superoleophobicity after several cycles of use or being applied in harsh environments. Although a few stable and self-repairing superoleophobic surfaces were developed, there is an unmet need to design more durable superoleophobic surfaces. The underlying determinants for realizing stability need to be studied carefully, such as substrate materials, surface morphology, and surface chemistry. Last but not least, superoleophobicity by itself does not fully satisfy the needs of practical application. Endowing superoleophobic surfaces with multiple functions and smart properties is the major trend in this research field.

The development trend of superoleophobicity may see an explosive growth towards the design, realization, and application of more complicated and subtle superoleophobic surfaces. With more and more scientists and engineers devoted to achieving superoleophobicity, the future of superoleophobic surfaces is bright and exciting, due to their great commercialization value and potential.

Acknowledgements

This work is supported by the National Science Foundation of China under the Grant no. 51335008, 61275008, and 61475124, the Special-funded programme on national key scientific instruments and equipment development of China under the Grant no. 2012YQ12004706, China Postdoctoral Science Foundation under the Grant no. 2016M600786, the Collaborative Innovation Center of Suzhou Nano Science and Technology and the International Joint Research Center for Micro/Nano Manufacturing and Measurement Technologies.

References

1 Y. Tian, B. Su and L. Jiang, *Adv. Mater.*, 2014, **26**, 6872–6897.
2 L. Wen, Y. Tian and L. Jiang, *Angew. Chem., Int. Ed.*, 2015, **54**, 3387–3399.

3 H. Bellanger, T. Darmanin, E. Taffin de Givenchy and F. Guittard, *Chem. Rev.*, 2014, **114**, 2694–2716.
4 Y. Lee, S. H. Park, K. B. Kim and J. K. Lee, *Adv. Mater.*, 2007, **19**, 2330–2335.
5 F. Chen, D. Zhang, Q. Yang, J. L. Yong, G. Du, J. Si, F. Yun and X. Hou, *ACS Appl. Mater. Interfaces*, 2013, **5**, 6777–6792.
6 J. N. Wang, Y. L. Zhang, Y. Liu, W. Zheng, L. P. Lee and H. B. Sun, *Nanoscale*, 2015, **7**, 7101–7114.
7 J. L. Yong, F. Chen, Q. Yang and X. Hou, *Soft Matter*, 2015, **11**, 8897–8906.
8 X. Yao, Y. Song and L. Jiang, *Adv. Mater.*, 2011, **23**, 719–734.
9 K. Liu, X. Yao and L. Jiang, *Chem. Soc. Rev.*, 2010, **39**, 3240–3255.
10 P. Roach, N. J. Shirtcliffe and M. I. Newton, *Soft Matter*, 2008, **4**, 224–240.
11 H. Teisala, M. Tuominen and J. Kuusipalo, *Adv. Mater. Interfaces*, 2014, **1**, 1300026.
12 Z. Chu and S. Seeger, *Chem. Soc. Rev.*, 2014, **43**, 2784–2798.
13 Z. Xue, M. Liu and L. Jiang, *J. Polym. Sci., Part B: Polym. Phys.*, 2012, **50**, 1209–1224.
14 T. Jiang, Z. Guo and W. Liu, *J. Mater. Chem. A*, 2015, **3**, 1811–1827.
15 J. Genzer and K. Efimenko, *Biofouling*, 2006, **22**, 339–360.
16 F. Xia and L. Jiang, *Adv. Mater.*, 2008, **20**, 2842–2858.
17 X.-M. Li, D. Reinhoudt and M. Crego-Calama, *Chem. Soc. Rev.*, 2007, **36**, 1350–1368.
18 Zen Yoshimitsu, Akira Nakajima, Toshiya Watanabe and Kazuhito Hashimoto, *Langmuir*, 2002, **18**, 5818–5822.
19 T. Darmanin and F. Guittard, *J. Mater. Chem. A*, 2014, **2**, 16319–16359.
20 P. Ragesh, V. A. Ganesh, S. V. Nair and A. S. Nair, *J. Mater. Chem. A*, 2014, **2**, 14773–14797.
21 Y. Zhang, Y. Chen, L. Shi, J. Li and Z. Guo, *J. Mater. Chem.*, 2012, **22**, 799–815.
22 S. Nishimoto and B. Bhushan, *RSC Adv.*, 2013, **3**, 671–690.
23 K. Liu and L. Jiang, *Annu. Rev. Mater. Res.*, 2012, **42**, 231–263.
24 L. Shen, B. Wang, J. Wang, J. Fu, C. Picart and J. Ji, *ACS Appl. Mater. Interfaces*, 2012, **4**, 4476–4483.
25 M. Barberoglou, V. Zorba, E. Stratakis, E. Spanakis, P. Tzanetakis, S. H. Anastasiadis and C. Fotakis, *Appl. Surf. Sci.*, 2009, **255**, 5425–5429.
26 X. Gao, X. Yan, X. Yao, L. Xu, K. Zhang, J. Zhang, B. Yang and L. Jiang, *Adv. Mater.*, 2007, **19**, 2213–2217.
27 M. J. Kreder, J. Alvarenga, P. Kim and J. Aizenberg, *Nat. Rev. Mater.*, 2016, **1**, 15003.
28 M. Nosonovsky and V. Hejazi, *ACS Nano*, 2012, **6**, 8488–8491.
29 J. Lv, Y. Song, L. Jiang and J. Wang, *ACS Nano*, 2014, **8**, 3152–3169.
30 F. Shi, J. Niu, J. Liu, F. Liu, Z. Wang, X. Q. Feng and X. Zhang, *Adv. Mater.*, 2007, **19**, 2257–2261.
31 H. Dong, M. Cheng, Y. Zhang, H. Wei and F. Shi, *J. Mater. Chem. A*, 2013, **1**, 5886–5891.
32 Y. Wu, Q. Wei, M. Cai and F. Zhou, *Adv. Mater. Interfaces*, 2015, **2**, 1400392.
33 G. McHale, M. I. Newton and N. J. Shirtcliffe, *Soft Matter*, 2010, **6**, 714–719.
34 N. J. Shirtcliffe, G. McHale, M. I. Newton and Y. Zhang, *ACS Appl. Mater. Interfaces*, 2009, **1**, 1316–1323.
35 G. McHale, N. J. Shirtcliffe, C. R. Evans and M. I. Newton, *Appl. Phys. Lett.*, 2009, **94**, 064104.
36 G.-H. Kim, B.-H. Lee, H. Im, S.-B. Jeon, D. Kim, M.-L. Seol, H. Hwang and Y.-K. Choi, *RSC Adv.*, 2016, **6**, 41914–41918.
37 S. Wang, T. Wang, P. Ge, P. Xue, S. Ye, H. Chen, Z. Li, J. Zhang and B. Yang, *Langmuir*, 2015, **31**, 4032–4039.
38 J. Songok, M. Tuominen, H. Teisala, J. Haapanen, J. Makela, J. Kuusipalo and M. Toivakka, *ACS Appl. Mater. Interfaces*, 2014, **6**, 20060–20066.
39 A. Ghosh, R. Ganguly, T. M. Schutzius and C. M. Megaridis, *Lab Chip*, 2014, **14**, 1538–1550.
40 B. P. Casavant, E. Berthier, A. B. Theberge, J. Berthier, S. I. Montanez-Sauri, L. L. Bischel, K. Brakke, C. J. Hedman, W. Bushman, N. P. Keller and D. J. Beebe, *Proc. Natl. Acad. Sci. U. S. A.*, 2013, **110**, 10111–10116.
41 B. Zhao, J. S. Moore and D. J. Beebe, *Science*, 2001, **291**, 1023–1026.
42 A. Vitale, M. Quaglio, S. L. Marasso, A. Chiodoni, M. Cocuzza and R. Bongiovanni, *Langmuir*, 2013, **29**, 15711–15718.
43 T.-i. Kim and K. Y. Suh, *Soft Matter*, 2009, **5**, 4131–4135.
44 K. W. Kwon, S. S. Choi, S. H. Lee, B. Kim, S. N. Lee, M. C. Park, P. Kim, S. Y. Hwang and K. Y. Suh, *Lab Chip*, 2007, **7**, 1461–1468.
45 H. X. Ren, X. Chen, X. J. Huang, M. Im, D. H. Kim, J. H. Lee, J. B. Yoon, N. Gu, J. H. Liu and Y. K. Choi, *Lab Chip*, 2009, **9**, 2140–2144.
46 E. P. Ivanova, J. Hasan, H. K. Webb, G. Gervinskas, S. Juodkazis, V. K. Truong, A. H. Wu, R. N. Lamb, V. A. Baulin, G. S. Watson, J. A. Watson, D. E. Mainwaring and R. J. Crawford, *Nat. Commun.*, 2013, **4**, 2838.
47 Q. Huang, L. Lin, Y. Yang, R. Hu, E. A. Vogler and C. Lin, *Biomaterials*, 2012, **33**, 8213–8220.
48 A. Ranella, M. Barberoglou, S. Bakogianni, C. Fotakis and E. Stratakis, *Acta Biomater.*, 2010, **6**, 2711–2720.
49 E. Fadeeva, V. K. Truong, M. Stiesch, B. N. Chichkov, R. J. Crawford, J. Wang and E. P. Ivanova, *Langmuir*, 2011, **27**, 3012–3019.
50 E. Stratakis, A. Ranella and C. Fotakis, *Biomicrofluidics*, 2011, **5**, 13411.
51 X. Liu, Y. Liang, F. Zhou and W. Liu, *Soft Matter*, 2012, **8**, 2070–2086.
52 M. Wang, C. Chen, J. Ma and J. Xu, *J. Mater. Chem.*, 2011, **21**, 6962–6967.
53 J. L. Yong, F. Chen, Q. Yang, D. Zhang, G. Du, J. Si, F. Yun and X. Hou, *J. Phys. Chem. C*, 2013, **117**, 24907–24912.
54 J. L. Yong, Q. Yang, F. Chen, D. Zhang, U. Farooq, G. Du and X. Hou, *J. Mater. Chem. A*, 2014, **2**, 5499–5507.
55 J. Li, Z. Jing, F. Zha, Y. Yang, Q. Wang and Z. Lei, *ACS Appl. Mater. Interfaces*, 2014, **6**, 8868–8877.
56 Z. Xue, Y. Cao, N. Liu, L. Feng and L. Jiang, *J. Mater. Chem. A*, 2014, **2**, 2445–2460.

57 L. Feng, Z. Zhang, Z. Mai, Y. Ma, B. Liu, L. Jiang and D. Zhu, *Angew. Chem., Int. Ed.*, 2004, **43**, 2012–2014.
58 S. Wang, Y. Song and L. Jiang, *Nanotechnology*, 2007, **18**, 015103.
59 Y. Yu, H. Chen, Y. Liu, V. Craig, L. H. Li and Y. Chen, *Adv. Mater. Interfaces*, 2014, **1**, 1300002.
60 J. L. Yong, Y. Fang, F. Chen, J. Huo, Q. Yang, H. Bian, G. Du and X. Hou, *Appl. Surf. Sci.*, 2016, **389**, 1148–1155.
61 N. J. Shirtcliffe, G. McHale and M. I. Newton, *Langmuir*, 2009, **25**, 14121–14128.
62 A. Nakajima, *NPG Asia Mater.*, 2011, **3**, 49–56.
63 D. Zahner, J. Abagat, F. Svec, J. M. Frechet and P. A. Levkin, *Adv. Mater.*, 2011, **23**, 3030–3034.
64 H. Mertaniemi, V. Jokinen, L. Sainiemi, S. Franssila, A. Marmur, O. Ikkala and R. H. Ras, *Adv. Mater.*, 2011, **23**, 2911–2914.
65 A. R. Parker and C. R. Lawrence, *Nature*, 2001, **414**, 33–34.
66 L. Zhai, M. C. Berg, F. C. Cebeci, Y. Kim, J. M. Milwid, M. F. Rubner and R. E. Cohen, *Nano Lett.*, 2006, **6**, 1213–1217.
67 R. P. Garrod, L. G. Harris, W. C. Schofield, J. Mcgettrick, L. J. Ward, D. O. Teare and J. P. Badyal, *Langmuir*, 2007, **23**, 689–693.
68 F. De Angelis, F. Gentile, F. Mecarini, G. Das, M. Moretti, P. Candeloro, M. L. Coluccio, G. Cojoc, A. Accardo, C. Liberale, R. P. Zaccaria, G. Perozziello, L. Tirinato, A. Toma, G. Cuda, R. Cingolani and E. Di Fabrizio, *Nat. Photonics*, 2011, **5**, 682–687.
69 Q. X. Zhang, Y. X. Chen, Z. Guo, H. L. Liu, D. P. Wang and X. J. Huang, *ACS Appl. Mater. Interfaces*, 2013, **5**, 10633–10642.
70 B.-B. Xu, Y.-L. Zhang, W.-Y. Zhang, X.-Q. Liu, J.-N. Wang, X.-L. Zhang, D.-D. Zhang, H.-B. Jiang, R. Zhang and H.-B. Sun, *Adv. Opt. Mater.*, 2013, **1**, 56–60.
71 J. L. Yong, Q. Yang, F. Chen, D. Zhang, G. Du, J. Si, F. Yun and X. Hou, *J. Micromech. Microeng.*, 2014, **24**, 035006.
72 A. Tuteja, W. Choi, M. Ma, J. M. Mabry, S. A. Mazzella, G. C. Rutledge, G. H. McKinley and R. E. Cohen, *Science*, 2007, **318**, 1618–1622.
73 A. Tuteja, W. Choi, J. M. Mabry, G. H. McKinley and R. E. Cohen, *Proc. Natl. Acad. Sci. U. S. A.*, 2008, **105**, 18200–18205.
74 http://www.surface-tension.de/.
75 S. Pan, A. K. Kota, J. M. Mabry and A. Tuteja, *J. Am. Chem. Soc.*, 2013, **135**, 578–581.
76 M. Liu, S. Wang, Z. Wei, Y. Song and L. Jiang, *Adv. Mater.*, 2009, **21**, 665–669.
77 X. Liu, J. Zhou, Z. Xue, J. Gao, J. Meng, S. Wang and L. Jiang, *Adv. Mater.*, 2012, **24**, 3401–3405.
78 J. L. Yong, F. Chen, Q. Yang, U. Farooq, H. Bian, G. Du and X. Hou, *Appl. Phys. A: Mater. Sci. Process.*, 2015, **119**, 837–844.
79 D. Wu, S. Z. Wu, Q. D. Chen, S. Zhao, H. Zhang, J. Jiao, J. A. Piersol, J. N. Wang, H. B. Sun and L. Jiang, *Lab Chip*, 2011, **11**, 3873–3879.
80 E. Zhang, Z. Cheng, T. Lv, L. Li and Y. Liu, *Nanoscale*, 2015, **7**, 19293–19299.
81 B. Wang, W. Liang, Z. Guo and W. Liu, *Chem. Soc. Rev.*, 2015, **44**, 336–361.
82 Z. Chu, Y. Feng and S. Seeger, *Angew. Chem., Int. Ed.*, 2015, **54**, 2328–2338.
83 J. L. Yong, F. Chen, Q. Yang, H. Bian, G. Du, C. Shan, J. Huo, Y. Fang and X. Hou, *Adv. Mater. Interfaces*, 2016, **3**, 1500650.
84 K. Li, J. Ju, Z. Xue, J. Ma, L. Feng, S. Gao and L. Jiang, *Nat. Commun.*, 2013, **4**, 2276.
85 C. F. Wang, F. S. Tzeng, H. G. Chen and C. J. Chang, *Langmuir*, 2012, **28**, 10015–10019.
86 W. Zhang, Z. Shi, F. Zhang, X. Liu, J. Jin and L. Jiang, *Adv. Mater.*, 2013, **25**, 2071–2076.
87 S. J. Gao, Z. Shi, W. B. Zhang, F. Zhang and J. Jin, *ACS Nano*, 2014, **8**, 6344–6352.
88 G. Ju, M. Cheng and F. Shi, *NPG Asia Mater.*, 2014, **6**, e111.
89 X. Yao, J. Gao, Y. Song and L. Jiang, *Adv. Funct. Mater.*, 2011, **21**, 4270–4276.
90 J. L. Yong, Q. Yang, F. Chen, H. Bian, G. Du, U. Farooq and X. Hou, *Adv. Mater. Interfaces*, 2015, **2**, 1400388.
91 Z. Cheng, H. Liu, H. Lai, Y. Du, K. Fu, C. Li, J. Yu, N. Zhang and K. Sun, *ACS Appl. Mater. Interfaces*, 2015, **7**, 20410–20417.
92 G. Li, Z. Zhang, P. Wu, S. Wu, Y. Hu, W. Zhu, J. Li, D. Wu, X. Li and J. Chu, *RSC Adv.*, 2016, **6**, 37463–37471.
93 B. Su, S. Wang, Y. Song and L. Jiang, *Soft Matter*, 2011, **7**, 51445149.
94 J. L. Yong, F. Chen, Q. Yang, D. Zhang, U. Farooq, G. Du and X. Hou, *J. Mater. Chem. A*, 2014, **2**, 8790.
95 J. L. Yong, Q. Yang, F. Chen, G. Du, C. Shan, U. Farooq, J. Wang and X. Hou, *RSC Adv.*, 2015, **5**, 40907–40911.
96 M. Jin, J. Wang, X. Yao, M. Liao, Y. Zhao and L. Jiang, *Adv. Mater.*, 2011, **23**, 2861–2864.
97 L. Chen, M. Liu, H. Bai, P. Chen, F. Xia, D. Han and L. Jiang, *J. Am. Chem. Soc.*, 2009, **131**, 10467–10472.
98 G. Li, Y. Lu, P. Wu, Z. Zhang, J. Li, W. Zhu, Y. Hu, D. Wu and J. Chu, *J. Mater. Chem. A*, 2015, **3**, 18675–18683.
99 X. Liu, J. Gao, Z. Xue, L. Chen, L. Lin, L. Jiang and S. Wang, *ACS Nano*, 2012, **6**, 5614–5620.
100 J. Zhang, X. Deng, H. J. Butt and D. Vollmer, *Langmuir*, 2014, **30**, 10637–10642.
101 K. Tsujii, T. Yamamoto, T. Onda and S. Shibuichi, *Angew. Chem., Int. Ed.*, 1997, **36**, 1011–1012.
102 J. L. Yong, F. Chen, Q. Yang, Y. Fang, J. Huo and X. Hou, *Chem. Commun.*, 2015, **51**, 9813–9816.
103 H. Zhao, K. Y. Law and V. Sambhy, *Langmuir*, 2011, **27**, 5927–5935.
104 M. Im, H. Im, J.-H. Lee, J.-B. Yoon and Y.-K. Choi, *Soft Matter*, 2010, **6**, 1401–1404.
105 L. Yuan, T. Wu, W. Zhang, S. Ling, R. Xiang, X. Gui, Y. Zhu and Z. Tang, *J. Mater. Chem. A*, 2014, **2**, 6952–6959.
106 A. Ahuja, J. A. Taylor, V. Lifton, A. A. Sidorenko, T. R. Salamon, E. J. Lobaton, A. P. Kolodner and T. N. Krupenkin, *Langmuir*, 2008, **24**, 9–14.
107 T. L. Liu and C. J. Kim, *Science*, 2014, **346**, 1096–1100.
108 A. K. Kota, Y. Li, J. M. Mabry and A. Tuteja, *Adv. Mater.*, 2012, **24**, 5838–5843.

109 A. K. Kota, G. Kwon and A. Tuteja, *NPG Asia Mater.*, 2014, **6**, e109.
110 A. K. Kota, J. M. Mabry and A. Tuteja, *Surf. Innovations*, 2013, **1**, 71–83.
111 L. Lin, M. Liu, L. Chen, P. Chen, J. Ma, D. Han and L. Jiang, *Adv. Mater.*, 2010, **22**, 4826–4830.
112 Y. Huang, M. Liu, J. Wang, J. Zhou, L. Wang, Y. Song and L. Jiang, *Adv. Funct. Mater.*, 2011, **21**, 4436–4441.
113 F. Zhang, W. B. Zhang, Z. Shi, D. Wang, J. Jin and L. Jiang, *Adv. Mater.*, 2013, **25**, 4192–4198.
114 X. Gao, L. P. Xu, Z. Xue, L. Feng, J. Peng, Y. Wen, S. Wang and X. Zhang, *Adv. Mater.*, 2014, **26**, 1771–1775.
115 K. He, H. Duan, G. Y. Chen, X. Liu, W. Yang and D. Wang, *ACS Nano*, 2015, **9**, 9188–9198.
116 Y. Cai, Q. Lu, X. Guo, S. Wang, J. Qiao and L. Jiang, *Adv. Mater.*, 2015, **27**, 4162–4168.
117 X. Deng, L. Mammen, H. J. Butt and D. Vollmer, *Science*, 2012, **335**, 67–70.
118 A. Steele, I. Bayer and E. Loth, *Nano Lett.*, 2009, **9**, 501–505.
119 T. Darmanin and F. Guittard, *J. Am. Chem. Soc.*, 2009, **131**, 7928–7933.
120 J. Zhang and S. Seeger, *Angew. Chem., Int. Ed.*, 2011, **50**, 6652–6656.
121 H. Wang, Y. Xue, J. Ding, L. Feng, X. Wang and T. Lin, *Angew. Chem., Int. Ed.*, 2011, **50**, 11433–11436.
122 Y. Hu, Q. Yang, F. Chen, H. Bian, Z. Deng, G. Du, J. Si, F. Yun and X. Hou, *Appl. Surf. Sci.*, 2014, **292**, 285–290.
123 A. K. Kota, G. Kwon, W. Choi, J. M. Mabry and A. Tuteja, *Nat. Commun.*, 2012, **3**, 1025.
124 J. Yang, H. Song, B. Chen, H. Tang and C. Li, *RSC Adv.*, 2014, **4**, 14227–14232.
125 H. Zhao and K. Y. Law, *Langmuir*, 2012, **28**, 11812–11818.
126 J. L. Yong, F. Chen, Q. Yang, U. Farooq, H. Bian, G. Du and X. Hou, *Appl. Phys. Lett.*, 2014, **105**, 071608.
127 Y. Cai, L. Lin, Z. Xue, M. Liu, S. Wang and L. Jiang, *Adv. Funct. Mater.*, 2014, **24**, 809–816.
128 P. Mazumder, Y. Jiang, D. Baker, A. Carrilero, D. Tulli, D. Infante, A. T. Hunt and V. Pruneri, *Nano Lett.*, 2014, **14**, 4677–4681.
129 J. L. Yong, F. Chen, Q. Yang, G. Du, C. Shan, H. Bian, U. Farooq and X. Hou, *J. Mater. Chem. A*, 2015, **3**, 9379–9384.
130 F. Chen, J. Song, Y. Lu, S. Huang, X. Liu, J. Sun, C. J. Carmalt, I. P. Parkin and W. Xu, *J. Mater. Chem. A*, 2015, **3**, 20999–21008.
131 H. Zhou, H. Wang, H. Niu, A. Gestos and T. Lin, *Adv. Funct. Mater.*, 2013, **23**, 1664–1670.
132 X. Wang, X. Liu, F. Zhou and W. Liu, *Chem. Commun.*, 2011, **47**, 2324–2326.
133 J. Li, L. Yan, H. Li, W. Li, F. Zha and Z. Lei, *J. Mater. Chem. A*, 2015, **3**, 14696–14702.
134 J. Li, D. Li, Y. Yang, J. Li, F. Zha and Z. Lei, *Green Chem.*, 2016, **18**, 541–549.
135 E. Zhang, Z. Cheng, T. Lv, Y. Qian and Y. Liu, *J. Mater. Chem. A*, 2015, **3**, 13411–13417.
136 J. L. Yong, F. Chen, Q. Yang, U. Farooq and X. Hou, *J. Mater. Chem. A*, 2015, **3**, 10703–10709.
137 H. Wang and Z. Guo, *Appl. Phys. Lett.*, 2014, **104**, 183703.
138 M. Zhang, T. Zhang and T. Cui, *Langmuir*, 2011, **27**, 9295–9301.
139 Z. Cheng, H. Lai, Y. Du, K. Fu, R. Hou, C. Li, N. Zhang and K. Sun, *ACS Appl. Mater. Interfaces*, 2014, **6**, 636–641.
140 Q. Cheng, M. Li, F. Yang, M. Liu, L. Li, S. Wang and L. Jiang, *Soft Matter*, 2012, **8**, 6740–6743.
141 M. Li, B. Wang, L. Heng and L. Jiang, *Adv. Mater. Interfaces*, 2014, **1**, 1400298.
142 L. Chen, M. Liu, L. Lin, T. Zhang, J. Ma, Y. Song and L. Jiang, *Soft Matter*, 2010, **6**, 2708–2712.
143 H. Liu, X. Zhang, S. Wang and L. Jiang, *Small*, 2015, **11**, 3338–3342.
144 C. Ding, Y. Zhu, M. Liu, L. Feng, M. Wan and L. Jiang, *Soft Matter*, 2012, **8**, 9064–9068.
145 M. Liu, X. Liu, C. Ding, Z. Wei, Y. Zhu and L. Jiang, *Soft Matter*, 2011, **7**, 4163–4165.
146 H. Feng, X. Xu, W. Hao, Y. Du, D. Tian and L. Jiang, *Phys. Chem. Chem. Phys.*, 2016, **18**, 16202–16207.
147 T. Darmanin and F. Guittard, *Mater. Today*, 2015, **18**, 273–285.
148 B. Bhushan, *Philos. Trans. R. Soc., A*, 2009, **367**, 1445–1486.
149 M. J. Liu, Y. M. Zheng, J. Zhai and L. Jiang, *Acc. Chem. Res.*, 2010, **43**, 368–377.
150 Y. L. Zhang, Q. D. Chen, Z. Jin, E. Kim and H. B. Sun, *Nanoscale*, 2012, **4**, 4858–4869.
151 W. Barthlott and C. Neinhuis, *Planta*, 1997, **202**, 1–8.
152 V. Zorba, E. Stratakis, M. Barberoglou, E. Spanakis, P. Tzanetakis, S. H. Anastasiadis and C. Fotakis, *Adv. Mater.*, 2008, **20**, 4049–4054.
153 L. Feng, Y. Zhang, J. Xi, Y. Zhu, N. Wang, F. Xia and L. Jiang, *Langmuir*, 2008, **24**, 4114–4119.
154 L. Feng, S. H. Li, Y. S. Li, H. J. Li, L. J. Zhang, J. Zhai, Y. L. Song, B. Q. Liu, L. Jiang and D. B. Zhu, *Adv. Mater.*, 2002, **14**, 1857–1860.
155 D. Wu, J.-N. Wang, S.-Z. Wu, Q.-D. Chen, S. Zhao, H. Zhang, H.-B. Sun and L. Jiang, *Adv. Funct. Mater.*, 2011, **21**, 2927–2932.
156 Y. Zheng, X. Gao and L. Jiang, *Soft Matter*, 2007, **3**, 178–182.
157 W. Barthlott, T. Schimmel, S. Wiersch, K. Koch, M. Brede, M. Barczewski, S. Walheim, A. Weis, A. Kaltenmaier, A. Leder and H. F. Bohn, *Adv. Mater.*, 2010, **22**, 2325–2328.
158 X. Gao and L. Jiang, *Nature*, 2004, **432**, 36.
159 D. L. Hu, B. Chan and J. W. Bush, *Nature*, 2003, **424**, 663–666.
160 K. Liu and L. Jiang, *Nano Today*, 2011, **6**, 155–175.
161 L. Zhang, Z. Zhou, B. Cheng, J. M. Desimone and E. T. Samulski, *Langmuir*, 2006, **22**, 8576–8580.
162 Y.-L. Zhang, H. Xia, E. Kim and H.-B. Sun, *Soft Matter*, 2012, **8**, 11217.
163 I. A. Larmour, S. E. J. Bell and G. C. Saunders, *Angew. Chem.*, 2007, **119**, 1740–1742.
164 Y. Zhao, Y. Tang, X. Wang and T. Lin, *Appl. Surf. Sci.*, 2010, **256**, 6736–6742.
165 N. J. Shirtcliffe, G. McHale, M. I. Newton, C. C. Perry and F. B. Pyatt, *Appl. Phys. Lett.*, 2006, **89**, 104106.

166 R. S. Seymour and S. K. Hetz, *J. Exp. Biol.*, 2011, **214**, 2175–2181.
167 R. Helbig, J. Nickerl, C. Neinhuis and C. Werner, *PLoS One*, 2011, **6**, e25105.
168 R. Hensel, A. Finn, R. Helbig, H.-G. Braun, C. Neinhuis, W.-J. Fischer and C. Werner, *Adv. Mater.*, 2014, **26**, 2029–2033.
169 A. B. D. Cassie and S. Baxter, *Trans. Faraday Soc.*, 1944, **40**, 546.
170 Q. Cheng, M. Li, Y. Zheng, B. Su, S. Wang and L. Jiang, *Soft Matter*, 2011, **7**, 5948–5951.
171 R. N. Wenzel, *Ind. Eng. Chem.*, 1936, **28**, 988–994.
172 R. J. Good, *J. Am. Chem. Soc.*, 1952, **74**, 5041–5042.
173 G. Whyman, E. Bormashenko and T. Stein, *Chem. Phys. Lett.*, 2008, **450**, 355–359.
174 E. Bormashenko, *Colloids Surf., A*, 2009, **345**, 163–165.
175 E. Bormashenko, *J. Phys. Chem. C*, 2009, **113**, 17275–17277.
176 M. Liu and L. Jiang, *Adv. Funct. Mater.*, 2010, **20**, 3753–3764.
177 J. Li, X. Liu, Y. Ye, H. Zhou and J. Chen, *J. Phys. Chem. C*, 2011, **115**, 4726–4729.
178 Z. Cheng, M. Du, H. Lai, N. Zhang and K. Sun, *Nanoscale*, 2013, **5**, 2776–2783.
179 J. L. Yong, Q. Yang, F. Chen, D. Zhang, G. Du, H. Bian, J. Si, F. Yun and X. Hou, *Appl. Surf. Sci.*, 2014, **288**, 579–583.
180 S. Wang and L. Jiang, *Adv. Mater.*, 2007, **19**, 3423–3424.
181 S.-M. Lee and T. H. Kwon, *J. Micromech. Microeng.*, 2007, **17**, 687–692.
182 S. Tian, L. Li, W. Sun, X. Xia, D. Han, J. Li and C. Gu, *Sci. Rep.*, 2012, **2**, 511.
183 H. Y. Erbil and C. E. Cansoy, *Langmuir*, 2009, **25**, 14135–14145.
184 K. Li, X. Zeng, H. Li, X. Lai, C. Ye and H. Xie, *Appl. Surf. Sci.*, 2013, **279**, 458–463.
185 A. Marmur, *Soft Matter*, 2012, **8**, 6867–6870.
186 G. Whyman and E. Bormashenko, *Langmuir*, 2011, **27**, 8171–8176.
187 S. S. Chhatre, W. Choi, A. Tuteja, K. C. Park, J. M. Mabry, G. H. McKinley and R. E. Cohen, *Langmuir*, 2010, **26**, 4027–4035.
188 M. Guo, B. Ding, X. Li, X. Wang, J. Yu and M. Wang, *J. Phys. Chem. C*, 2010, **114**, 916–921.
189 G.-R. Choi, J. Park, J.-W. Ha, W.-D. Kim and H. Lim, *Macromol. Mater. Eng.*, 2010, **295**, 995–1002.
190 W. Choi, A. Tuteja, S. Chhatre, J. M. Mabry, R. E. Cohen and G. H. McKinley, *Adv. Mater.*, 2009, **21**, 2190–2195.
191 J. Yang, Z. Zhang, X. Men, X. Xu and X. Zhu, *New J. Chem.*, 2011, **35**, 576–580.
192 H. Meng, S. Wang, J. Xi, Z. Tang and L. Jiang, *J. Phys. Chem. C*, 2008, **112**, 11454–11458.
193 W. S. Y. Wong, G. Liu, N. Nasiri, C. Hao, Z. Wang and A. Tricoli, *ACS Nano*, 2017, **11**, 587–596.
194 W. S. Y. Wong, G. Liu and A. Tricoli, *Small*, 2017, **13**, 1603688.
195 D. Wang, X. Wang, X. Liu and F. Zhou, *J. Phys. Chem. C*, 2010, **114**, 9938–9944.
196 H. Wang, Y. Xue and T. Lin, *Soft Matter*, 2011, **7**, 8158–8161.
197 S. Srinivasan, S. S. Chhatre, J. M. Mabry, R. E. Cohen and G. H. McKinley, *Polymer*, 2011, **52**, 3209–3218.
198 K. Ellinas, M. Chatzipetrou, I. Zergioti, A. Tserepi and E. Gogolides, *Adv. Mater.*, 2015, **27**, 2231–2235.
199 S. Wooh, H. Huesmann, M. N. Tahir, M. Paven, K. Wichmann, D. Vollmer, W. Tremel, P. Papadopoulos and H. J. Butt, *Adv. Mater.*, 2015, **27**, 7338–7343.
200 H. Vahabi, W. Wang, S. Movafaghi and A. K. Kota, *ACS Appl. Mater. Interfaces*, 2016, **8**, 21962–21967.
201 Y. Lu, J. Song, X. Liu, W. Xu, Y. Xing and Z. Wei, *ACS Sustainable Chem. Eng.*, 2013, **1**, 102–109.
202 S. P. P. Kobaku, A. K. Kota, D. H. Lee, J. M. Mabry and A. Tuteja, *Angew. Chem., Int. Ed.*, 2012, **51**, 10109–10113.
203 Z. He, M. Ma, X. Lan, F. Chen, K. Wang, H. Deng, Q. Zhang and Q. Fu, *Soft Matter*, 2011, **7**, 6435–6443.
204 H. Zhou, H. Wang, H. Liu and T. Lin, *Sci. Rep.*, 2013, **3**, 2964.
205 J. Yang, Z. Zhang, X. Xu, X. Zhu, X. Men and X. Zhou, *J. Mater. Chem.*, 2012, **22**, 2834–2837.
206 S. Pan, R. Guo and W. Xu, *AIChE J.*, 2014, **60**, 2752–2756.
207 S. Taleb, T. Darmanin and F. Guittard, *ACS Appl. Mater. Interfaces*, 2014, **6**, 7953–7960.
208 T. S. Wong, S. H. Kang, S. K. Tang, E. J. Smythe, B. D. Hatton, A. Grinthal and J. Aizenberg, *Nature*, 2011, **477**, 443–447.
209 H. F. Bohn and W. Federle, *Proc. Natl. Acad. Sci. U. S. A.*, 2004, **101**, 14138–14143.
210 U. Manna and D. M. Lynn, *Adv. Mater.*, 2015, **27**, 3007–3012.
211 S. Nishioka, M. Tenjimbayashi, K. Manabe, T. Matsubayashi, K. Suwabe, K. Tsukada and S. Shiratori, *RSC Adv.*, 2016, **6**, 47579–47587.
212 M. Röhrig, M. Mail, M. Schneider, H. Louvin, A. Hopf, T. Schimmel, M. Worgull and H. Hölscher, *Adv. Mater. Interfaces*, 2014, **1**, 1300083.
213 N. Vogel, R. A. Belisle, B. Hatton, T. S. Wong and J. Aizenberg, *Nat. Commun.*, 2013, **4**, 2167.
214 M. J. Hancock, K. Sekeroglu and M. C. Demirel, *Adv. Funct. Mater.*, 2012, **22**, 2223–2234.
215 Y. Fang, J. L. Yong, F. Chen, J. Huo, Q. Yang, H. Bian, G. Du and X. Hou, *Appl. Phys. A: Mater. Sci. Process.*, 2016, **122**, 827.
216 Y. Lai, X. Gao, H. Zhuang, J. Huang, C. Lin and L. Jiang, *Adv. Mater.*, 2009, **21**, 3799–3803.
217 C. Li, R. Guo, X. Jiang, S. Hu, L. Li, X. Cao, H. Yang, Y. Song, Y. Ma and L. Jiang, *Adv. Mater.*, 2009, **21**, 4254–4258.
218 X. D. Zhao, H. M. Fan, X. Y. Liu, H. Pan and H. Y. Xu, *Langmuir*, 2011, **27**, 3224–3228.
219 D. Zhang, F. Chen, Q. Yang, J. L. Yong, H. Bian, Y. Ou, J. Si, X. Meng and X. Hou, *ACS Appl. Mater. Interfaces*, 2012, **4**, 4905–4912.
220 M. Jin, X. Feng, J. Xi, J. Zhai, K. Cho, L. Feng and L. Jiang, *Macromol. Rapid Commun.*, 2005, **26**, 1805–1809.
221 J. L. Yong, F. Chen, Q. Yang, D. Zhang, H. Bian, G. Du, J. Si, X. Meng and X. Hou, *Langmuir*, 2013, **29**, 3274–3279.

222 F. Chen, D. Zhang, Q. Yang, X. Wang, B. Dai, X. Li, X. Hao, Y. Ding, J. Si and X. Hou, *Langmuir*, 2011, **27**, 359–365.
223 E. Mele, S. Girardo and D. Pisignano, *Langmuir*, 2012, **28**, 5312–5317.
224 W. Li, G. Fang, Y. Li and G. Qiao, *J. Phys. Chem. B*, 2008, **112**, 7234–7243.
225 M. Morita, T. Koga, H. Otsuka and A. Takahara, *Langmuir*, 2005, **21**, 911–918.
226 J. L. Yong, Q. Yang, F. Chen, D. Zhang, G. Du, H. Bian, J. Si and X. Hou, *RSC Adv.*, 2014, **4**, 8138–8143.
227 J. Y. Chung, J. P. Youngblood and C. M. Stafford, *Soft Matter*, 2007, **3**, 1163–1169.
228 K. Sekeroglu, U. A. Gurkan, U. Demirci and M. C. Demirel, *Appl. Phys. Lett.*, 2011, **99**, 63703.
229 C. Py, P. Reverdy, L. Doppler, J. Bico, B. Roman and C. N. Baroud, *Phys. Rev. Lett.*, 2007, **98**, 156103.
230 D. Zhang, F. Chen, Q. Yang, J. Si and X. Hou, *Soft Matter*, 2011, **7**, 8337–8342.
231 S. Neuhaus, N. D. Spencer and C. Padeste, *ACS Appl. Mater. Interfaces*, 2012, **4**, 123–130.
232 S. Z. Wu, D. Wu, J. Yao, Q. D. Chen, J. N. Wang, L. G. Niu, H. H. Fang and H. B. Sun, *Langmuir*, 2010, **26**, 12012–12016.
233 S.-G. Park, J. H. Moon, H. C. Jeon and S.-M. Yang, *Soft Matter*, 2012, **8**, 4567–4570.
234 J. N. Wang, R. Q. Shao, Y. L. Zhang, L. Guo, H. B. Jiang, D. X. Lu and H. B. Sun, *Chem. – Asian J.*, 2012, **7**, 301–304.
235 A. T. Paxson and K. K. Varanasi, *Nat. Commun.*, 2013, **4**, 1492.
236 W. Xu and C. H. Choi, *Phys. Rev. Lett.*, 2012, **109**, 024504.
237 K. Golovin, D. H. Lee, J. M. Mabry and A. Tuteja, *Angew. Chem., Int. Ed.*, 2013, **52**, 13007–13011.
238 B. Li, J. Zhang, Z. Gao and Q. Wei, *J. Mater. Chem. A*, 2016, **4**, 953–960.
239 X. Deng, L. Mammen, Y. Zhao, P. Lellig, K. Müllen, C. Li, H.-J. Butt and D. Vollmer, *Adv. Mater.*, 2011, **23**, 2962–2965.
240 J. T. Han, S. Y. Kim, J. S. Woo and G.-W. Lee, *Adv. Mater.*, 2008, **20**, 3724–3727.
241 P. A. Levkin, F. Svec and J. M. Frechet, *Adv. Funct. Mater.*, 2009, **19**, 1993–1998.
242 Y. Chen, Y. Zhang, L. Shi, J. Li, Y. Xin, T. Yang and Z. Guo, *Appl. Phys. Lett.*, 2012, **101**, 033701.
243 Y. L. Zhang, J. N. Wang, Y. He, Y. He, B. B. Xu, S. Wei and F. S. Xiao, *Langmuir*, 2011, **27**, 12585–12590.
244 J. Bravo, L. Zhai, Z. Wu, R. E. Cohen and M. F. Rubner, *Langmuir*, 2007, **23**, 7293–7298.
245 Y. Li, F. Liu and J. Sun, *Chem. Commun.*, 2009, 2730–2732.
246 R. G. Karunakaran, C. H. Lu, Z. Zhang and S. Yang, *Langmuir*, 2011, **27**, 4594–4602.
247 L. Xu, R. G. Karunakaran, J. Guo and S. Yang, *ACS Appl. Mater. Interfaces*, 2012, **4**, 1118–1125.
248 Y. Liu, X. Chen and J. H. Xin, *J. Mater. Chem.*, 2009, **19**, 5602–5611.
249 T. Verho, C. Bower, P. Andrew, S. Franssila, O. Ikkala and R. H. Ras, *Adv. Mater.*, 2011, **23**, 673–678.
250 C.-H. Xue and J.-Z. Ma, *J. Mater. Chem. A*, 2013, **1**, 4146–4161.
251 Z. Guo, F. Zhou, J. Hao and W. Liu, *J. Am. Chem. Soc.*, 2005, **127**, 15670–15671.
252 H. S. Lim, J. H. Baek, K. Park, H. S. Shin, J. Kim and J. H. Cho, *Adv. Mater.*, 2010, **22**, 2138–2141.
253 B. Deng, R. Cai, Y. Yu, H. Jiang, C. Wang, J. Li, L. Li, M. Yu, J. Li, L. Xie, Q. Huang and C. Fan, *Adv. Mater.*, 2010, **22**, 5473–5477.
254 B. Li and J. Zhang, *Chem. Commun.*, 2016, **52**, 2744–2747.
255 J. Ou, W. Hu, S. Liu, M. Xue, F. Wang and W. Li, *ACS Appl. Mater. Interfaces*, 2013, **5**, 10035–10041.
256 H. Wang, H. Zhou, A. Gestos, J. Fang and T. Lin, *ACS Appl. Mater. Interfaces*, 2013, **5**, 10221–10226.
257 H. Wang, H. Zhou, A. Gestos, J. Fang, H. Niu, J. Ding and T. Lin, *Soft Matter*, 2013, **9**, 277–282.
258 H. Zhou, H. Wang, H. Niu, J. Fang, Y. Zhao and T. Lin, *Adv. Mater. Interfaces*, 2015, **2**, 1400559.
259 Z. Cheng, H. Lai, Y. Du, K. Fu, R. Hou, N. Zhang and K. Sun, *ACS Appl. Mater. Interfaces*, 2013, **5**, 11363–11370.
260 Z. Wang, L. Zhu, W. Li and H. Liu, *ACS Appl. Mater. Interfaces*, 2013, **5**, 10904–10911.
261 B. Wang and Z. Guo, *Chem. Commun.*, 2013, **49**, 9416–9418.
262 Z. Cheng, C. Ding, H. Liu, Y. Zhu and L. Jiang, *Nanoscale*, 2014, **6**, 190–194.
263 M. A. Gondal, M. S. Sadullah, M. A. Dastageer, G. H. McKinley, D. Panchanathan and K. K. Varanasi, *ACS Appl. Mater. Interfaces*, 2014, **6**, 13422–13429.
264 D. Ge, L. Yang, C. Wang, E. Lee, Y. Zhang and S. Yang, *Chem. Commun.*, 2015, **51**, 6149–6152.
265 Y.-Q. Liu, Y.-L. Zhang, X.-Y. Fu and H.-B. Sun, *ACS Appl. Mater. Interfaces*, 2015, **7**, 20930–20936.
266 L. Li, Z. Liu, Q. Zhang, C. Meng, T. Zhang and J. Zhai, *J. Mater. Chem. A*, 2015, **3**, 1279–1286.
267 J. L. Yong, Q. Yang, F. Chen, D. Zhang, H. Bian, Y. Ou, J. Si, G. Du and X. Hou, *Appl. Phys. A: Mater. Sci. Process.*, 2013, **111**, 243–249.
268 L. P. Xu, J. Zhao, B. Su, X. Liu, J. Peng, Y. Liu, H. Liu, G. Yang, L. Jiang, Y. Wen, X. Zhang and S. Wang, *Adv. Mater.*, 2013, **25**, 606–611.
269 L. Zhang, Y. Zhong, D. Cha and P. Wang, *Sci. Rep.*, 2013, **3**, 2326.
270 W. Ma, H. Xu and A. Takahara, *Adv. Mater. Interfaces*, 2014, **1**, 1300092.
271 Y.-K. Lai, Y.-X. Tang, J.-Y. Huang, F. Pan, Z. Chen, K.-Q. Zhang, H. Fuchs and L.-F. Chi, *Sci. Rep.*, 2013, **3**, 3009.
272 Y. Zhu, F. Zhang, D. Wang, X. F. Pei, W. Zhang and J. Jin, *J. Mater. Chem. A*, 2013, **1**, 5758–5765.
273 L. Heng, T. Guo, B. Wang, Y. Zhang and L. Jiang, *RSC Adv.*, 2015, **5**, 102378.
274 M. Y. Shen, C. H. Crouch, J. E. Carey and E. Mazur, *Appl. Phys. Lett.*, 2004, **85**, 5694–5696.
275 J. Bonse, S. Baudach, J. Krüger, W. Kautek and M. Lenzner, *Appl. Phys. A: Mater. Sci. Process.*, 2014, **74**, 19–25.
276 R. Wang, K. Hashimoto, A. Fujishima, M. Chikuni, E. Kojima, A. Kitamura, M. Shimohigoshi and T. Watanabe, *Nature*, 1997, **388**, 431–432.
277 K. Liu, M. Cao, A. Fujishima and L. Jiang, *Chem. Rev.*, 2014, **114**, 10044–10094.

278 D. Wang, Y. Liu, X. Liu, F. Zhou, W. Liu and Q. Xue, *Chem. Commun.*, 2009, 7018–7020.
279 Y. Liu, Z. Lin, W. Lin, K. S. Moon and C. P. Wong, *ACS Appl. Mater. Interfaces*, 2012, **4**, 3959–3964.
280 D. Tian, X. Zhang, Y. Tian, Y. Wu, X. Wang, J. Zhai and L. Jiang, *J. Mater. Chem.*, 2012, **22**, 19652–19657.
281 J. Yang, Z. Zhang, X. Men, X. Xu and X. Zhu, *Langmuir*, 2010, **26**, 10198–10202.
282 Y. Sawai, S. Nishimoto, Y. Kameshima, E. Fujii and M. Miyake, *Langmuir*, 2013, **29**, 6784–6789.
283 Y. Gao, M. Cheng, B. Wang, Z. Feng and F. Shi, *Adv. Mater.*, 2010, **22**, 5125–5128.
284 F. Xia, L. Feng, S. Wang, T. Sun, W. Song, W. Jiang and L. Jiang, *Adv. Mater.*, 2006, **18**, 432–436.
285 T. Sun, G. Wang, L. Feng, B. Liu, Y. Ma, L. Jiang and D. Zhu, *Angew. Chem., Int. Ed.*, 2004, **43**, 357–360.
286 G. Ju, M. Cheng, M. Xiao, J. Xu, K. Pan, X. Wang, Y. Zhang and F. Shi, *Adv. Mater.*, 2013, **25**, 2915–2919.
287 L. Xu, X. Lu, M. Li and Q. Lu, *Adv. Mater. Interfaces*, 2014, **1**, 1400011.
288 S. S. Chhatre, A. Tuteja, W. Choi, A. Revaux, D. Smith, J. M. Mabry, G. H. McKinley and R. E. Cohen, *Langmuir*, 2009, **25**, 13625–13632.
289 X.-D. Zhao, H.-M. Fan, J. Luo, J. Ding, X.-Y. Liu, B.-S. Zou and Y.-P. Feng, *Adv. Funct. Mater.*, 2011, **21**, 184–190.
290 M. Im, D.-H. Kim, J.-H. Lee, J.-B. Yoon and Y.-K. Choi, *Langmuir*, 2010, **26**, 12443–12447.
291 L. Xu, Q. Ye, X. Lu and Q. Lu, *ACS Appl. Mater. Interfaces*, 2014, **6**, 14736–14743.
292 X. Hong, A. X. Gao and L. Jiang, *J. Am. Chem. Soc.*, 2007, **129**, 1478–1479.
293 Z. Cheng, L. Feng and L. Jiang, *Adv. Funct. Mater.*, 2008, **18**, 3219–3225.
294 Y. Zhao, J. Fang, H. Wang, X. Wang and T. Lin, *Adv. Mater.*, 2010, **22**, 707–710.
295 D. Wu, S. Z. Wu, Q. D. Chen, Y. L. Zhang, J. Yao, X. Yao, L. G. Niu, J. N. Wang, L. Jiang and H. B. Sun, *Adv. Mater.*, 2011, **23**, 545–549.
296 S. Zhao, H. Xia, D. Wu, C. Lv, Q.-D. Chen, K. Ariga, L.-Q. Liu and H.-B. Sun, *Soft Matter*, 2013, **9**, 4236–4240.
297 F. Guo and Z. Guo, *RSC Adv.*, 2016, **6**, 36623–36641.
298 T. Chen, H. Liu, H. Yang, W. Yan, W. Zhu and H. Liu, *RSC Adv.*, 2016, **6**, 43937–43949.
299 T. Sun and G. Qing, *Adv. Mater.*, 2011, **23**, H57–H77.
300 Z. Hu, X. Zhang, Z. Liu, K. Huo, P. K. Chu, J. Zhai and L. Jiang, *Adv. Funct. Mater.*, 2014, **24**, 6381–6388.
301 X. Zhou, Z. Zhang, X. Xu, F. Guo, X. Zhu, X. Men and B. Ge, *ACS Appl. Mater. Interfaces*, 2013, **5**, 7208–7214.
302 C.-H. Xue, Y.-R. Li, J.-L. Hou, L. Zhang, J.-Z. Ma and S.-T. Jia, *J. Mater. Chem. A*, 2015, **3**, 10248–10253.
303 N. Sakai, A. Fujishima, T. Watanabe and K. Hashimoto, *J. Phys. Chem. B*, 2003, **107**, 1028–1035.
304 G. Caputo, C. Nobile, T. Kipp, L. Blasi, V. Grillo, E. Carlino, L. Manna, R. Cingolani, P. D. C. And and A. Athanassiou, *J. Phys. Chem. C*, 2008, **112**, 701–714.
305 X. Chen and A. Selloni, *Chem. Rev.*, 2014, **114**, 9281–9282.
306 M. Dahl, Y. Liu and Y. Yin, *Chem. Rev.*, 2014, **114**, 9853–9889.
307 F. Zuo, L. Wang, T. Wu, Z. Zhang, B. Dan and P. Feng, *J. Am. Chem. Soc.*, 2010, **132**, 11856–11857.
308 S. Livraghi, S. Maurelli, M. C. Paganini, M. Chiesa and E. Giamello, *Angew. Chem., Int. Ed.*, 2011, **50**, 8038–8040.
309 G. Liu, L.-C. Yin, J. Wang, P. Niu, C. Zhen, Y. Xie and H.-M. Cheng, *Energy Environ. Sci.*, 2012, **5**, 9603–9610.
310 A. Naldoni, M. Allieta, S. Santangelo, M. Marelli, F. Fabbri, S. Cappelli, C. L. Bianchi, R. Psaro and V. D. Santo, *J. Am. Chem. Soc.*, 2012, **134**, 7600–7603.
311 Q. Xiang, J. Yu and M. Jaroniec, *J. Am. Chem. Soc.*, 2012, **134**, 6575–6578.
312 T. R. Gordon, M. Cargnello, T. Paik, F. Mangolini, R. T. Weber, P. Fornasiero and C. B. Murray, *J. Am. Chem. Soc.*, 2012, **134**, 6751–6761.
313 D. Tian, L. He, N. Zhang, X. Zheng, Y. Dou, X. Zhang, Z. Guo and L. Jiang, *Adv. Funct. Mater.*, 2016, **26**, 7986–7992.
314 Z. Wang, Y. Xu, Y. Liu and L. Shao, *J. Mater. Chem. A*, 2015, **3**, 12171–12178.
315 S. Li, J. Huang, M. Ge, C. Cao, S. Deng, S. Zhang, G. Chen, K. Zhang, S. S. Al-Deyab and Y. Lai, *Adv. Mater. Interfaces*, 2015, **2**, 1500220.
316 Y. Cao, X. Zhang, L. Tao, K. Li, Z. Xue, L. Feng and Y. Wei, *ACS Appl. Mater. Interfaces*, 2013, **5**, 4438–4442.
317 J. Song, S. Huang, Y. Lu, X. Bu, J. E. Mates, A. Ghosh, R. Ganguly, C. J. Carmalt, I. P. Parkin, W. Xu and C. M. Megaridis, *ACS Appl. Mater. Interfaces*, 2014, **6**, 19858–19865.
318 J. Y. Huang, S. H. Li, M. Z. Ge, L. N. Wang, T. L. Xing, G. Q. Chen, X. F. Liu, S. S. Al-Deyab, K. Q. Zhang, T. Chen and Y. K. Lai, *J. Mater. Chem. A*, 2015, **3**, 2825–2832.
319 B. Cortese, D. Caschera, F. Federici, G. M. Ingo and G. Gigli, *J. Mater. Chem. A*, 2014, **2**, 6781–6789.
320 Q. Liu, A. A. Patel and L. Liu, *ACS Appl. Mater. Interfaces*, 2014, **6**, 8996–9003.
321 Z. Xue, S. Wang, L. Lin, L. Chen, M. Liu, L. Feng and L. Jiang, *Adv. Mater.*, 2011, **23**, 4270–4273.
322 Z. Cheng, J. Wang, H. Lai, Y. Du, R. Hou, C. Li, N. Zhang and K. Sun, *Langmuir*, 2015, **31**, 1393–1399.
323 W. Zhang, Y. Zhu, X. Liu, D. Wang, J. Li, L. Jiang and J. Jin, *Angew. Chem., Int. Ed.*, 2014, **53**, 856–860.
324 Y. Dong, J. Li, L. Shi, X. Wang, Z. Guo and W. Liu, *Chem. Commun.*, 2014, **50**, 5586–5589.
325 G. J. Dunderdale, C. Urata, T. Sato, M. W. England and A. Hozumi, *ACS Appl. Mater. Interfaces*, 2015, **7**, 18915–18919.
326 M. Tao, L. Xue, F. Liu and L. Jiang, *Adv. Mater.*, 2014, **26**, 2943–2948.
327 R. Yang, P. Moni and K. K. Gleason, *Adv. Mater. Interfaces*, 2015, **2**, 1400489.
328 Q. Wen, J. Di, L. Jiang, J. Yu and R. Xu, *Chem. Sci.*, 2013, **4**, 591–595.
329 H. Song, D. L. Chen and R. F. Ismagilov, *Angew. Chem., Int. Ed.*, 2006, **45**, 7336–7356.
330 Y. L. Sun, W. F. Dong, R. Z. Yang, X. Meng, L. Zhang, Q. D. Chen and H. B. Sun, *Angew. Chem., Int. Ed.*, 2012, **51**, 1558–1562.

331 X. Li, Y. Ding, J. Shao, H. Tian and H. Liu, *Adv. Mater.*, 2012, **24**, OP165–OP169.
332 F. Chen, Z. Deng, Q. Yang, H. Bian, G. Du, J. Si and X. Hou, *Opt. Lett.*, 2014, **39**, 606–609.
333 X. H. Lee, I. Moreno and C. C. Sun, *Opt. Express*, 2013, **21**, 10612–10621.
334 C. Li and H. Jiang, *Appl. Phys. Lett.*, 2012, **100**, 231105.
335 A. O. Ashtiani and H. Jiang, *Appl. Phys. Lett.*, 2013, **103**, 111101.
336 Y. S. Lu, H. Tu, Y. Xu and H. Jiang, *Appl. Phys. Lett.*, 2013, **103**, 261113.
337 Z. Ding and B. Ziaie, *Appl. Phys. Lett.*, 2009, **94**, 081111.
338 X. Jin, D. Guerrero, R. Klukas and J. F. Holzman, *Appl. Phys. Lett.*, 2014, **105**, 031102.
339 Q. Zhu, Q. Pan and F. Liu, *J. Phys. Chem. C*, 2011, **115**, 17464–17470.
340 Y. Liu, J. Ma, T. Wu, X. Wang, G. Huang, Y. Liu, H. Qiu, Y. Li, W. Wang and J. Gao, *ACS Appl. Mater. Interfaces*, 2013, **5**, 10018–10026.
341 A. Zhang, M. Chen, C. Du, H. Guo, H. Bai and L. Li, *ACS Appl. Mater. Interfaces*, 2013, **5**, 10201–10206.
342 S. J. Choi, T. H. Kwon, H. Im, D. I. Moon, D. J. Baek, M. L. Seol, J. P. Duarte and Y. K. Choi, *ACS Appl. Mater. Interfaces*, 2011, **3**, 4552–4556.
343 Y. Gao, Y. S. Zhou, W. Xiong, M. Wang, L. Fan, H. Rabiee-Golgir, L. Jiang, W. Hou, X. Huang, L. Jiang, J. F. Silvain and Y. F. Lu, *ACS Appl. Mater. Interfaces*, 2014, **6**, 5924–5929.
344 X. Huang, B. Sun, D. Su, D. Zhao and G. Wang, *J. Mater. Chem. A*, 2014, **2**, 7973–7979.
345 T. Sun, G. Qing, B. Su and L. Jiang, *Chem. Soc. Rev.*, 2011, **40**, 2909–2921.
346 Y. Mao, Q. Sun, X. Wang, Q. Ouyang, L. Han, L. Jiang and D. Han, *Appl. Phys. Lett.*, 2009, **95**, 013704.
347 B. Chang, M. Zhang, G. Qing and T. Sun, *Small*, 2015, **11**, 1097–1112.
348 X. Zhang, L. Wang and E. Levänen, *RSC Adv.*, 2013, **3**, 12003–12020.
349 I. Banerjee, R. C. Pangule and R. S. Kane, *Adv. Mater.*, 2011, **23**, 690–718.
350 J. Y. Huang, Y. K. Lai, F. Pan, L. Yang, H. Wang, K. Q. Zhang, H. Fuchs and L. F. Chi, *Small*, 2014, **10**, 4865–4873.
351 J. Zhao, X. Zhang, N. Chen and Q. Pan, *ACS Appl. Mater. Interfaces*, 2012, **4**, 3706–3711.
352 X. Zhang, J. Zhao, Q. Zhu, N. Chen, M. Zhang and Q. Pan, *ACS Appl. Mater. Interfaces*, 2011, **3**, 2630–2636.
353 E. Bormashenko, A. Musin, R. Grynuov and R. Pogreb, *Colloid Polym. Sci.*, 2015, **293**, 567–572.